NASA Contractor Report 3440

Charged Particle Concepts for Fog Dispersion

Walter Frost, Frank G. Collins,
and David Koepf

NASA

NASA Contractor Report 3440

Charged Particle Concepts for Fog Dispersion

Walter Frost, Frank G. Collins,
and David Koepf
FWG Associates, Inc.
Tullahoma, Tennessee

ACKNOWLEDGMENTS

TABLE OF CONTENTS

LIST OF TABLES

NOMENCLATURE

a	Particle radius (μm)
A	Area (m^2)
b	Parameter in description of circular turbulent jet
c_p	Specific heat at constant pressure (J/kg K)
C	Cunningham correction factor
C_D	Drag coefficient
D_o	Relative dispersion of droplet density
D_v	Diffusivity of water vapor in air
$D_{1,2}$	Einstein relation $D_{1,2} = Z_{1,2}kT/e$
e	Electronic charge (c)
e_s	Vapor pressure over water (N/m^2)
E	Electric field (V/m)
E_o	Average electric field in corona discharge (V/m)
E_s	Electric field at particle surface (V/m)
E_T	Electric field at top of tower (V/m)
F_D	Drag force (N)
F_E	Electric force (N)
F_G	Gravitational force (N)
g	Gravity (m/s^2)
H	Maximum height of charged field in Gourdine theory (m)
H	Height of structure (m)
I_j	Current leaving nozzle (c/s)
$(\tilde{I}_{1,2})_D$	Rate of attachment of positive/negative ions due to diffusion (c/s)

$(\tilde{I}_{1,2})_E$ Rate of attachment of positive/negative ions due to electrical field attraction (c/s)

$\vec{J}$ Current density (c/s m^2)

k Boltzmann constant

k_T Thermal conductivity of air (W/mK)

K Eddy diffusion coefficient

Kn Knudsen number

ℓ Liquid water content

ℓ_1 Sum of water content $\ell_1 = q_v + \ell_c + \ell_f$

ℓ_2 Sum of water content $\ell_2 = q_v + \ell_c + \ell_f + \ell_p$

ℓ_o Threshold liquid water content for conversion

L Latent heat of vaporization (J/kg)

m Mass of particle (kg)

n Number of charges on a particle

$\hat{n}$ Unit vector normal to an area

n_f Droplet size distribution function (m^{-1})

n_s Saturated number of charges on a particle

n_1 Positive free small ions

n_2 Negative free small ions

N Charged particle number density (m^{-3})

N Number density of droplets (m^{-3})

N_{BJ} Charged particle number density between jets (m^{-3})

N_i Ion number density in corona region (m^{-3})

N_J Charged particle number density in jet (m^{-3})

N_{Jo} Charge number density at nozzle exit (m^{-3})

P Pressure (N/m^2)

P_o Environmental reference state pressure (N/m^2)

q	Charge on particle or droplet (c)
$\hat{q}$	Water vapor plus liquid water content of charged droplets ($\hat{q} = q_v + \ell_c$)
q_v	Water vapor mixing ratio
q_{vs}	Saturated water vapor mixing ratio
Q	Total current from a spherical source (c/s)
r	Radius (m)
$\hat{r}$	Unit vector in radial direction
r_{cf}	Position vector of a small colliding droplet with respect to center of large droplet being impacted (m)
R	Radius of cylindrical region of uniform charge density (m)
R	Specific gas constant for air (J/kg K)
R_j	Exit radius of nozzle (m)
Re	Reynolds number
R_v	Specific gas constant for water vapor (J/kg K)
s	Saturation ratio, $s = q_v/q_{vs}$
<S>	Mean separation probability
$S(\alpha_1)$	Angular separation probability function
t	Time (s)
t_m	Length of time particle is in corona region (s)
t_o	Time constant for field charging (s)
T	Temperature (°K)
u	Horizontal fluid velocity (m/s)
$\vec{u}$	Fluid dynamics velocity (m/s)
u_j	Velocity at nozzle exit (m/s)
v	Particle speed (m/s)
v*	Terminal speed of particle (m/s)

$\overline{v}$ rms speed of ions (m/s)

v_r Relative speed (m/s)

v_j Volume flow rate from nozzle (m^3/s)

w Vertical fluid flow (m/s)

V Relative velocity of droplet (m/s)

V_{cf} Relative velocity between charged droplet and fog droplet (m/s)

x Downstream distance along jet centerline from nozzle exit (m)

x Horizontal distance (m)

z Vertical position (m)

Z Particle mobility (m^2/Vs)

Z_i Ion mobility (m^2/Vs)

Z_{max} Particle mobility when the surface field is the breakdown field (m^2/Vs)

α Ionic recombination coefficient

α Spreading factor for cirular turbulent jet

α_1 Angle of colliding droplet relative to velocity of impacting droplet

$\gamma_{1,2}$ Positive nondimensional constants

ε_o Permitivity of free space (c/Vm)

η Collision efficiency

$<\theta>$ Potential temperature of environmental reference state (°K)

θ' Deviation of potential temperature from reference state (°K)

κ_e Dielectric strength of particle

λ Mean free path of air (m)

$\hat{\lambda}$ Exponent in Marshall-Palmer distribution

μ Coefficient of viscosity of air (kg/ms)

ρ Density of particle (kg/m^3)

ρ_a Density of air (kg/m^3)

ρ_e Charge density (c/m^3)

ρ_T Total charge density (c/m^3)

$<\rho>$ Density of the environmental reference state (kg/m^3)

ρ_w Density of water (kg/m^3)

τ Acceleration time constant of particle (s)

ϕ' Entropy (J/kg K)

ϕ_e Electrical potential (V)

ψ Streamline (s^{-1})

ω Vorticity (kg/m^3s)

Subscripts

c   Designates charged droplet

f   Designates fog droplet

p   Designates precipitating droplet

x   Component in x direction

z   Component in z direction

Supercripts

pol   Denotes polarization

coal   Denotes coalescence

1.0 INTRODUCTION

Charged particle techniques hold promise for dispersing warm fog in
the terminal area of commercial airports. A survey of research relative
to this technique and a discussion of competitive techniques such as
thermal air, etc., is given in Christensen and Frost [1-1]. The present
report focuses on features of the technique which require further study.
The physical principles upon which the technique is based and the major
experiments carried out in the past towards verification of the tech-
nique are described in Section 2.0. The fundamentals of the nozzle
operation are given in Section 3.0. A complete discussion of the char-
acteristics of the nozzle and the theory of particle charging internally
in the nozzle are described. Information from the extensive literature
on electrostatic precipitation relative to environmental pollution
control is incorporated into this discussion. The section ends with a
description of some of the preliminary and simplified analyses reported
in the literature on the jet characteristics and its interaction with
neighboring jets.

From the survey reported in Reference [1-1], it is evident that
much needs to be learned relative to the interaction of the charged
particles expelled by the nozzle and the fog droplets. The mechanisms of
charge transfer, coalescence, etc., are somewhat understood by cloud
physicists [1-2, 1-3], but this understanding has not
been applied to the problem in hand. Also, since the charged particles
themselves result in the formation of the atmospheric electric field
which causes the charged fog droplets to be driven to the ground, the
physical process is highly dynamic. Modeling of the above-described
fog and jet interaction would be useful to optimize the nozzle design;
however, it is believed that the state of the art is such that an effec-
tive nozzle can be designed [1-4, 1-5] and the effectiveness of the fog
dispersal technique evaluated experimentally. An understanding of the
basic unsolved equations governing the process is useful, however, to
interpreting the experimental results; therefore, Section 4.0 presents

the equation governing the transfer of water substances and of electrical charge. A brief description of several semi-empirical, mathematical expressions necessary as input to the governing equations is given. A solution technique and the formulation of boundary conditions to analyzing the jet interaction with fog and the formation of the electric field requires further development.

Section 5.0 describes the necessary ingredients of a field experiment to verify the system once a prototype is built. The necessary equipment, number of nozzles, accuracy of the instruments, parameters to be measured, etc., are discussed based on the extent of our existing knowledge. The purpose of Section 5.0 is to provide insight as to the magnitude of the field program necessary to verify the fog dispersal system.

References

1-1. Christensen, L. S., and W. Frost. "Fog Dispersion," NASA CR 3255, March 1980.

1-2. Mason, B. J. The Physics of Clouds. New York: Oxford University Press, 1971.

1-3. Chalmers, J. A. Atmospheric Electricity. New York: Pergamon Press, 1967.

1-4. Willke, T. L. "Current Production in a Cylindrical Geometry Electrofluid Dynamic Generator," U.S. Air Force, Aerospace Research Laboratories, Report No. ARL 71-0245, October 1971.

1-5. Lawson, M. O. "Ion Generation by Corona Discharge for Electro-Fluid Dynamic Energy Conversion Processes," U.S. Air Force, Aerospace Research Laboratories, Report No. ARL 64-76, October 1964.

2.0 CHARGED PARTICLE FOG DISPERSAL CONCEPT
AND BACKGROUND RESEARCH

The concept of fog dispersal by charged particle techniques stems from existing evidence that electric forces have profound effect on the growth of water droplets in warm clouds and in fogs by collision and coalescence. Carroz, et al. [2-1] and Cochet [2-2] have shown theoretically that highly charged droplets possess much larger collection efficiencies than similar but uncharged droplets. Also, the successful introduction of large quantities of highly charged droplets into confined regions of fog results in the generation of a substantial electric field, which modify the natural fog over regions beyond the immediate influence of charged materials. A general consensus [2-2, 2-3] indicates that electric fields greater than 20 kV/m are required to influence significantly the stability of a natural fog; and while there may be considerable difficulty in engineering these large electric fields, the potential rewards from an aviation operational point of view are large enough to warrant further investigation.

Gourdine Systems, Inc., [2-4] appear to be the first to propose a system having practical application for fog dispersal at airports. Their concept involved using a matrix of charged particle spray guns installed along and around an airport runway to propel charged water droplets into the fog. An electric charge was thereby imparted to the fog droplets, causing them to precipitate to the ground under the action of space charged induced electric fields or through enhanced coalescence and precipitation under gravitational forces. Application of this concept calls for the development of a charged particle spray gun which must charge the particles (charged carriers) internally and propel the particles to the necessary heights to affect the clearing which allows aircraft operations to continue. Secondly, to provide the optimum spray gun design and matrix array for efficient warm fog dispersal, the charged particle/fog droplet interaction must be understood. In particular, the extent and intensity of the electric field which can be generated under

3

various climatic conditions, i.e., wind, fog density, turbulence, etc., must be known. The mechanism of transferring charge to the fog droplets and of their following the electric field to ground, as well as the mechanism of coalescence which enhances droplet growth and their migration to the ground by gravitational forces is not understood. In view of the experimental and analytical difficulties which must be overcome to develop a comprehensive model of this mechanism it is recommended that a systematic development and testing of a prototype system be carried out. The effectiveness and economic viability of this system can be established in this manner without a complete knowledge of the charged particle interactions.

The principle upon which a charged particle spray gun operates is illustrated in Figure 2.1. Figure 2.1a illustrates the principle of an electrical gas dynamics direct energy conversion nozzle. A gas containing uncharged particles flows through a corona discharge and down a dielectric channel. In the corona region molecular ions are injected into the flow and some of these ions attach to the water droplets and are swept downstream. The particles are discharged to a sharp, pointed electrode collector downstream and the current passes through an external resistance. Thus, energy in the flowing gas is converted to high-voltage electrical energy. That is, the energy lost while flowing from the ionizer, corona discharge region, to the collector appears as electric energy, or heat, in the external resistance.

In the fog dispersal mode the collecting electrode is eliminated and the charged particles are carried into the atmosphere by the flow energy. Thus, kinetic energy of the flowing gas and particles is converted into electric potential energy in the form of a large cloud of highly charged particles. Since the charged particles dispersed to the atmosphere find their way back to ground potential through the atmosphere, the air becomes the external resistance, dissipating electrical energy as heat through collisions between the air molecules and the charged particles. The larger the size cloud of charges the longer the path to ground and the larger the external resistance. For a given current output, the larger the external resistance the larger are the voltage and power that must be generated to maintain the charged cloud.

4
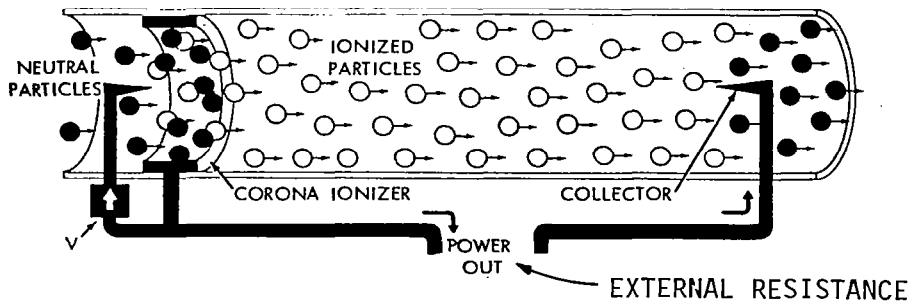
a) Energy mode.
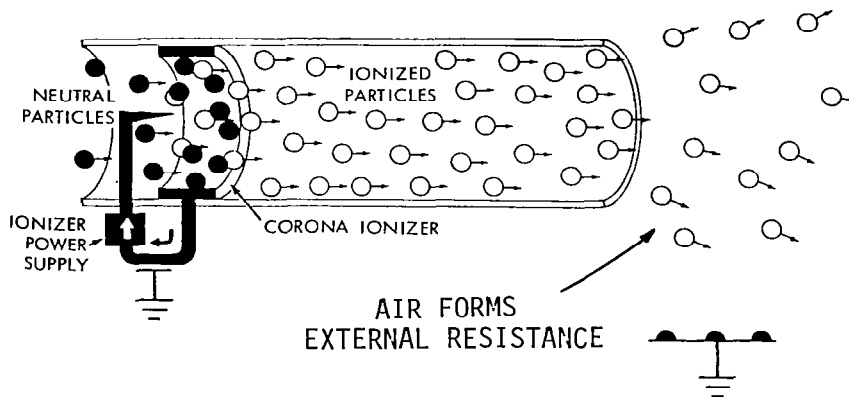
b) Fog dispersal mode.

Figure 2.1   Principle of charged particle fog dispersal technique
             [2-4].

5

Therefore, in order to establish a cloud of charged fog droplets of the same polarity, a charged particle spray gun must raise the charges to a high electrical potential energy with respect to ground, typically several thousand volts, and propel these charged particles to sufficient heights to affect fog clearing.

The initial spray gun used by Gourdine Systems, Inc. [2-4] used a high-speed jet of air to carry the charged submicron water droplets into the fog. The jet of air along with turbulent diffusion pushes the charged particles to a height which preliminary experiments and calculations suggest can be on the order of 30 m. Continuous injection of the charged water droplets from the spray guns maintains a constant space charge electric field. The fog particles having acquired a charge from interaction with the charge carriers are then considered to follow the electric field and precipitate to the ground. A mathematical model of this mechanism is given in later sections.

To test this system a laboratory and a field study were carried out. A complete description of these studies is given in References [2-5] and [2-6]. A summary of a full-scale field study, conducted in the Panama Canal Zone [2-7], is given in the following sections to provide the reader with an understanding of the practical approach to warm fog dispersal and to familiarize him with the limited background information available.

2.1 Summary of the Full-Scale Field Experiment in the Panama Canal Zone

A description of the experimental apparatus utilized in the Panama Canal Zone full-scale field experiment as detailed in References [2-4] and [2-7] is given along with some of the estimated and measured characteristics of the system. Also, the reported results of the experiment are summarized.

In the Panama experiment, sixteen spray guns were set up in a 4x4 array with 38.1 m (125 ft) separation between guns. Figure 2.2 schematically illustrates this array and the location of the major fog monitoring instrumentation sites. The meteorological van containing most of the instrumentation was located some distance from the array to avoid the possibility of distortion of results by grounding effects of the metal tower. Two visibility monitoring stations were utilized: the

EGD Spray Gun System

1 kw, 115 V AC Portable
Gasoline Generator

Prevailing Wind

38.1 m
(125 ft)

38.1 m
(125 ft)

114.4 m
(375 ft)

South Mobile
Videograph

East-West Access Road

114.4 m
(375 ft)

North Stationary
Videograph

Meteorological Van
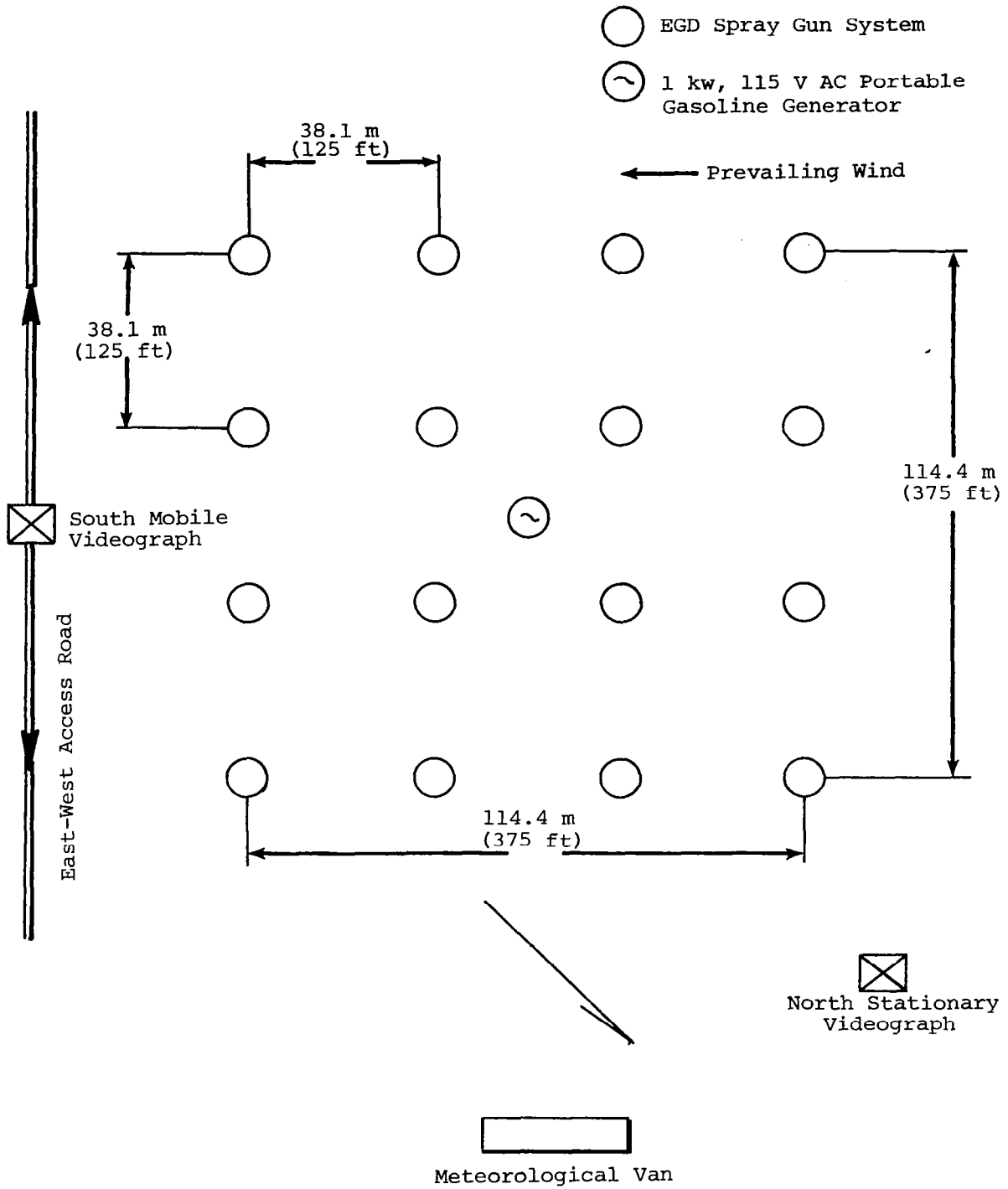
Figure 2.2 Panama Canal Zone field experiment arrangement [2-7].

7

south mobile videograph and the north stationary videograph. In all cases, reported data were measured with the south mobile videograph.

During the test period, ten field tests were carried out. Of these, 40 percent of the experiments produced some effect on surface visibility. These effects are discussed subsequently.

Space charge distribution measurements were made during only two of the runs. These measurements indicated the existence of charged particles at an altitude of at least 30.5 m (100 ft) and of the right order of magnitude (-3×10^{-7} c/m^3) corresponding to approximately 15×10^6 V at a height of 30.5 m (100 ft) [2-4]. Data at the center of the array, however, shows a factor of three less than expected, and the space charge distribution according to measurements was, in general, nonuniform.

Electric field distribution measurements were made during all tests to provide an indirect measurement of the relative distribution of ground current density. Measurements indicated a field strength of -4×10^4 V/m at a distance of 77.8 m (255 ft) downwind of the test array. Figure 2.3 from Reference [2-4] summarizes the time and space relationship mapping of the electric field distribution.

2.1.1 Description of Experimental Apparatus

A charged particle spray gun in operation is illustrated in Figure 2.4 [2-7]. The system consists of a nozzle or spray gun, a supply and control hand cart, and a gasoline-driven air compressor. Sixteen of these units were constructed and used in the experimental program.

Charged particle spray gun. A schematic of the spray gun nozzle is shown in Figure 2.5. The major dimensions and working principles are illustrated. A stream of saturated compressed air enters the spray gun and passes through a nozzle as illustrated in Figure 2.5. The air expands to supersonic conditions, cooling sufficiently to form droplets of water. As the droplets pass through the corona discharge region of the nozzle, they acquire a charge. The charged particles are then carried by supersonic airflow down the dielectric channel and exhaust to the atmosphere forming the space-charged cloud.

The operating characteristics of the spray guns utilized in the Panama experiment, as reported in Reference [2-4], are given in Table 2.1.

X EGD Spray Gun

◯ 6 ft Circle

● Center of each four spray guns. Top number, scanner faces X. Bottom number, scanner faces away from X. Number in ( ) indicates time in hours. Midway measurement omitted for clarity.

⊗ 2.3×10^5 ⊗ 2.8×10^5 ⊗ 1.8×10^5 ⊗ 2.5×10^5
   2.3×10^5 1.5×10^5 1.0×10^5 1.8×10^5

        ● 4×10^4 ●   ● 4×10^4
          (0340)   (0337)

⊗ 2.5×10^5 ⊗ 1.5×10^5 ⊗ 2.0×10^5 ⊗ 2.5×10^5
   1.5×10^5 1.0×10^5 1.0×10^5 1.5×10^5

◄──────────   ● 3.8×10^4 ● 2.8×10^4 ● 2.0×10^4
   85 yds   (0328)   ·   (0325)   (0323)
4×10^4

⊗ 2.8×10^5 ⊗ 2.4×10^5 ⊗ 2.5×10^5 ⊗ 3.0×10^5
   2.0×10^5 1.4×10^5 1.5×10^5 1.8×10^5

        ● 3.0×10^4 ● 1.5×10^4 ● 2.8×10^4
          (0255)   (0305)   (0317)

⊗ 2.5×10^5 ⊗ 2.6×10^5 ⊗ 2.0×10^5 ⊗ 3.0×10^5 v/m
   2.0×10^5 1.5×10^5 1.5×10^5 1.4×10^5 v/m
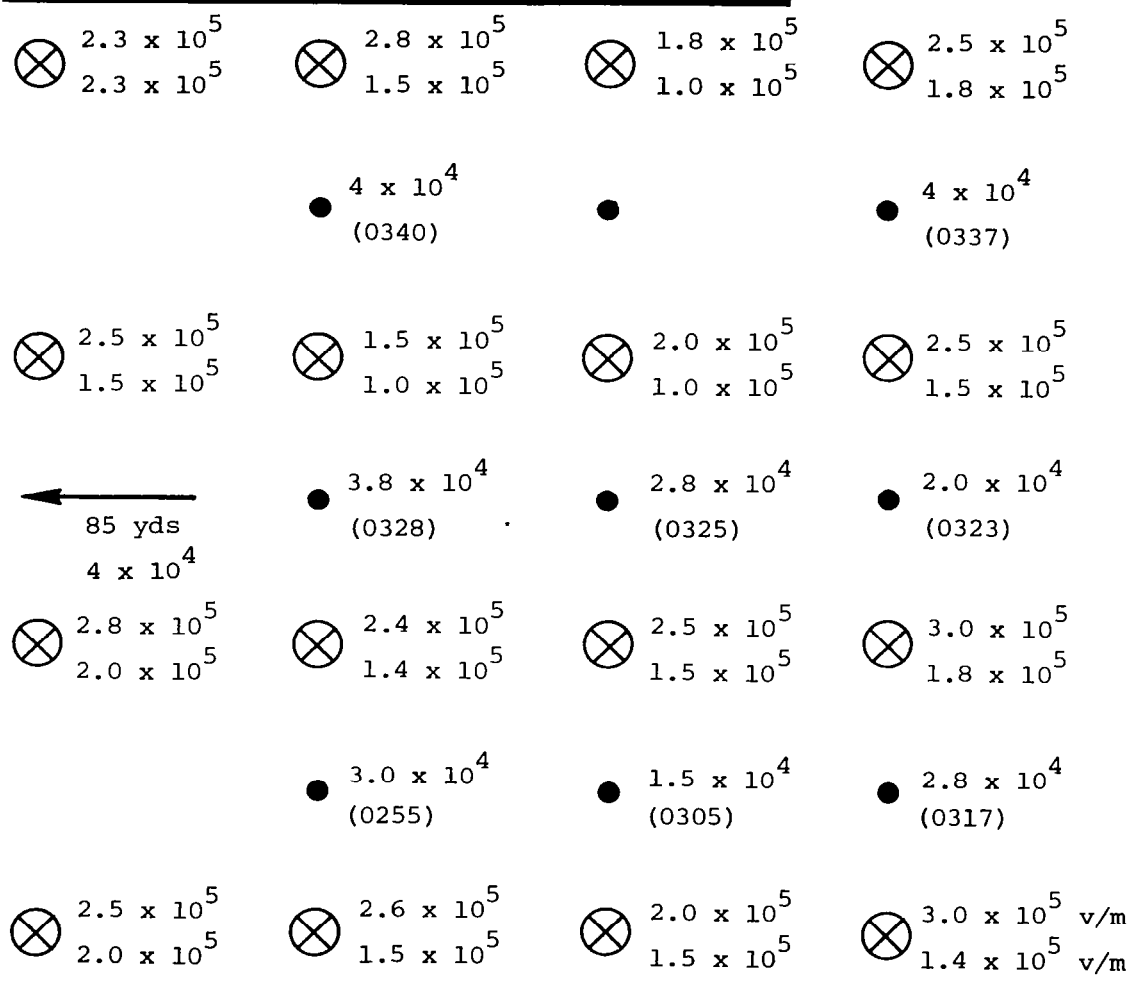
Date: 11/23/72

V-G-6D

Background, $+3.5 \times 10^3$ V/m
          (0245)

Figure 2.3 Typical electric field mapping (relative ground-current density distribution) as reported in Reference [2-4].

9
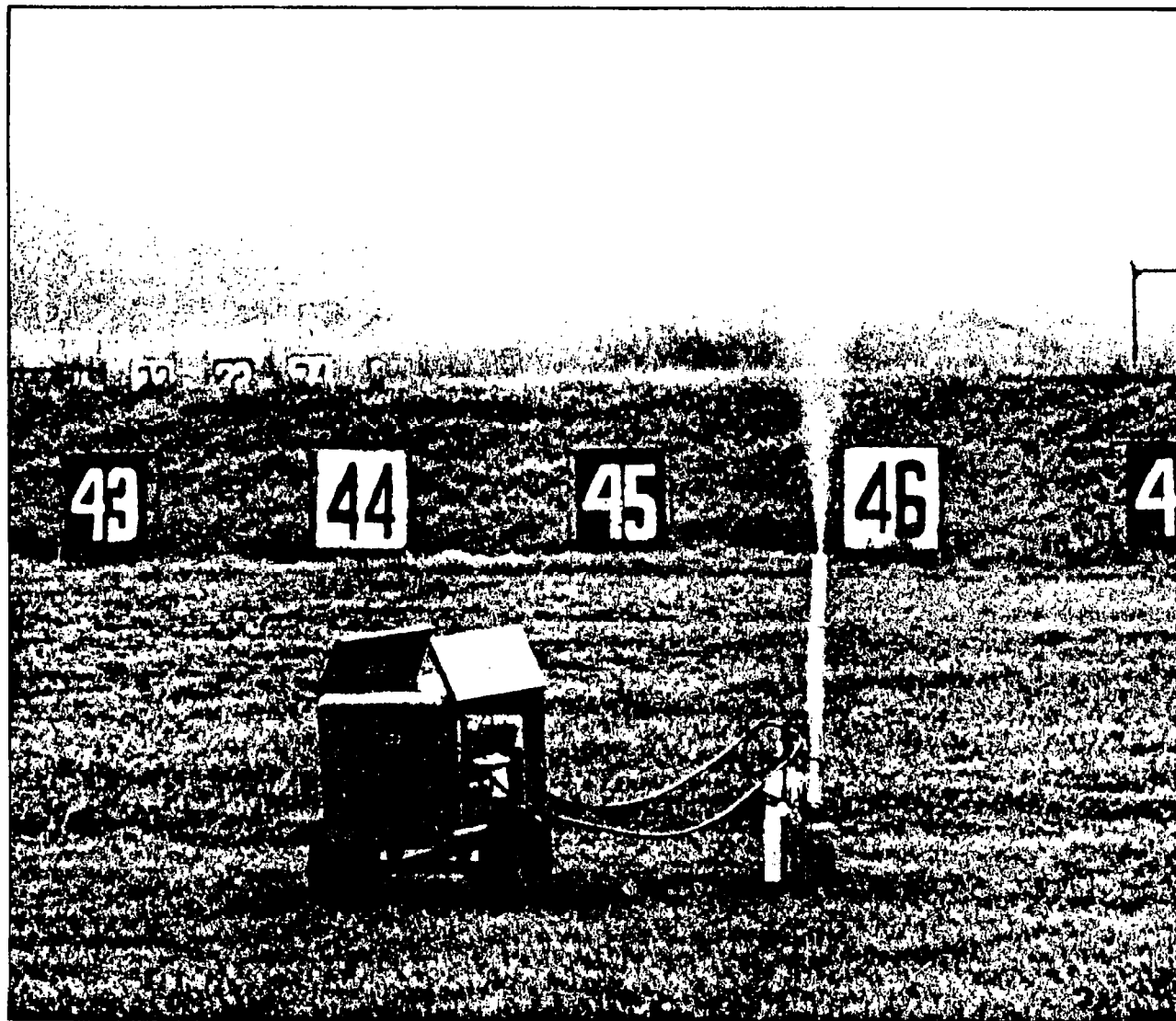
Figure 2.4   Charged particle spray gun in operation [2-7].
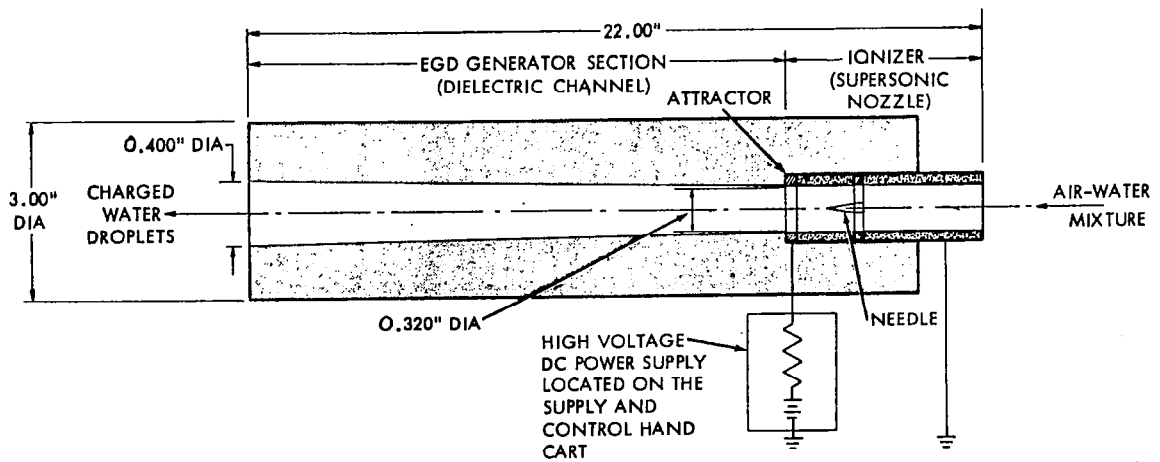
Figure 2.5 Schematic of spray gun nozzle [2-4].

TABLE 2.1 Operating Characteristics of Spray Gun Used in Panama Experiment [2-4].

Ionizer voltage	9 $\sim$ 10 kV
Compressor line pressure	75 psig
Volumetric flow rate of air	50 scfm
Water consumption	38 cc/min, or 6.34 x 10^{-4} kg/s
Short-circuited current	100 $\sim$ 135 x 10^{-6} A
Load voltage (2 x 10^9 Ω load)	70 $\sim$ 80 kV
Mach number	1.35
Charge/mass ratio*	0.213 c/kg
Droplet radius**	10^{-7} m
Droplet charge	8.92 x 10^{-19} c
Droplet mobility	5.7 x 10^{-8} m^2/Vs

$$\frac{*\text{Charge/droplet}}{\text{Mass/Droplet}} = \frac{\text{Short-Circuited Current (A)}}{\text{Water Consumption (kg/s)}}$$

    **Derived from experimental charge/mass ratio and by using diffusion charging mechanism for particles in a supersonic channel.

11

The method of measuring the load voltage and the short-circuited current are illustrated in Figure 2.6. Optimum outputs were achieved by adjusting simultaneously the air/water mixture and the high voltage applied to the ionizer.

As described in Section 3.0, one drawback to this type of spray gun nozzle, identified by the present authors, is that the particles do not remain in the corona region sufficiently long to become fully charged. As will be shown, the time required to fully charge a particle is on the order of milliseconds whereas at sonic speeds the droplets pass through the corona region in microseconds.

Auxiliary equipment. The other components making up the system are illustrated in Figure 2.7. All supplies, controls, and regulators necessary to operate this spray gun were mounted on a mobile hand cart. A water tank with all controls and regulators was mounted in the front and a high-voltage DC power supply with a 110 AC volt input supplied from a portable gas-driven generator along with a stand for the charged particle spray gun were mounted in the rear. An electrical power distribution network was employed to provide power to all 16 mobile units from the centrally located gas-driven generator.

Air provided by a portable air compressor entered the system at the water tank inlet. The air pressure was controlled by a regulator and fed through an on/off valve to the water tank. Pressurized water entered a capillary tube in the water tank, passed through a flow meter and through a capillary coil where it was mixed with a second air supply. Mixing of the compressed air and water took place in a section of pressure hose, and the air/water mixture was supplied to the charged particle spray gun. The required water flow rate was controlled by adjusting the metering valve on the flow meter.

2.1.2 Parameters Measured and Instrumentation

The parameters measured during the field program were:

- Atmospheric transmissivity (visibility versus time)

- Wind speed and direction versus time

LOAD VOLTAGE PROBE (WITH 2×10^9 Ω LOAD RESISTOR)

μ AMMETER

HANDLE

SPRAY
GUN

SPRAY
GUN
STAND

GROUND CLIP

LOAD VOLTAGE MEASUREMENT

CORONA TIP

μ AMMETER

SPRAY
GUN

SPRAY
GUN
STAND

GROUND CLIP

SHORT-CIRCUITED CURRENT
MEASUREMENT
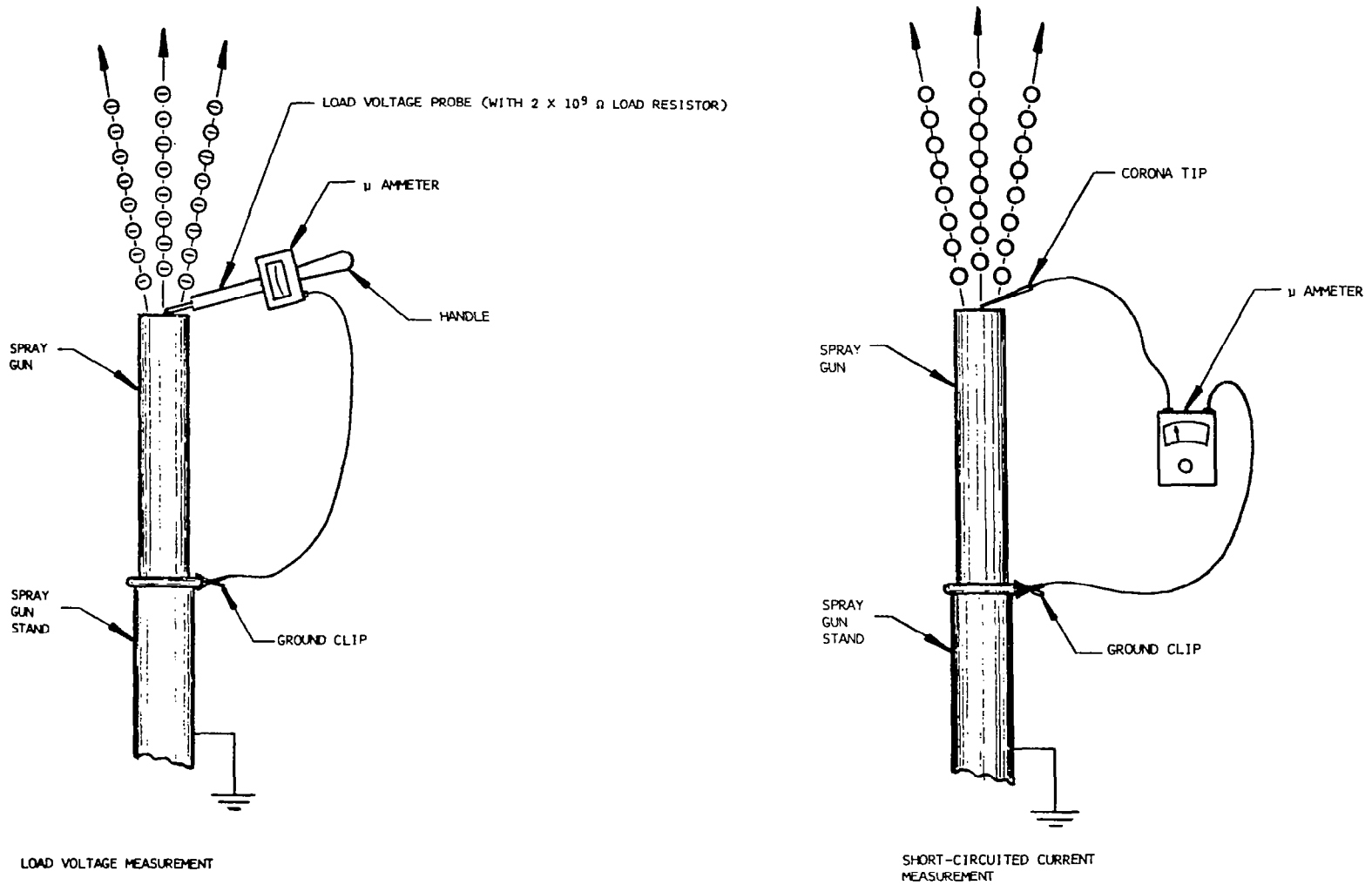
Figure 2.6   Illustrates measurement of load voltage and of short-circuited
current [2-4].
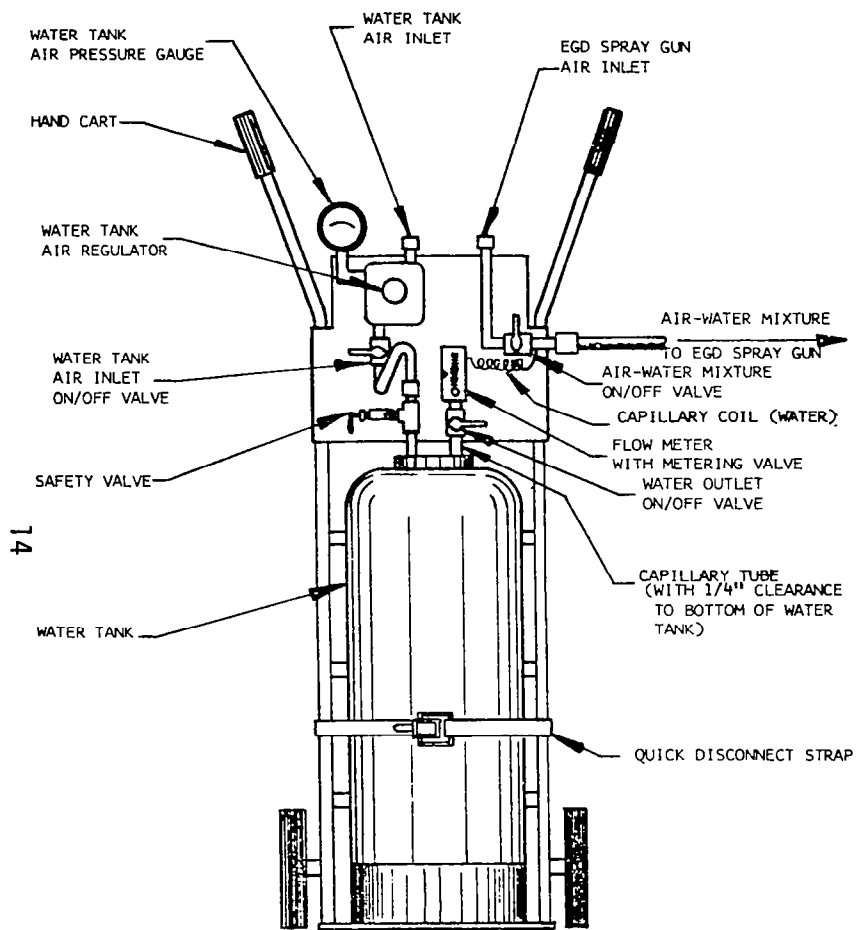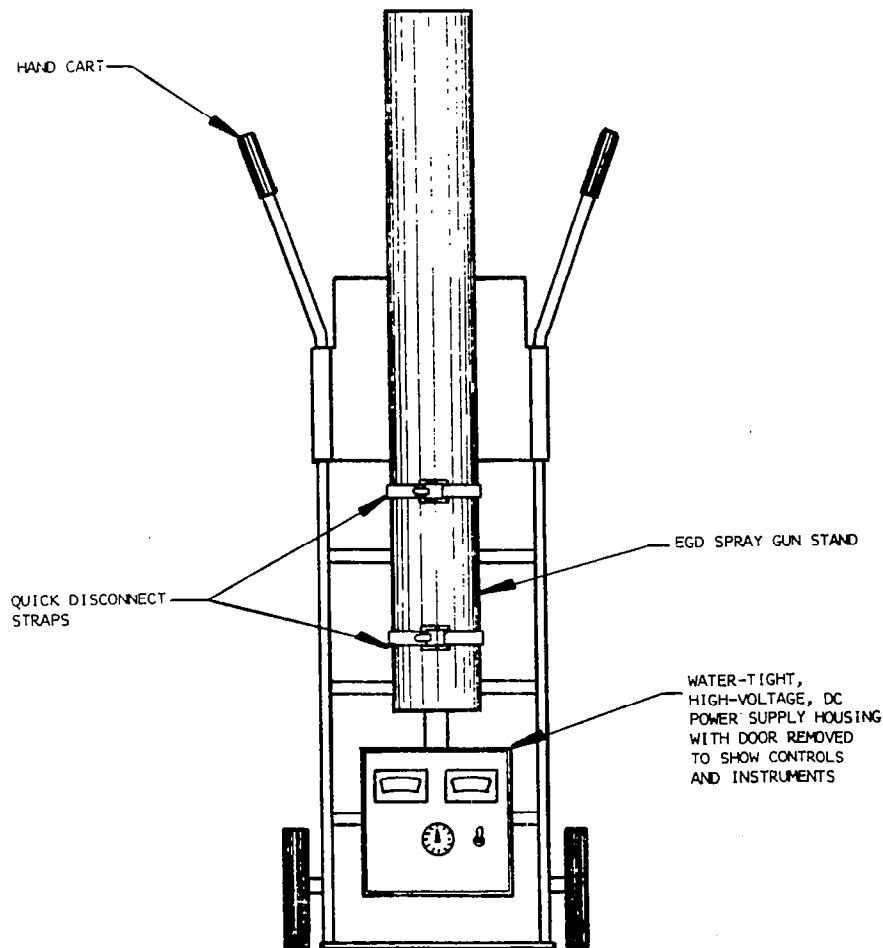
Figure 2.7 Schematic of charged particle spray gun unit used in Panama experiment [2-4].

- Fog drop size distribution and concentration versus time and altitude

- Atmospheric temperature and dew point, or relative humidity versus time

- Atmospheric electrical potential gradient versus time

- Atmospheric space-charge distribution versus time and altitude

- Ground-current density distribution versus time

Space-charge density distribution. A space-charge density probe supported by a balloon-borne platform was used to measure the space-charge density distribution. Details of the probe are given in Reference [2-4]. It consisted mainly of an aluminum cylinder with a spherical brass ball centered axially in the middle. The ball was connected to the input of an electrometer and the cylinder was electrically grounded. The potential measured in the space-charge cloud is in direct proportion to the space-charge density and the diameter of the cylinder squared. The output of the probe was telemetered to a ground receiver.

Ground-current density distribution. The ground current density distribution was measured indirectly by mapping the electric field as obtained by a portable electric field scanner. The ground current density was then estimated from the electric field map and the measured space-charge density distribution. To determine an absolute distribution of ground-current density, the mobility of the charged particles must be known.

Visibility. Visibility was measured with videographs located as illustrated in Figure 2.2. The videograph, a product of Sperry-Rand, Ltd., operates on measurement of backscattered light.

Fog drop size distribution and concentration. Fog drops were collected on hand-held gelatin-coated slides.

Other climatological parameters. Temperature, dew point, wind direction and speed were measured from a 15.2 m (50 ft) instrumented tower. The meteorological van and tower were located somewhat out of the spray gun array to avoid distortion of the electrical field resulting from grounding effects of the metal tower. Measurements of temperature and

relative humidity were recorded at ground level while wind direction and speed were recorded from sensors on the instrumented tower installed at an altitude 15.9 m (52 ft) above ground level. Time is recorded in local standard time and visibility in nautical miles.

2.2 Test Results

This section summarizes the test results as presented in Reference [2-7]. Ten fog dispersal tests were performed. Two of the ten tests conducted were not evaluated because of equipment malfunction and premature breakup of the natural fog. Figure 2.8 reproduced from Reference [2-7] summarizes results of the remaining eight dispersal tests. All visibilities were recorded by the south mobile videograph and are expressed in nautical miles (NMI).

November 16--Tests V-G(2) and V-G(3). In test V-G(2) the spray guns were turned on at approximately 0435. With the exception of a slight pulse at the beginning of the tests, visibility averaged 0.2 NMI. Sixty minutes after spraying began the visibility increased steadily reaching a peak of 3.9 NMI 8 min after spraying was terminated at 0545. Visibility then decreased abruptly to near its original value in approximately 4 min. Temperature and relative humidity remained constant at 75° F and 100 percent, respectively, during the test. Winds were recorded calm throughout the test period with a slight southerly drift in fog being noted.

Test V-G(3) was a continuation of test V-G(2). Here the spray guns were activated at 0615 and continued to operate until 0645. Wind speed was recorded as calm except for a brief 2-minute period of 2 to 4 kts at 0630. The prevailing wind direction during the test was equally divided between WSW (250 deg) and NW (315 deg). Visibility initially at 0.2 NMI improved reaching a peak of 0.8 NMI in 22 min from activating the spray guns. Following spray termination a steady decreasing trend in visibility was recorded.

Visual observers indicated that the sky was totally obscured throughout V-G(2) and V-G(3). Temperature increased from 75° F to 76° F, and relative humidity decreased from 100 percent to 97 percent during this test period.

16
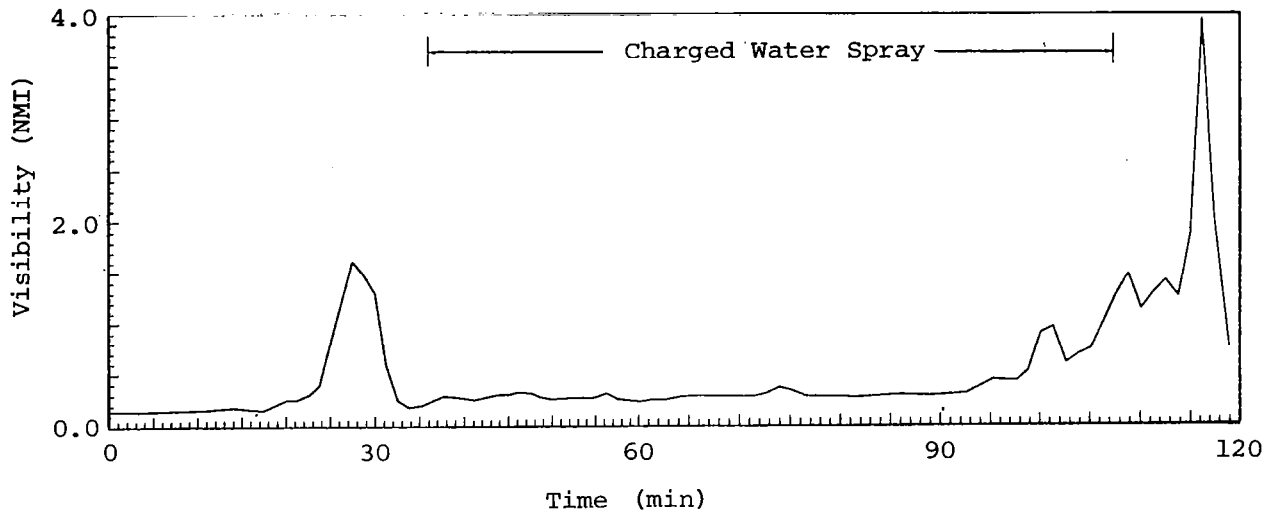
a) Visibility plot--test V-G(2).
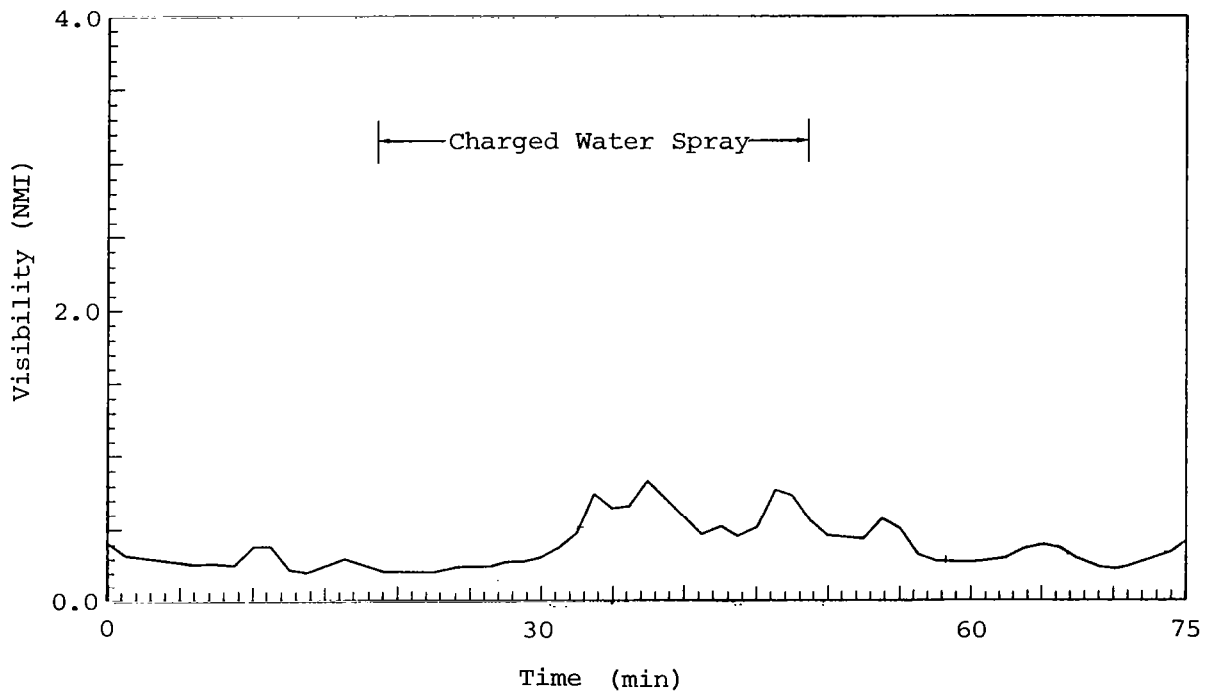
b) Visibility plot--test V-G(3).

Figure 2.8   Test results of the Panama field experiment as reported in
Reference [2-7].

17
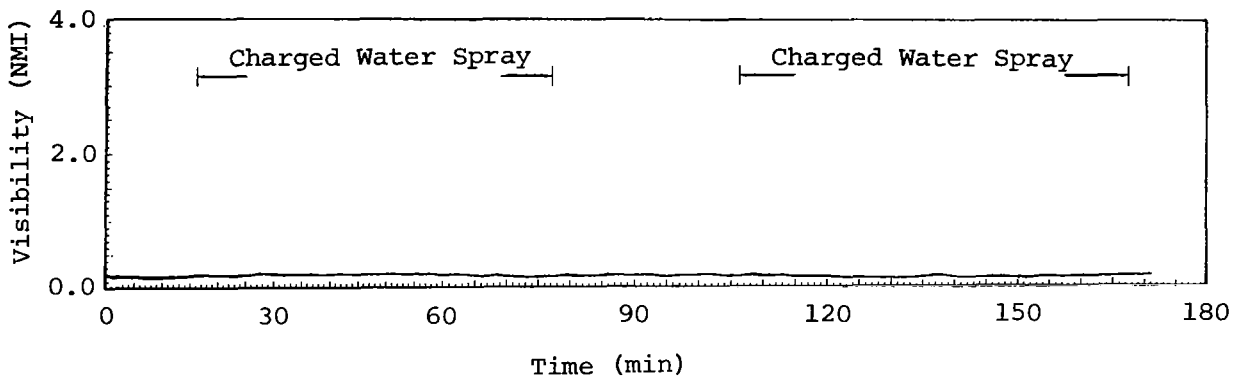
c) Visibility plot--test V-G(4) and (5).
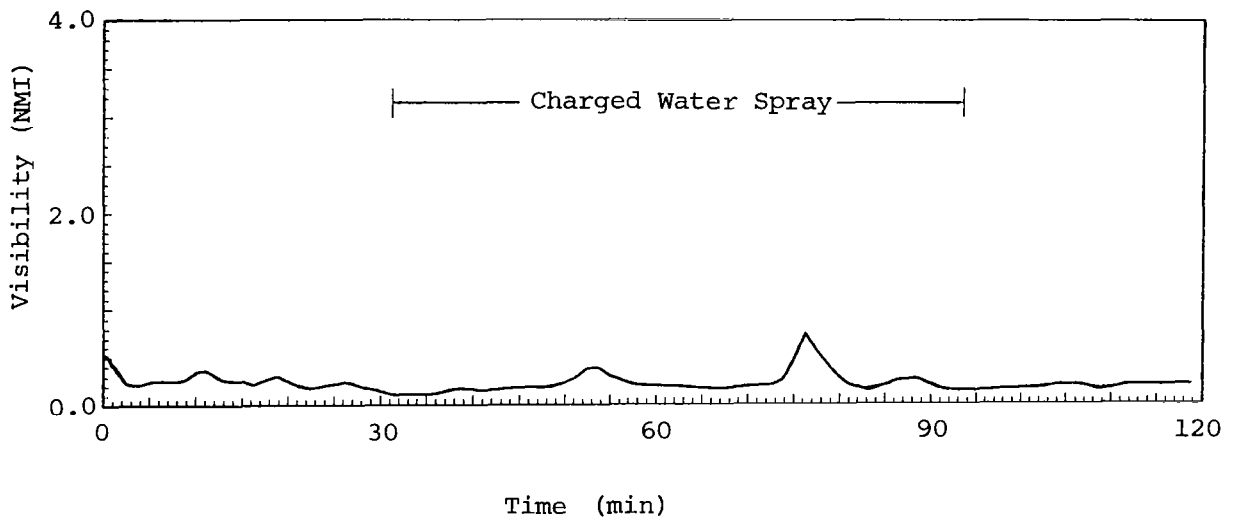
d) Visibility plot--test V-G(6).

Figure 2.8 (continued).

18
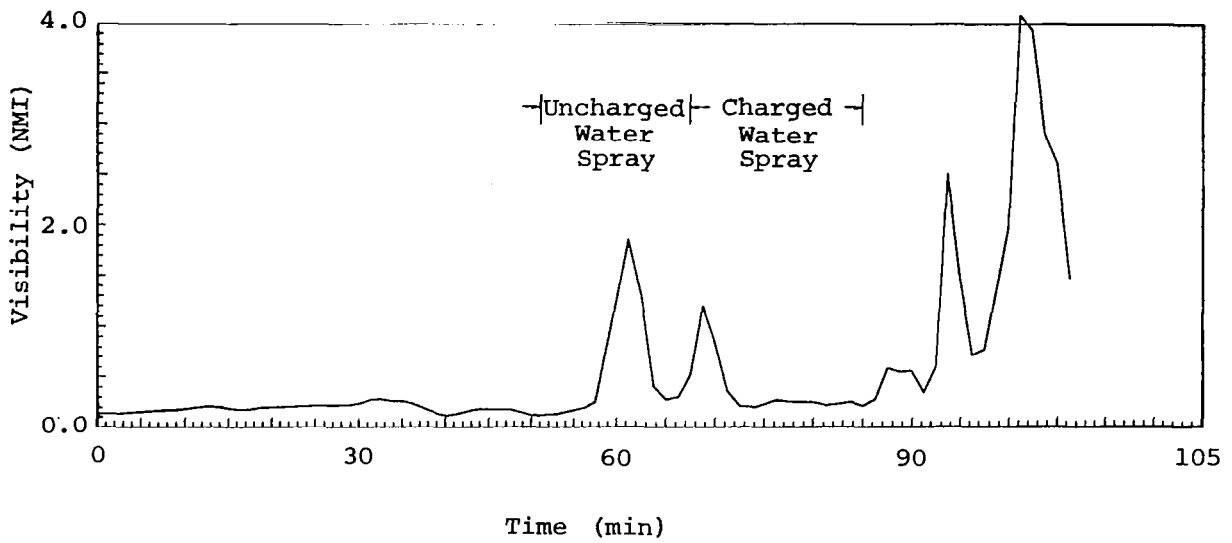
e) Visibility plot--test V-G(7).
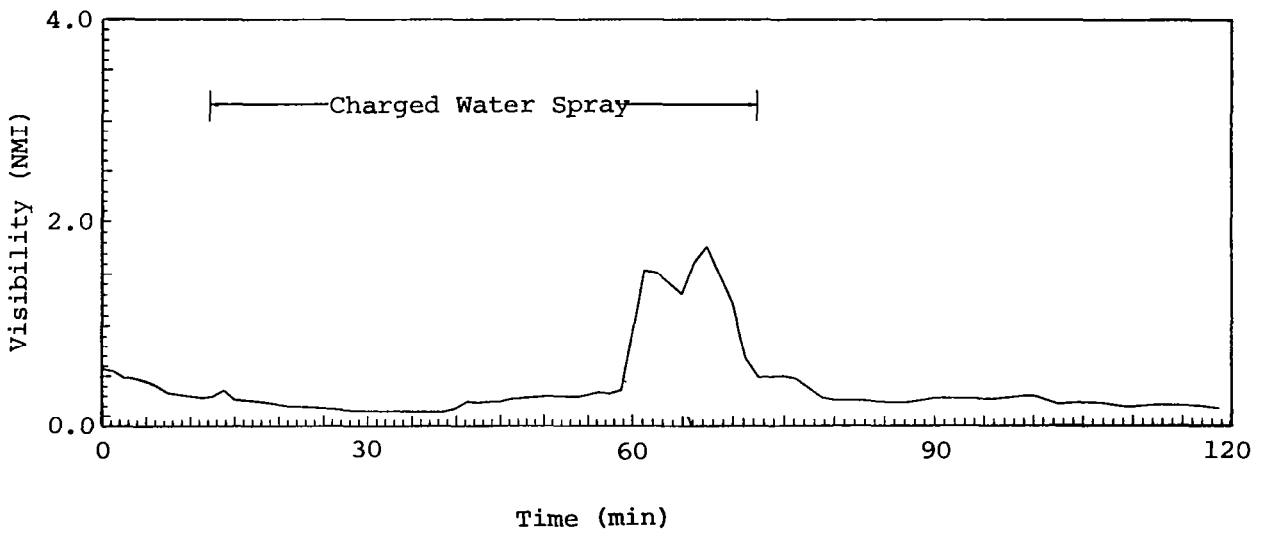
f) Visibility plot--test V-G(9).

Figure 2.8 (continued).
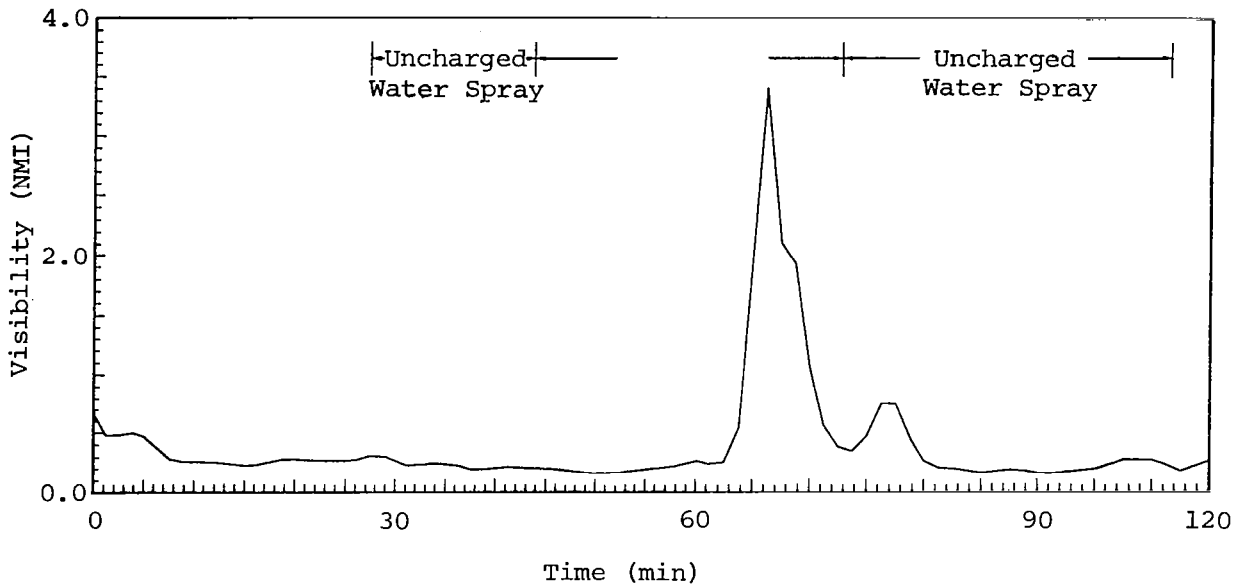
g) Visibility plot--test V-G(10).

Figure 2.8 (concluded).

November 18--Tests V-G(4) and V-G(5). Spray guns were operated
from 0400 to 0500 for V-G(4) and from 0530 to 0630 for V-G(5). Both the
south and north videograph plots showed poor visibility throughout both
test periods. Wind speed varied from 1 to 5 kts during V-G(4), dimin-
ished to calm except for a 20-minute period of 1 to 3 kts from 0550 to
0610 during V-G(5). The prevailing wind direction during test V-G(4)
was WNW (295 deg). This direction held during the first half of test
V-G(5) becoming WSW (240 deg) during the second half. It should be noted
that in both cases the wind was such as to carry the cleared fog patch
away from either of the videograph systems.

Temperature and relative humidity were constant at 74° F and 100
percent, respectively, throughout both test periods.

Sky conditions were partially obscured with stars intermittently
visible during test V-G(4), becoming totally obscure during test V-G(5).

November 23--Tests V-G(6) and V-G(7). Spraying began for test
V-G(6) at 0255 and was terminated at 0400. Visibility was recorded at
0.1 NMI as spraying began. A clearing pulse peaking at 0.4 NMI occurred

20

20 min after spraying began and a second pulse peaking at 0.7 NMI occurred 24 min later. Visibility stabilized at 0.1 to 0.2 NMI after the spraying was terminated.

Stars were visible though partially obscured throughout the test period.

For test V-G(7) the spray system was activated from 0445 to 0520. Uncharged water was used until 0500 and charged water was used the remainder of the time. Winds were calm with a slight southerly drift of the fog.

A visibility pulse having a peak of 1.8 NMI 10 min after uncharged spraying began, and a second pulse peaking at 1.2 NMI 1 min after charged spraying began occurred. A third major clearing trend began as the treatment was terminated, reaching a peak of 4.1 NMI 16 min after spraying ended. Visual observations reflected these trends.

November 24--Tests V-G(9) and V-G(10). For test V-G(9) the spray system was activated at 0245 and continued for one hour. Winds were calm to slight with direction W (270 deg) to N (360 deg) during periods of slight (less than 2 kts winds). Visibility remained at approximately 0.3 NMI during the first 48 min of treatment after which a significant clearing pulse peaking at 1.8 NMI occurred followed by a decline to nearer the original value as spraying was terminated.

As shown in the figure, both charged and uncharged spraying was utilized for test V-G(10). Winds during the test period remained uncharged from V-G(9), continuing calm to slight. Uncharged water spraying began at 0415, and at approximately 0430 charged spraying was initiated and continued for 35 min. Five minutes after charged spraying was initiated, a gradual increasing trend in visibility began. Nineteen minutes after the charged spraying began a sharp increase in visibility occurred peaking at 3.4 NMI 4 min later. An equally sharp decrease in visibility occurred as charging was terminated. During the final uncharged phase, visibility returned to its original value of approximately 0.2 NMI.

2.3 Reported Conclusions from the Field Tests

Of the ten fog dispersal field tests conducted in the Panama Canal Zone, the conclusions reproduced from Reference [2-7] were:

1. Visibility improvement occurred during the treatment or treatment lag period in six out of eight test cases.

2. The magnitude and persistence of visibility improvement, as well as the treatment lag time to achieve such improvement, varied widely from case to case causing inconsistent results.

3. Under the test conditions that existed, the spray system was incapable of sustaining a fog clearing once it was achieved. Several times visibility improvement occurred during the treatment, only to deteriorate while treatment was still in progress. This failure may have been due to too strong a wind flow thus prohibiting cumulative effects.

4. Variation in wind flow and/or low-level air turbulence may have caused test distortion on the day treatment effects failed to occur.

5. Applying statistical visibility treatments (as described in Reference [2-7]), it was concluded that clearing effects were achieved on three of the four test days and in six out of eight test cases.

Conclusions drawn from the same tests by Reference [2-4] may be summarized as follows.

1. The electric field and space-charge density were nonuniform in the field test.

2. The fog closed in after shutdown of the spray guns indicating that visibility improvements observed during spray gun operations were actually under persistent fog conditions.

3. The height to which the space charge was propelled by the spray guns was verified experimentally to be of 30.5 m (100 ft) minimum by the measurement of the space-charge density probe.

4. Instrumentation recorded fog clearings in general were obtained under favorable conditions of calm wind. Visual clearings were also observed under conditions of unfavorable wind speed. Based on theoretical analysis [2-4], a moving fog of the order of 0.3 NMI/hr would mask the clearing effect of a 4x4 spray gun array as utilized in the Panama Canal experiment.

Finally, Reference [2-4] concludes that although the effectiveness of a fog dispersal system had been demonstrated in the field and in the laboratory [2-5], its principal mechanism, either precipitation due to a space charge induced electric field or gravitational fallout due to enhanced electrical coalescence, needs more field data with regard to fog droplet size and liquid water content of treated and untreated fogs, and more elaborate instrumentation to measure the size of water droplets introduced by the spray guns. It should be noted that collecting precipitating fog droplets on hand-held gelatin-coated slides resulted in erratic data [2-7]. The droplet data gathered was thus inadequate to show changes in droplet size and distribution with time. The limited data, however, did show that while the median drop diameter did not increase greatly (5.1 μm), the upward shift in size distribution as indicated by a 20.6 percent increase in the 30 to 60 μm range and a 15.5 percent decrease in the 0 to 30 μm range tends to support droplet growth by coalescence.

Reference [2-4] recommends more detailed experimental investigation. In keeping with this it is recommended that a nozzle configuration be determined and a single unit built for testing. Preliminary results from such tests will provide quidance to larger scale tests. The remaining sections of this report describe the current analytical information and analyses techniques available to study the problem in hand. Section 3.0 describes information relative to the nozzle design and concludes with some of the simpler analyses of the nozzle jets carried out to date. Section 4.0 describes the necessary equations and analytical approach required to estimate analytically the interaction of the charged carriers issuing from the nozzle with the droplets distributed in the fog.

References

2-1. Carroz, J. W., P. St.-Amad, and D. R. Cruise. "The Use of Highly Charged Hygroscopic Drops for Fog Dispersal," Naval Weapons Center, China Lake, California, 1972.

2-2. Cochet, R. "Evolution d'une Gouttelette d'eau Chargee dans un Nuage on un Brouillard a Temperature Positive," ACAD (Paris) COMPT REND, Vol. 233, 1951, p. 190.

2-3. Moore, C. B., and B. Vonnegut. "Estimates of Raindrop Collection Efficiencies in Electrified Clouds," American Geophysics Union, Geophysical Monograph No. 5, 1960, pp. 291-304.

2-4. Chiang, T. K. "Field Evaluation of an Electrogasdynamic Fog Dispersal Concept," Part I, FAA-RD-73-33, February 1973.

2-5. Jiusto, J. E. "Laboratory Evaluation of an Electrogasdynamic Fog Dispersal Concept," FAA-RD-72-99, 1972.

2-6. Chiang, T. K., and M. C. Gourdine. "Electrogasdynamic Fog Dispersal Test and Evaluation for a Ground-Based System," Internal report for FAA by Gourdine Systems, Inc., Livingston, New Jersey, January 1973.

2-7. Wright, T., and R. Clark. "Field Evaluation of an Electrogasdynamic Fog Dispersal Concept," Part II, FAA-RD-73-33, February 1973.

3.0 NOZZLE CHARACTERISTICS

This section describes the fundamentals of the nozzle operation.
A discussion of the characteristics of the nozzle and the theory of
particle charging internally within the nozzle is described. The exten-
sive literature on electrostatic precipitation techniques available in
the environmental pollution literature is incorporated into the discus-
sion. A description of some of the preliminary and simplified analyses
reported in the literature on the jet characteristics and its interaction
with neighboring jets concludes Section 3.0.

3.1 Particle Charging in a Corona Discharge

The charged particle fog dispersal technique (CPFDT) requires a
high current source of unipolarity charged particles. This is currently
provided by passing a high-speed saturated airstream through a corona
discharge (see Figure 3.1) [3-1 through 3-6]. An understanding of the
operation of the CPFDT requires a detailed examination of the corona
discharge and the charge transfer that occurs in the corona discharge
region.

A corona discharge occurs in a high pressure gas when a high
voltage is applied between a small wire or other form of electrode with
a very small radius of curvature and a large grounded electrode which
surrounds the wire (Figure 3.2). A very high electric field occurs near
the wire which accelerates any free electrons which are present, causing
them to produce additional electrons upon impact with neighboring gas
molecules. This initiates an avalanche which produces large quantities
of electrons and positive ions near the wire. The highly mobile elec-
trons quickly move toward the grounded electrode and into a region of
smaller electric field where they can no longer generate additional
electrons. If electronegative molecules, such as O_2, CO_2, or H_2O are
present, then the electrons attach themselves to these molecules forming
stable ions. Because of their considerably smaller mobility, the ions

25
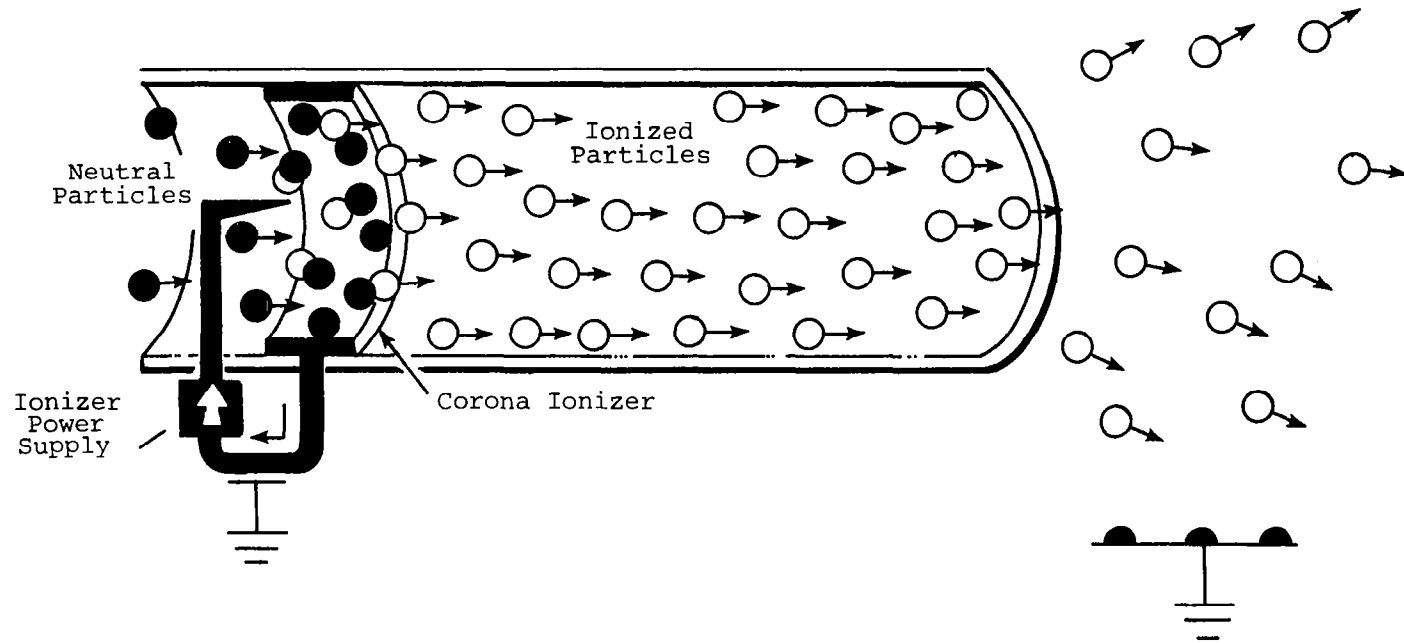
Figure 3.1 Operating principle of charged particle fog dispersal technique [3-7].

Droplet

Region
of Corona Glow

Free
electrons

Form Negative Ions

Electrons

Wire

Electrons

Positive Ions

Electrons and Ions Formed
in Region Close to
Wire Where E is Very Large

Gas Molecule
(Electronegative)

E smaller so more electrons
are not formed here. Electrons
attach themselves to electronegative
atoms (O_2, CO_2, H_2O) to form stable
ions which drift very slowly toward the
positive electrode.

Figure 3.2 Physics of corona discharge [3-9].

drift only slowly toward the grounded electrode and a stable space charge is formed in the region between the corona glow, which is close to the wire, and the surrounding electrode.

If particles, such as water droplets, are passed through the space charge, then it is possible for them to pick up charges from the ions. The process of charging a water droplet is complicated, but it is common practice to simplify the analysis of the general process and distinguish two main processes, namely, field charging and diffusion charging [3-8, 3-9, 3-10]. Field charging accurately describes the charging of particles having a radius greater than 0.5 μm while diffusion charging is an approximate description of the charging of particles having a radius less than 0.2 μm [3-8]. The charging of intermediate-sized particles must be described by the combination of both types of charging [3-9]. In the following discussion, it is assumed that the particles are spherical.

3.1.1 Field Charging

First, consider the field charging process. Let E_o be the mean electric field in the space charge region (10^5 to 10^6 V/m). The electric potential and flux lines surrounding an uncharged spherical particle which is placed in this field are shown in Figure 3.3. If an ion is brought in the neighborhood of the particle as a result of its motion in the electric field, then an induced dipole is generated in the particle and the ion is attracted to the particle (Figure 3.4). This process continues (Figure 3.5) until a saturation charge is acquired on the particle and all other charges are repelled (Figure 3.6). The particle acquires charge according to the relation [3-8] (mks units are used throughout the following sections)

$$\frac{n}{n_s} = \frac{t}{t + t_o} \tag{3-1}$$

where n_s is the saturation number of charges

$$n_s = K \frac{4\pi\varepsilon_o E_o a^2}{e} \tag{3-2}$$

28
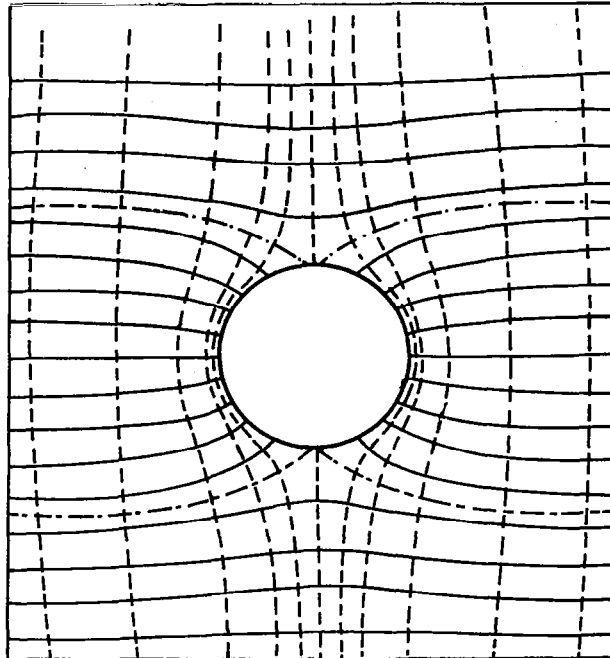
Figure 3.3 Potential and flux lines around an uncharged spherical particle [3-9, 3-14].
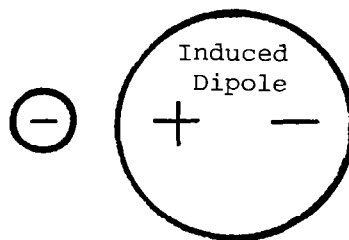
Figure 3.4 Dipole induced in spherical particle due to presence of nearby charged particle [3-9].
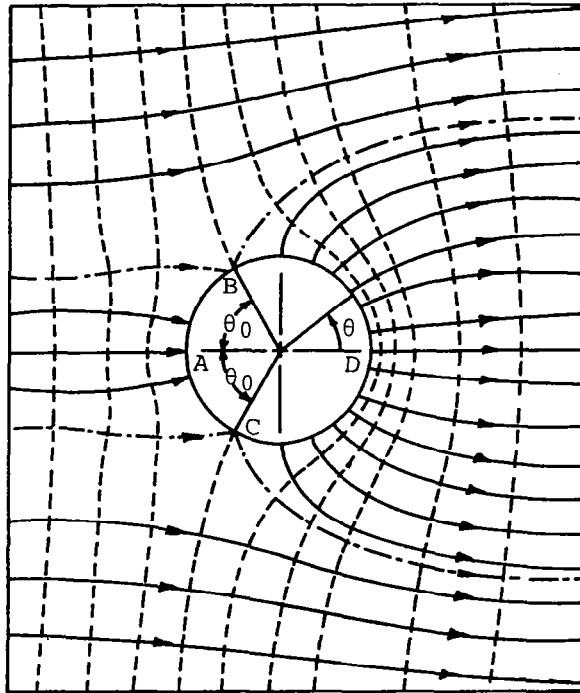
Figure 3.5   Potential and field lines around a partially charged
spherical particle [3-14].
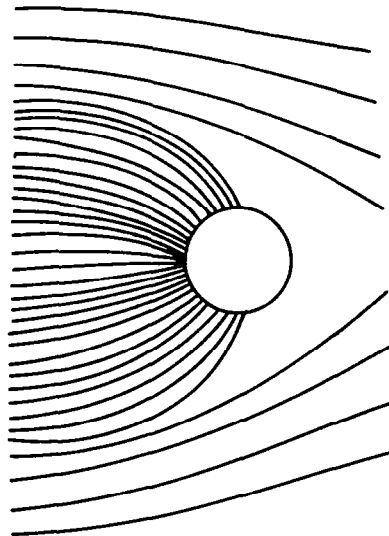
Figure 3.6   Field lines around a fully charged spherical particle [3-9].

$$K = \begin{cases} 3; & \text{conducting particle} \\ \dfrac{3\kappa_e}{\kappa_e + 2}; & \text{dielectric particle} \end{cases} \qquad (3\text{-}2)$$

and

$$t_o = \frac{4\varepsilon_o}{N_i\, e\, Z_i} \qquad (3\text{-}3)$$

Ion mobilities, Z_i, are of the order of 10^{-4} m^2/Vs (see Figure 3.14, page 50, and Table 3.9, page 52) and the ion number density in the space charge, N_i, is of the order of 10^{15} m^{-3}. For water $K = 2.93$, but it will be assumed to be equal to 3.0, for convenience, in the following equations.

Using the numerical values for the physical constants, Equations 3-2 and 3-3 can be written as

$$n_s = 2.08 \times 10^9\, a^2\, E_o \qquad \text{(charges)} \qquad (3\text{-}4)$$

$$t_o = \frac{2.21 \times 10^8}{N_i\, Z_i} \qquad \text{(s)} \qquad (3\text{-}5)$$

Calculated values are given in Tables 3.1 and 3.2. The electric field at the surface of a spherical particle is given by

$$E_s = \frac{ne}{4\pi\varepsilon_o a^2} \qquad (3\text{-}6)$$

$$E_s = \frac{1.44 \times 10^{-9}\, n}{a^2} \qquad \text{(V/m)}$$

Note that if the particle has a saturation charge, then (see Table 3.2)

$$E_s = KE_o \simeq 3E_o \qquad \text{(V/m)} \qquad (3\text{-}7)$$

The charge is built up relatively slow and after $9t_o$ has only reached 90 percent of the saturation charge (Figure 3.7). Thus, a particle will have to remain in the space charge for a relatively long time to be able to acquire maximum charge.

31

Table 3.1 Time Constant for Field Charging with a Mobility of $Z_i = 10^{-4}$ m^2/Vs.

N_i (#/m^3)	t_o (s)
10^{13}	2.21×10^{-1}
10^{14}	2.21×10^{-2}
10^{15}	2.21×10^{-3}
10^{16}	2.21×10^{-4}
10^{17}	2.21×10^{-5}

Table 3.2 Saturation Charge and Surface Field for Field Charging.

E_o (V/m)	a (m)	n_s (charges)	E_s (V/m)
10^5	5×10^{-7}	52	3.0×10^5
	10^{-6}	208	3.0×10^5
	10^{-5}	2.08×10^3	3.0×10^5
10^6	5×10^{-7}	520	3.0×10^6
	10^{-6}	2.08×10^3	3.0×10^6
	10^{-5}	2.08×10^5	3.0×10^6
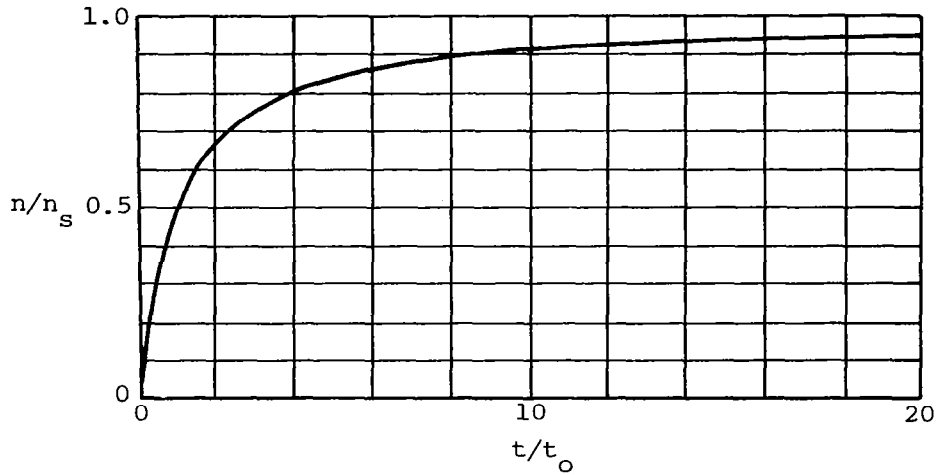
Figure 3.7 Charge buildup for a field charged particle [3-9].

If the particles stay in the corona space charge region long enough to acquire the saturation charge, then the maximum current that can leave the nozzle is related to the nozzle particle mass flow rate. The charge to mass ratio for particles of density, ρ, is given by

$$\frac{q}{m} = \frac{9\epsilon_o E_o}{a\rho}\left(\frac{t}{t + t_o}\right) \qquad (3\text{-}8)$$

For water

$$\frac{q}{m} = 7.97 \times 10^{-14} \frac{E_o}{a}\left(\frac{t}{t + t_o}\right) \qquad (c/kg)$$

Written in terms of the particle surface field

$$\frac{q}{m} = \frac{3\epsilon_o E_s}{a\rho} \qquad (3\text{-}9)$$

and for water

$$\frac{q}{m} = 2.66 \times 10^{-14} \frac{E_s}{a} \qquad (c/kg) \qquad (3\text{-}10)$$

The surface field cannot be greater than 3×10^6 V/m to prevent a corona discharge [3-3, 3-10]. Therefore, the charge to mass ratio has a maximum for a given particle size which increases with decreasing particle size

33

(Figure 3.8). Values of q/m for t much greater than t_o are given in Table 3.3. Note that Equation 3-10 is valid for all size water droplets.

The particle can acquire charge until the electrical stresses are greater than the surface stresses. If that occurs, then the particle becomes unstable and loses mass and charge due to the Rayleigh instability. Instability occurs if

$$E_s^2 > \frac{4\sigma}{\varepsilon_o a} \qquad (V^2/m^2) \qquad\qquad (3-11)$$

or, for water at 20° C,
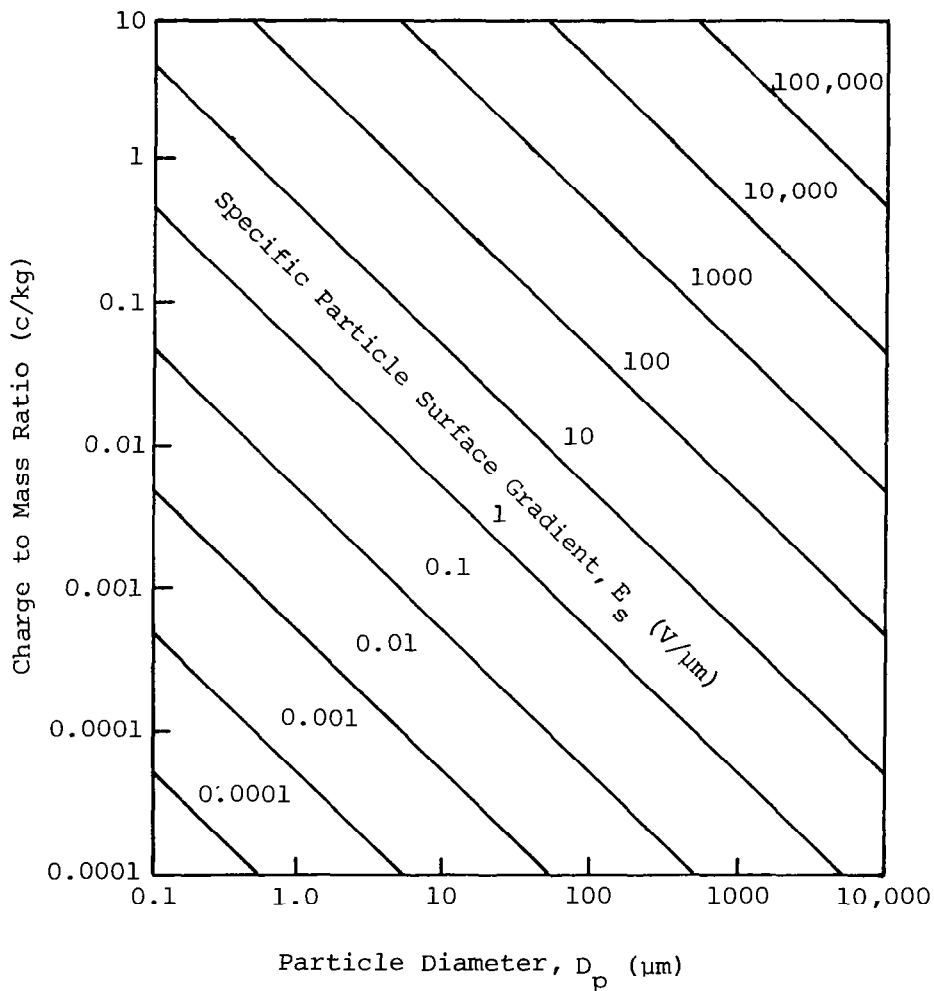
Figure 3.8 Charge to mass ratio for spherical particles in air [3-10].

34

Table 3.3 Charge to Mass Ratio for Field Charging.

E_o (V/m)	a (m)	q/m (c/kg)
10^5	5×10^{-8}	0.159
	10^{-7}	7.97×10^{-2}
	5×10^{-7}	1.59×10^{-2}
	10^{-6}	7.97×10^{-3}
	10^{-5}	7.97×10^{-4}
10^6	5×10^{-8}	1.59
	10^{-7}	0.797
	5×10^{-7}	1.59×10^{-1}
	10^{-6}	7.97×10^{-2}
	10^{-5}	7.97×10^{-3}

$$E_s > \frac{1.81 \times 10^5}{a^{1/2}} \qquad \text{(V/m)} \qquad (3\text{-}12)$$

E_s will be equal to the maximum value 3×10^6 V/m for a particle of radius 3.6×10^{-3} m. This is much larger than any particles used in the CPFDT and so the Rayleigh instability is not a limitation to the maximum particle charge.

3.1.2 Diffusion Charging

Small particles (radius $\leqslant 0.2$ μm) collide with ions that are brought in contact with them as a result of thermal diffusion. This process was first examined by Arendt and Kallman [3-11] and simplified by White [3-8]. The White expression for the number of charges acquired by a particle as a function of time is given by

$$n = \frac{4\pi\varepsilon_o akT}{e^2} \ln\left(1 + \frac{a\bar{v}N_i e^2}{4\varepsilon_o kT} t\right) \qquad \text{(charges)} \qquad (3\text{-}13)$$

35

Assuming nitrogen ions at 300° K, this expression can be written as

$$n = 1.795 \times 10^7 \ a \ \ell n(1 + 7.37 \times 10^{-5} \ N_i at) \quad \text{(charges)} \quad (3\text{-}14)$$

This expression is plotted in Figure 3.9.

Several differences should be noted between the two types of charging processes. First, the diffusion charging expression is independent of the electric field in the corona space charge, but this must be considered to be an approximation, albeit an accurate one, for the smaller particles. Second, a saturation charge does not exist for diffusion charging. However, the particle can never acquire a charge greater than that required to produce a breakdown field at the particle surface (3×10^6 V/m). The time to reach the breakdown surface field is given in Table 3.4. If the particles have acquired enough charge to achieve a breakdown surface field of 3×10^6 V/m, then the number of charges on the particle is given by (Equation 3-6)

$$n = \frac{4\pi\epsilon_o}{e} \ a^2 E_s$$

$$n = 2.08 \times 10^{15} \ a^2 \quad \text{(charges)} \quad (3\text{-}15)$$

In the previously used nozzles (see Section 3.2) which had only a single corona region through which the water droplets rapidly proceeded, the particles were not in the corona region long enough to acquire either the saturation charge for the field charged particles or to approach the breakdown field for the diffusion charged particles. Therefore, more charge could be emitted by passing the particles through an extended corona region or multiple corona regions. Also, it is apparent that smaller droplets can carry a relatively greater amount of charge since the maximum possible charge to mass ratio (at breakdown field, for example) increases as the droplet diameter decreases. Mobility considerations, to be discussed later, indicate that there is probably an optimum range of droplets sizes which will deliver the maximum charge to the greatest heights in the fog.
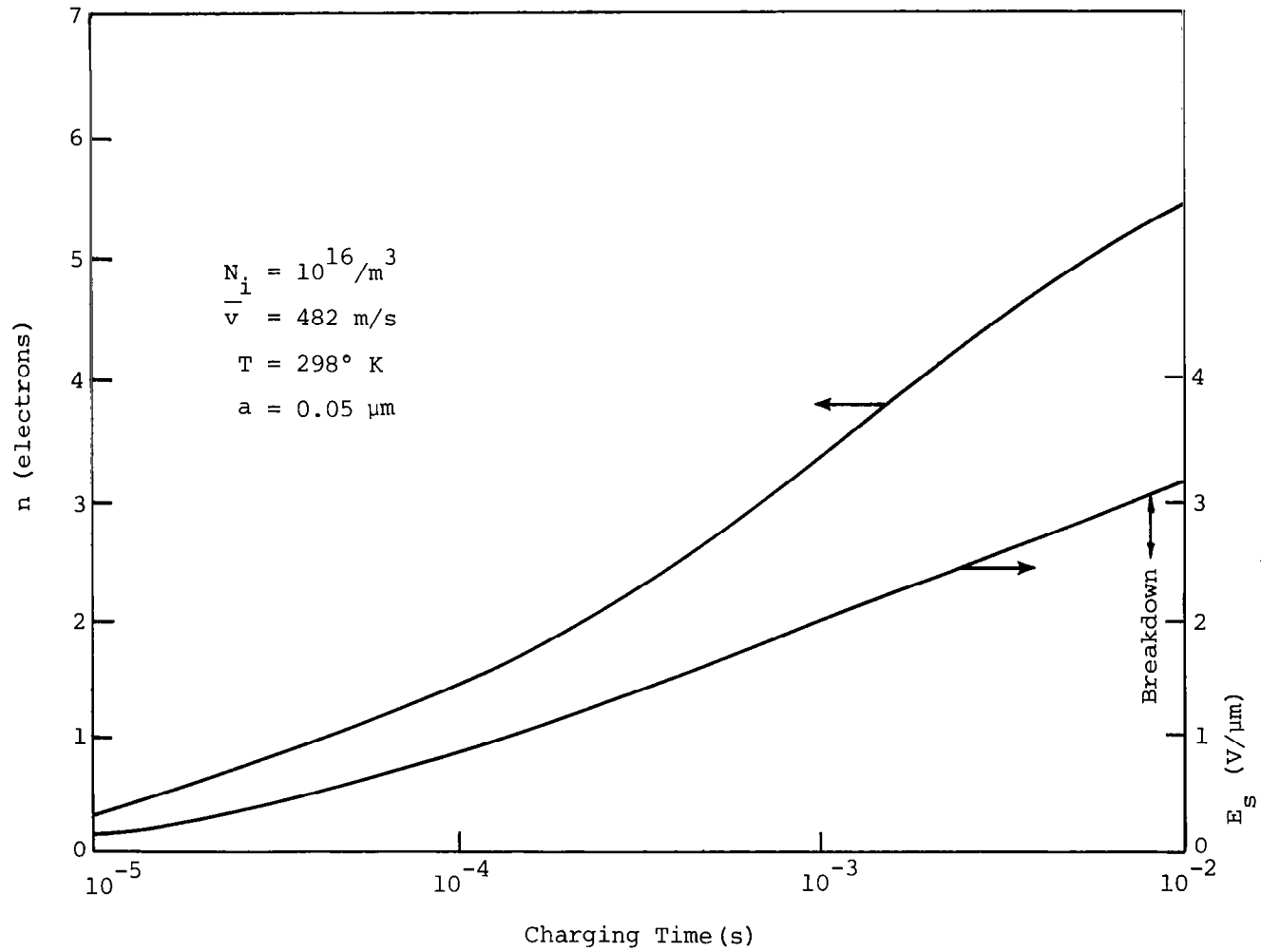
Figure 3.9 Diffusion charging according to White's equation [3-8].

Table 3.4 Time to Reach Breakdown Surface Field ($N_i = 10^{16}/m^{-3}$).

a (m)	t (s)
10^{-8}	2.97×10^{-4}
5×10^{-8}	8.90×10^{-3}
7×10^{-8}	6.51×10^{-2}
10^{-7}	1.48
2×10^{-7}	8.07×10^{4}

3.1.3 Charged Particle Mobility

For a system of moving charged particles in an electric field, $\vec{E}$, the current density, $\vec{J}$, is related to the field through the conductivity of the media. In the present case, this relationship can be written as

$$\vec{J} = \rho_e Z \vec{E} = \rho_e \vec{v} \tag{3-16}$$

where Z is called the mobility of the charged particle of charge density, ρ_e, and $\vec{v}$ is the drift velocity of the particle in the field or the velocity relative to the fluid. The mobility can be calculated once the drift velocity is known. Consider a spherical particle of charge, q, initially at rest in a field, E. The field will accelerate the particle in the field direction and its motion will be resisted by the fluid dynamic drag. Assume that the particles are small enough so that the Stokes' drag law is valid. This assumption will be examined later. Then, the particle acceleration is described by the following equations, assuming a negatively charged particle.

$F_D = 6\pi\mu av$ ⟵ ⟶ $F_E = qE$

⟵ E

38
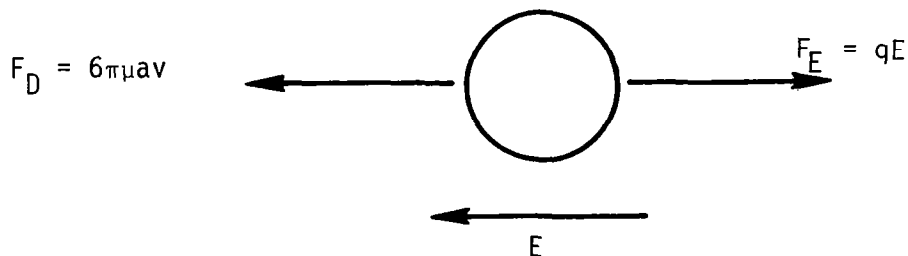
$$m \frac{dv}{dt} = qE - 6\pi\mu av$$

$$v = \frac{qE}{6\pi\mu a}\left(1 - e^{-t/\tau}\right) = v^*\left(1 - e^{-t/\tau}\right) \tag{3-17}$$

$$v^* = \frac{qE}{6\pi\mu a} = \frac{neE}{6\pi\mu a} \tag{3-18}$$

$$\tau = \frac{m}{6\pi\mu a} \tag{3-19}$$

The charged particle is accelerated to its terminal velocity, v^*, in about 5τ. For air at $20°$ C, the terminal velocity is given by

$$v^* = 4.63 \times 10^{16} \frac{nE}{a} \quad (m/s) \tag{3-20}$$

where E is the electric field surrounding the particle which has n charges. Once the particle leaves the nozzle, the field is created by the charge density itself. If the jet is modeled as a cylindrical region of constant radius equal to the jet exit radius, R_j, and having a uniform charge density, then the field created by the charges alone at the edge of the jet is $E = R_j \rho_e / 2\varepsilon_o$ and at the edge of the jet

$$v^* = 2.61 \times 10^5 \frac{R_j \rho_e n}{a} \tag{3-21}$$

This value of v^* is useful for understanding the electrostatic spreading rate of the jet. To obtain a numerical value for v^*, Equation 3-1 or 3-13 must be used for the number of charges on the particle. First, assume the particles are field charged and have achieved the saturation charge. This assumption will yield the maximum v^*. Then, if K = 3.0,

$$v^* = 5.45 \times 10^4 E_o a R_j \rho_e \tag{3-22}$$

Note that this same equation holds for diffusion charged particles which have acquired the breakdown field at their surface. It is necessary to keep in mind that E_o is the mean electric field in the corona region where the particles were charged while the accelerating field in the jet is created by ρ_e.

To be able to use this expression, it is necessary to have an estimate of ρ_e. Applying a one-dimensional control-volume analysis to the jet and assuming that ρ_e and u_j are uniform over the nozzle exit, then the current leaving the jet is given by

$$I_j = \int \vec{J} \cdot \hat{n} dA = \int \rho_e \vec{u}_j \cdot \hat{n} dA = R_j^2 \rho_e u_j \quad \text{(c/s)} \tag{3-23}$$

Values of I_j and u_j as measured by Gourdine [3-2] are given in Table 3.5. Equation 3-23 was used to calculate the ρ_e values given in the table. Using the maximum ρ_e (for the small nozzle), values of v* were calculated and are given in Table 3.6. Gourdine estimated that the particle radius in his nozzle was about 10^{-7} m.

Table 3.5   Characteristics of Nozzles Used by Gourdine [3-2].

	Large	Medium	Small
Radius, R_j (m)	3.12×10^{-3}	1.56×10^{-3}	1.0×10^{-3}
Current (A) ($E_r(0) = 10^6$ V/m)	160×10^{-6}	80×10^{-6}	51.3×10^{-6}
q/m (c/kg)	0.125	0.25	0.392
Z (m^2/Vs)	6×10^{-8}	1.2×10^{-7}	1.9×10^{-7}
u_j (m/s)	415	415	415
v_j (m^3/s)*	1.27×10^{-2}	3.17×10^{-3}	1.3×10^{-3}
ρ_e (c/m^3)*	1.26×10^{-2}	2.52×10^{-2}	3.95×10^{-2}

*Calculated values.

Next, consider the terminal velocity for diffusion charged particles. Rather than using Equation 3-13 for n, it is more meaningful to assume that the particle has built-up charge so that the particle surface field equals the breakdown field, i.e., $E_s = 3E_0 = 3 \times 10^6$ V/m and then from Equation 3-6

$$ne = 4\pi\varepsilon_0 a^2 E_s = 3.34 \times 10^{-4} a^2 \quad \text{(c)} \tag{3-24}$$

40

Table 3.6 Terminal Velocity for Particles in Small Jet.

E_0 (V/m)	a (m)	v* (m/s)	Re
10^5	5×10^{-7}	1.1×10^{-2}	1.0×10^{-3}
	10^{-6}	2.2×10^{-2}	2.9×10^{-3}
	10^{-5}	2.2×10^{-1}	2.9×10^{-1}
10^6	5×10^{-7}	1.1×10^{-1}	1.0×10^{-2}
	10^{-6}	2.2×10^{-1}	2.9×10^{-2}
	10^{-5}	2.2	2.9

Then the maximum terminal velocity at the edge of a cylindrical region of uniform charge density is

$$v^* = 5.45 \times 10^{10} \, R_j \rho_e a \qquad (m/s) \qquad (3\text{-}25)$$

This expression gives a value for $v^* = 0.214$ m/s for the large jet of Gourdine [3-2].

For spherical water droplets moving in air, the acceleration time constant, τ, is given by

$$\tau = 1.21 \times 10^7 a^2 \qquad (s) \qquad (3\text{-}26)$$

Values are given in Table 3.7. Under most circumstances the acceleration time constant is much smaller than the characteristic charging times (see Table 3.1, page 32, and Table 3.4, page 38) and, therefore, the particles can be assumed to be always moving at their terminal velocity corresponding to the charge which they carry at the time. Then from Equations 3-16 and 3-18 the mobility is defined as

$$Z = \frac{q}{6\pi\mu a} = \frac{ne}{6\pi\mu a} \qquad (3\text{-}27)$$

For a field charged particle

Table 3.7 Acceleration Time Constant for Water Droplets in Air.

a (m)	τ (s)
10^{-8}	1.21×10^{-9}
10^{-7}	1.21×10^{-7}
10^{-6}	1.21×10^{-5}
10^{-5}	1.21×10^{-3}

$$Z = \frac{2\varepsilon_o K E_o a}{3\mu}\left(\frac{t}{t + t_o}\right) \tag{3-28}$$

$$Z = 9.65 \times 10^{-7} E_o a \left(\frac{t}{t + t_o}\right) \quad (m^2/Vs)$$

and for a diffusion charged particle

$$Z = \frac{2\varepsilon_o kT}{3\mu e} \ell n\left(1 + \frac{e^2 \bar{v} N_i a}{4\varepsilon_o kT} t_m\right) \tag{3-29}$$

$$Z = 8.31 \times 10^{-9} \ell n[1 + 7.37 \times 10^{-5} N_i a t_m] \quad (m^2/Vs)$$

where t_m is the length of time the particle remained in the corona space charge. If t_m was long enough so that the particle has acquired the breakdown field at its surface, then Equation 3-29 can be replaced by

$$Z_{max} = \frac{2\varepsilon_o E_s a}{3\mu} , \quad E_s = 3 \times 10^6 \text{ V/m} \tag{3-30}$$

$$Z_{max} = 0.965a \quad (m^2/Vs)$$

Note that Ruhnke [3-3] incorrectly gave the expression $Z = 10a$, and this accounts for the order of magnitude difference between the mobility estimates of Ruhnke and those of Gourdine [3-2].

Values of the mobility determined from Equation 3-28 for field charge particles are shown in Figure 3.10 for $t \gg t_o$ and for diffusion charged particles according to Equation 3-29 are shown in Figure 3.11.

42
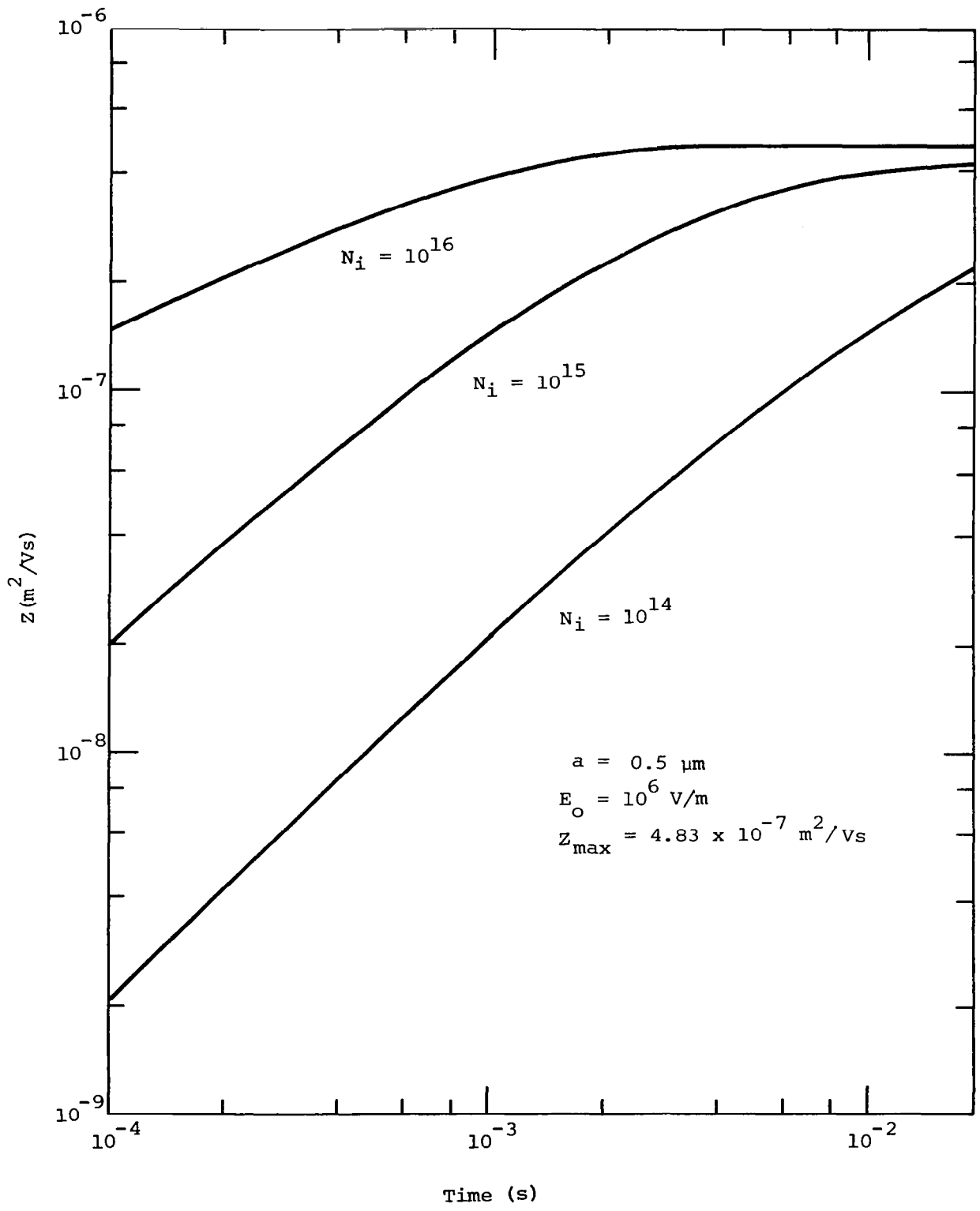
Figure 3.10   Mobility of field charged particles as a function of time
spent in a corona discharge.

43
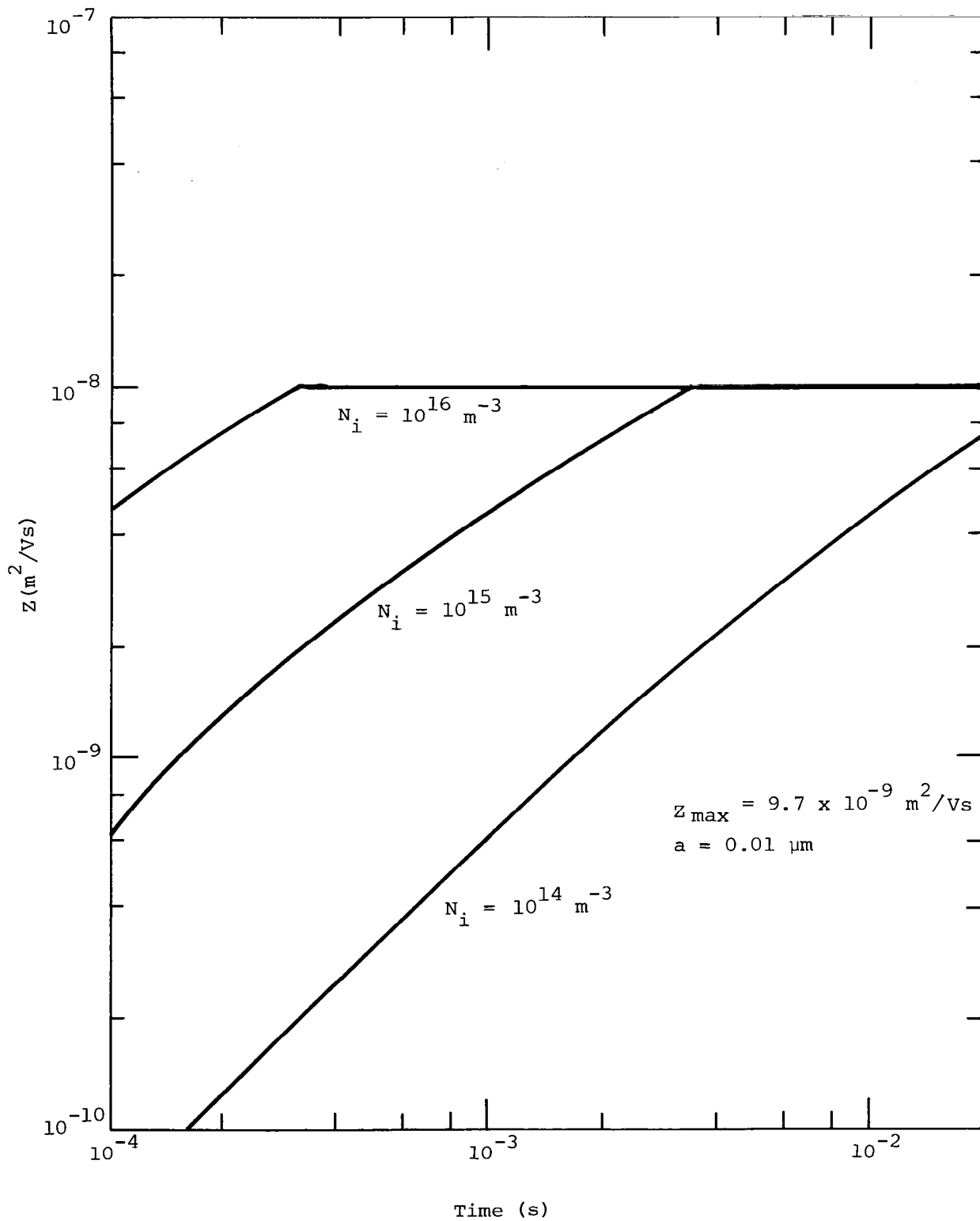
a) $a = 0.01$ μm.

Figure 3.11   Mobility of diffusion charged particles as a function of time spent in corona discharge.

The figure shows a log-log plot with axis $Z(m^2/Vs)$ versus Time (s). Three curves are labeled:

$N_i = 10^{16}$ m^{-3}

$N_i = 10^{15}$ m^{-3}

$N_i = 10^{14}$ m^{-3}

$a = 0.05$ μm

$Z_{max} = 4.8 \times 10^{-8}$ m^2/ Vs

Time (s)

b) a = 0.05 μm.
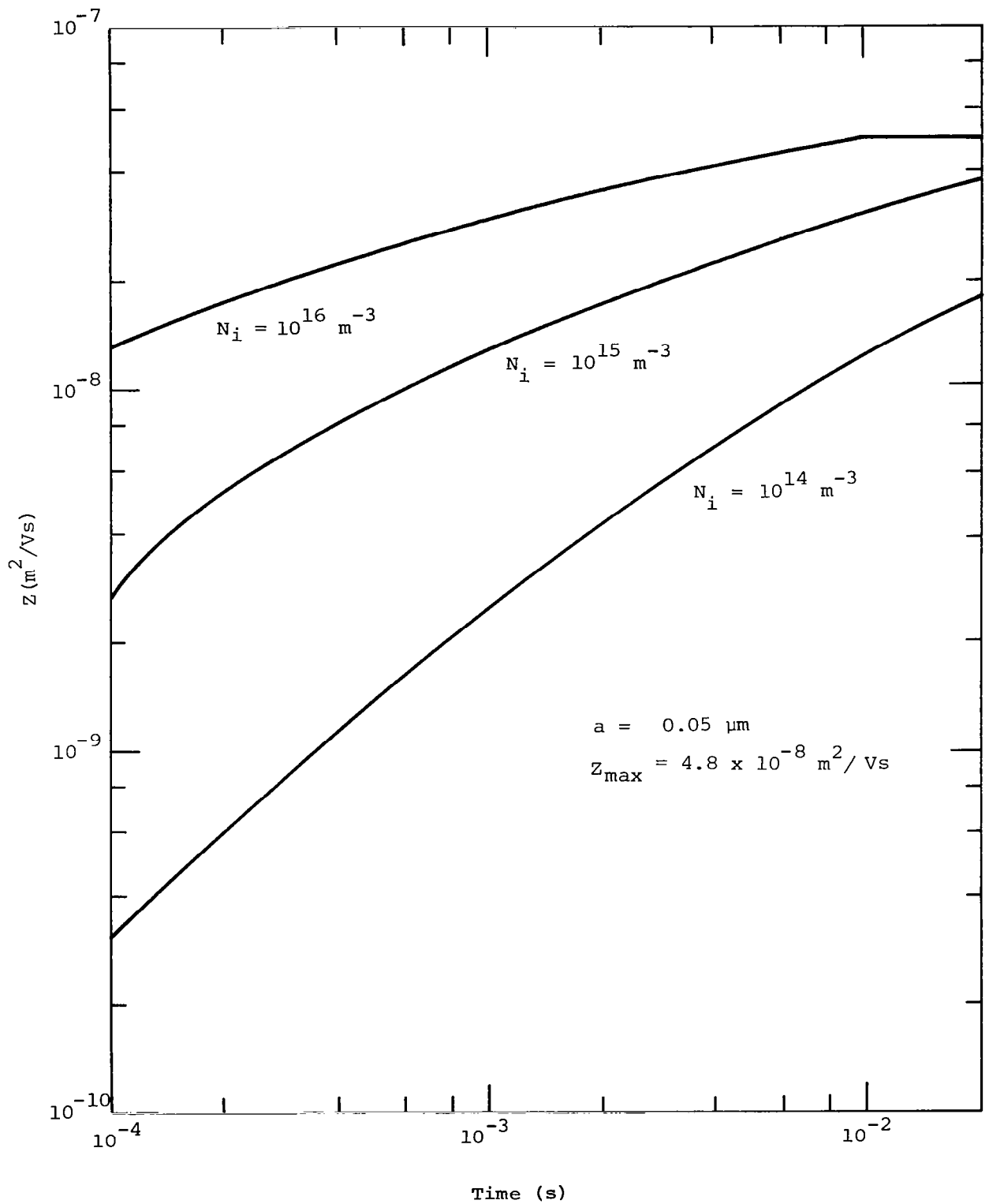
Figure 3.11 (continued).

c) a = 0.1 μm.
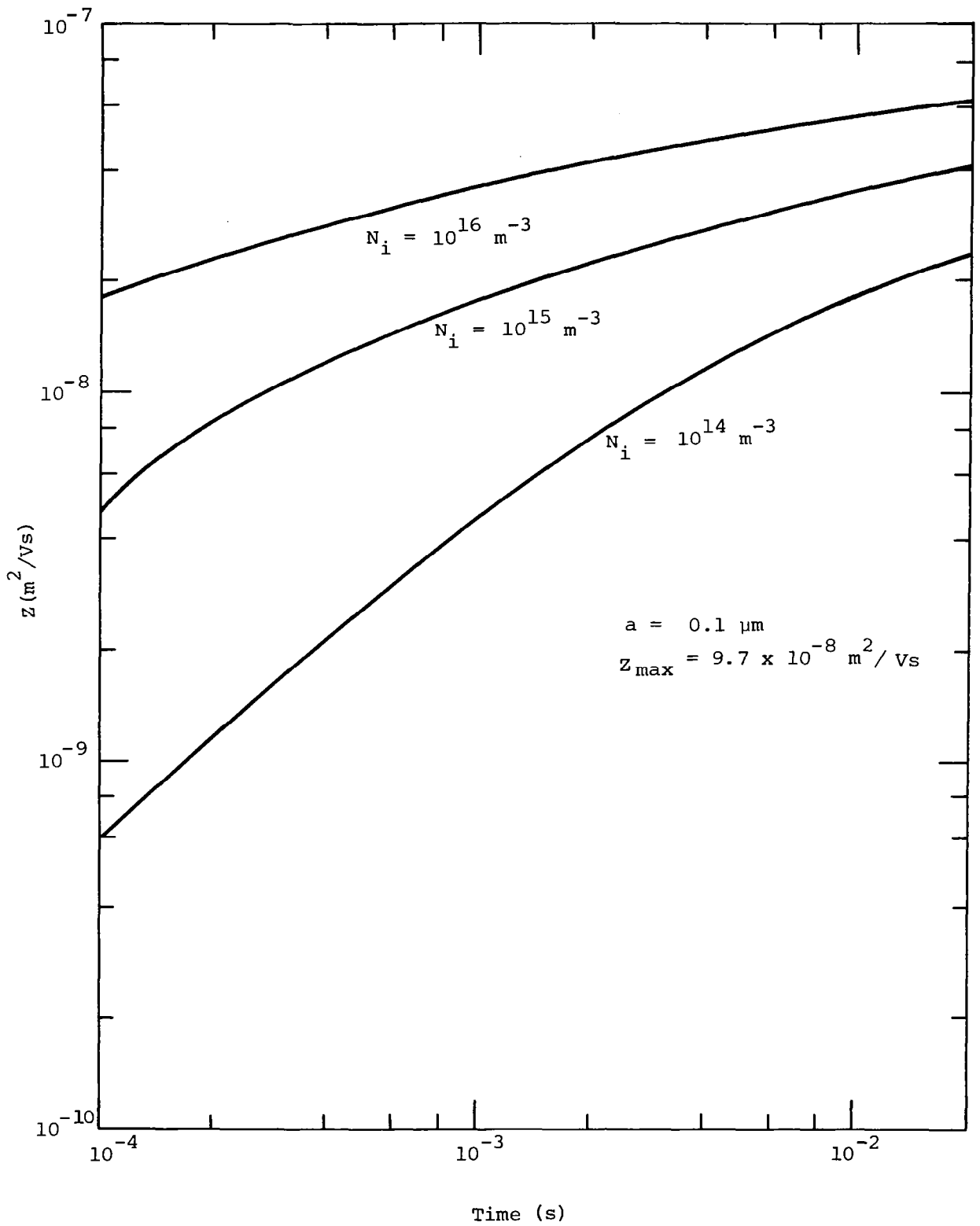
Figure 3.11 (continued).

In all cases the mobility increases as the length of time that the particle remains in the corona region increases. The particles eventually can reach the breakdown field at their surface and reach Z_{max} given by Equation 3-30. For most particles this is not expected to occur with the previously used nozzles because the particles probably do not spend longer than 10^{-4} seconds in the corona (see Section 3.2). The mobility for various particle sizes at a fixed charging time is shown in Figure 3.12.

From this analysis it appears that it is desirable to design a nozzle system that produces the smallest possible droplets, because the charge to mass ratio increases for decreasing size. It would also be desirable to keep the particles in the corona region long enough for them to acquire the maximum possible charge and to design the corona discharge with the maximum ion density. This would probably require a modification of the previously used nozzles. Also, for a given electric field the smaller the particle the smaller the mobility (see Equations 3-28 and 3-29) so that the particle should be able to proceed further into the fog. However, an analysis of the turbulent jet, including the effects of turbulent diffusion, will probably indicate that diffusive effects will be too great for the smallest particles and thus an optimum size will exist. This analysis remains to be performed.

It should be noted that the particle mobilities are much smaller than electron or ion mobilities. The mobilities of electrons in gases are of the order of 0.4 m^2/Vs (Figure 3.13) and about 10^{-4} m^2/Vs for ions (Figure 3.14 and Table 3.8). It is for this reason that the particles can leave the corona region and proceed to great distances in the jet before the electric field effects disperse them.

The equation for the mobility of the water droplet, Equation 3-27, was derived assuming that the Stokes' drag law was valid. However, that is true only if the Reynolds number based on the sphere diameter is much less than one. Assuming air, the droplet Reynolds number based on the particle diameter is

$$Re = \frac{2\rho_a v_r a}{\mu} = 1.32 \times 10^5 v_r a \tag{3-31}$$
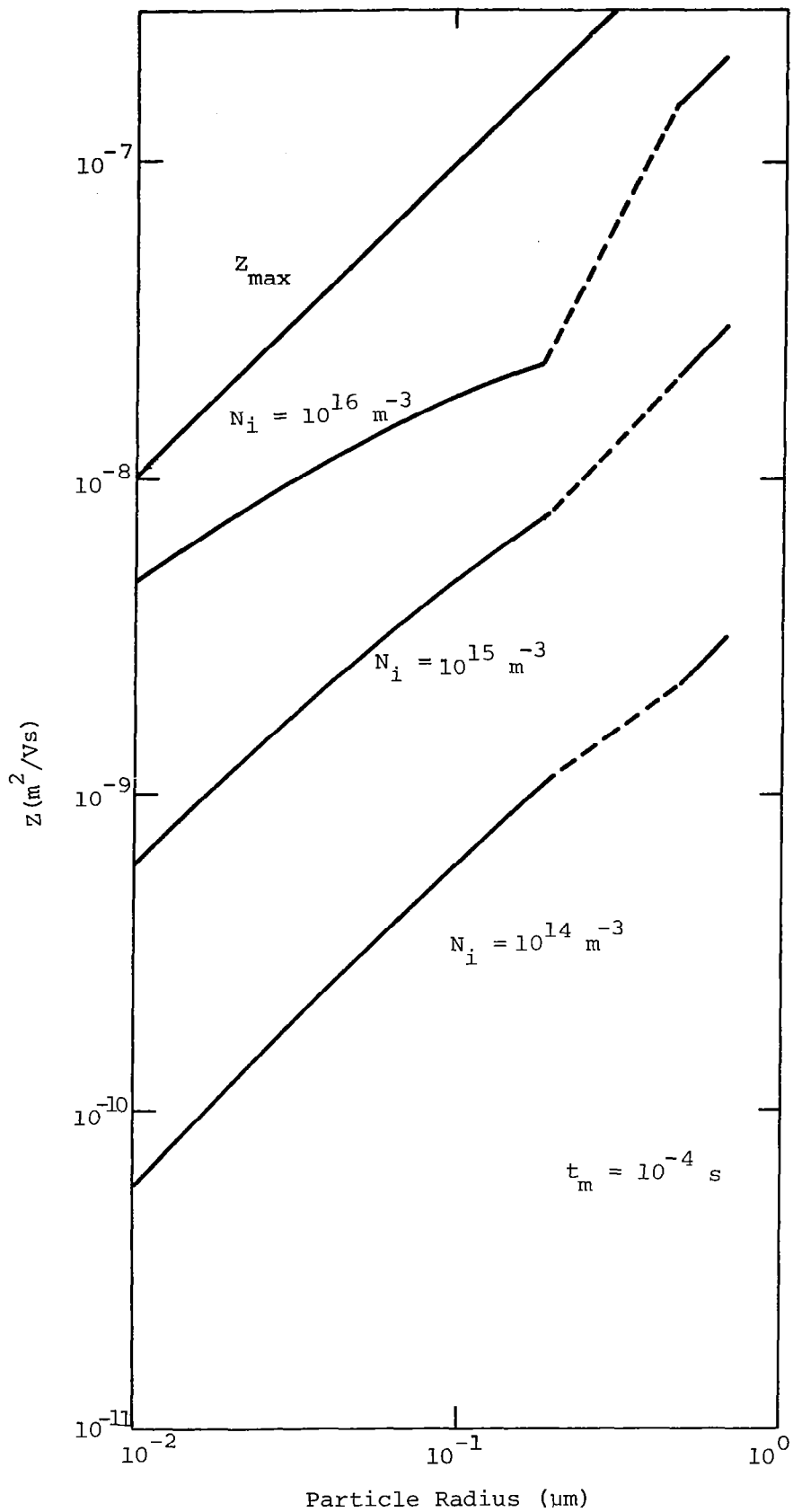
Figure 3.12 Mobility for fixed charging time.
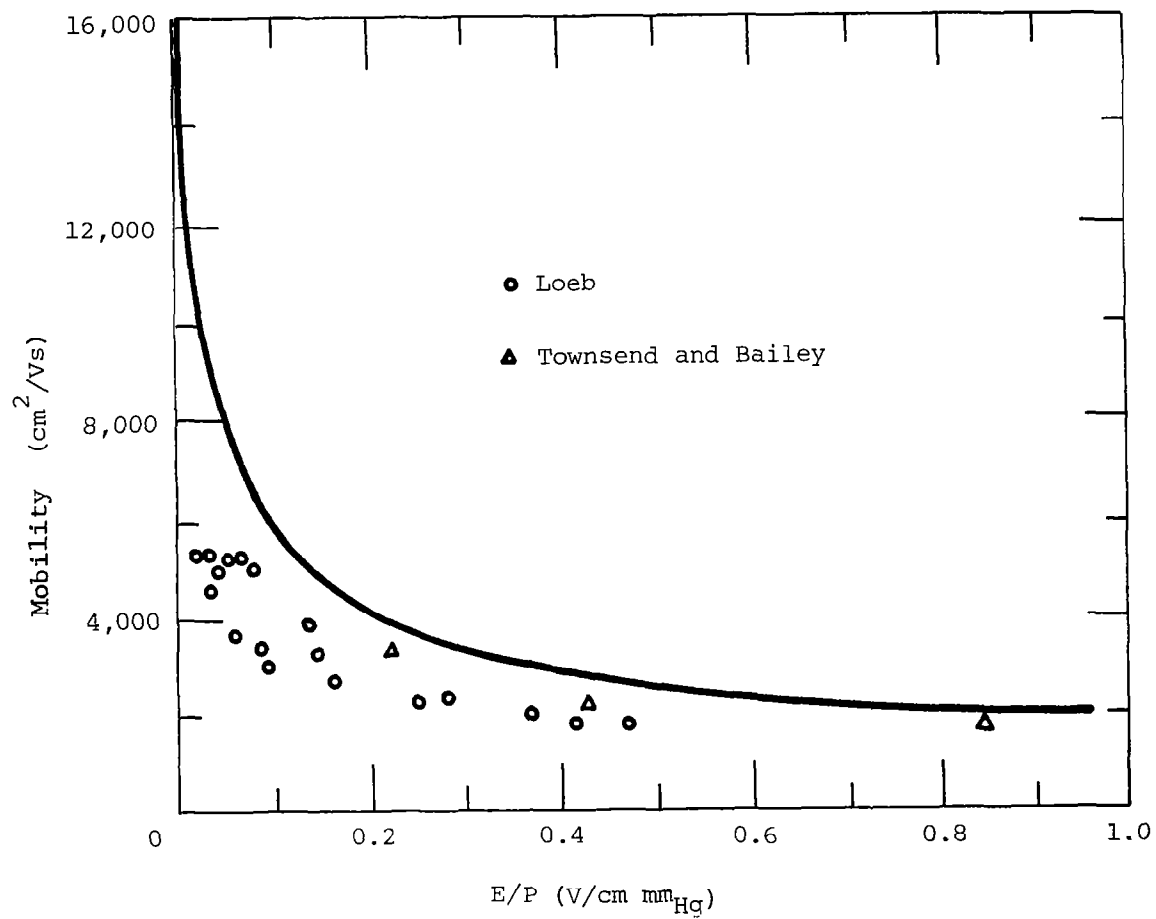
Figure 3.13 Electron mobility in hydrogen [3-15].
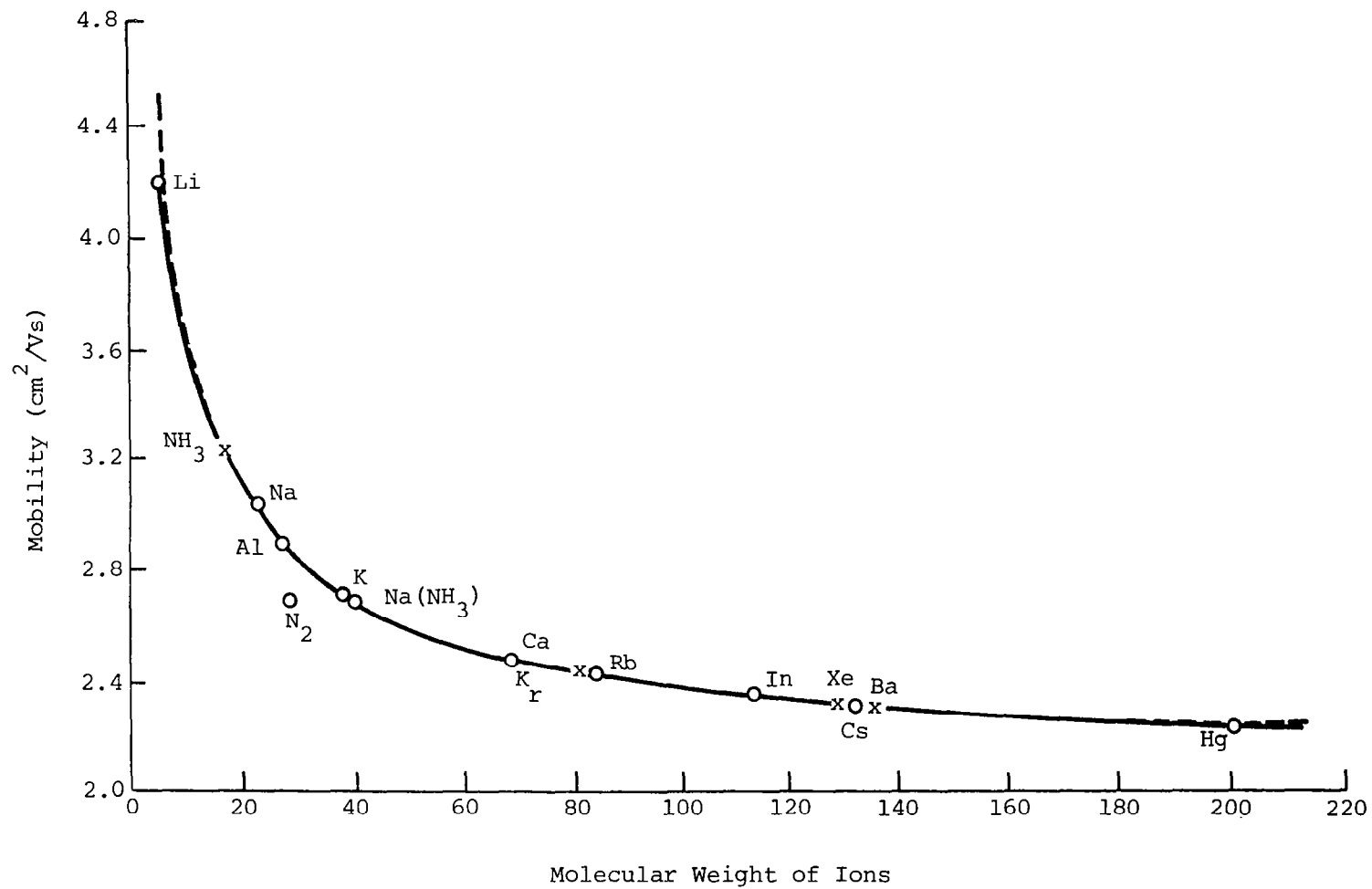
Figure 3.14 Mobility of positive ions in nitrogen (K in cm^2/Vs) [3-15].

Table 3.8 Mobility of Singly Charged Gaseous Ions at 0° C and 760 mm Hg [3-15].

| Gas | cm^2/Vs | |
	Z^-	Z^+
Air (dry)	2.10	1.36
Air very pure	2.50	1.80
A	1.70	1.37
A very pure	206.00	1.31
Cl_2	0.74	0.74
CCl_4	0.31	0.30
C_2H_2	0.83	0.78
C_2H_5Cl	0.38	0.36
C_2H_5OH	0.37	0.36
CO	1.14	1.10
CO_2 dry	0.98	0.84
H_2	8.15	5.90
H_2 very pure	7,900.00	----
HCl	0.62	0.53
H_2O at 100° C	0.95	1.10
H_2S	0.56	0.62
He	6.30	5.09
He very pure	500.00	5.09
N_2	1.84	1.27
N_2 very pure	145.00	1.28
NH_3	0.66	0.56
N_2O	0.90	0.82
Ne	----	9.90
O_2	1.80	1.31
SO_2	0.41	0.41

Z^- = mobility of negative ion.

Z^+ = mobility of positive ion.

where v_r is the particle speed relative to the airspeed. Typical Reynolds numbers are given in Table 3.6, page 41, assuming that the particles are moving with v^* through still air. For the sizes of particles most likely to occur in the jets (less than 1 μm) the Reynolds numbers are sufficiently small so that the Stokes' drag law is valid. However, the particle diameters are so small that rarefraction effects become important. The first rarefaction effect manifests itself as slip over the surface. This results in a decrease in the drag compared to the Stokes' drag. It is usual to apply the Cunningham correction factor [3-14] to the continuum results previously given. The correction factor is given in terms of the Knudsen number, which is defined as

$$Kn = \lambda/a = 6.67 \times 10^{-8}/a \tag{3-32}$$

where λ is the mean free path length in air at standard conditions. The Cunningham correction factor is

$$C = 1 + Kn(1.257 + 0.400 \, e^{-1.10/Kn}) \tag{3-33}$$

Values are given in Table 3.9 and Figure 3.15. The previous results must be corrected as follows. The particle drag is given by

$$F_D = 6\pi\mu a v/C \tag{3-34}$$

the terminal velocity becomes (see Equation 3-18)

Table 3.9 Knudsen Number and Cunningham Correction Factor.

a (m)	Kn = λ/a	C
10^{-8}	6.600	11.650
5×10^{-8}	3.300	2.911
10^{-7}	0.660	1.890
2×10^{-7}	0.330	1.424
5×10^{-7}	0.170	1.168
10^{-6}	0.066	1.084
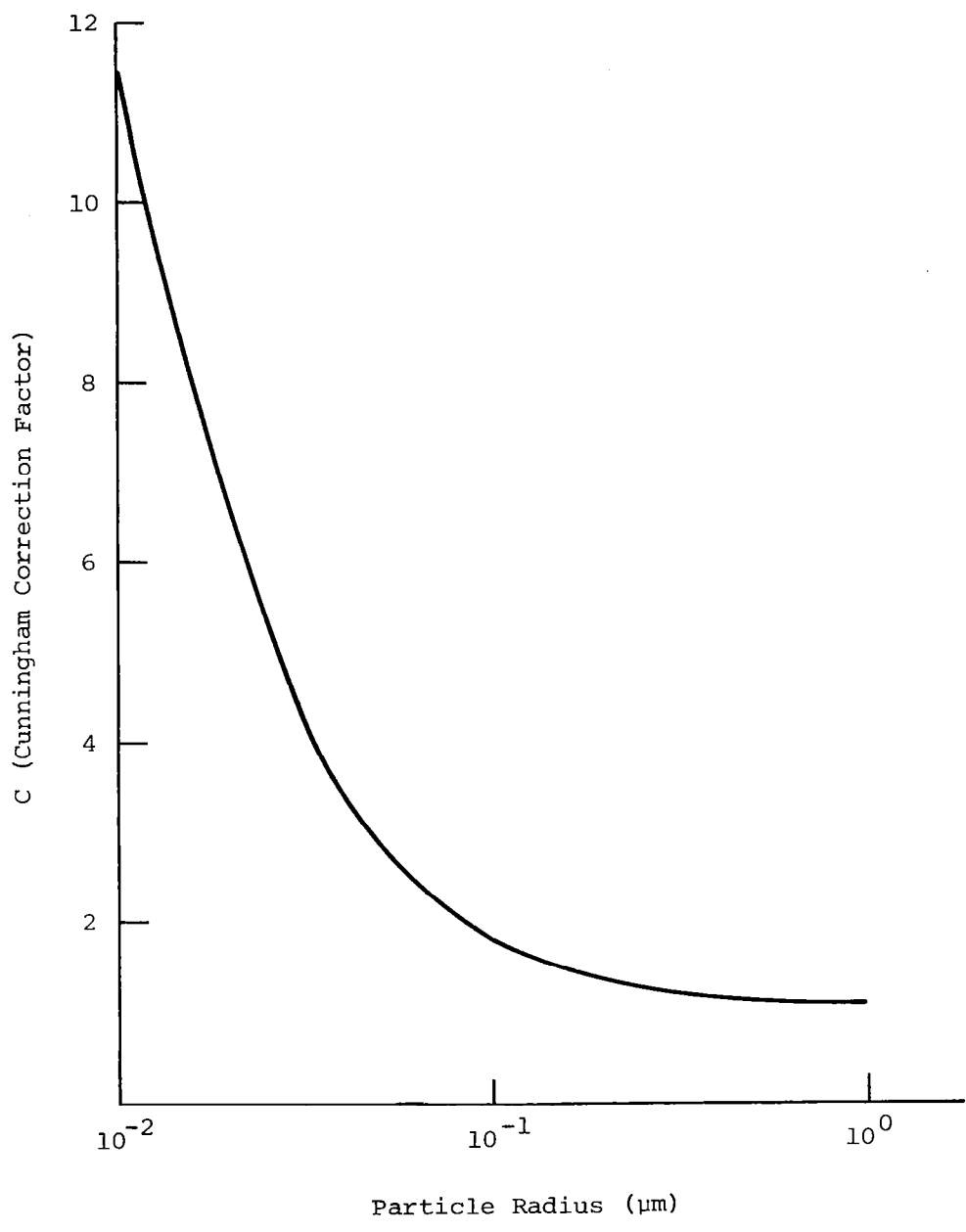
Figure 3.15 Cunningham correction factor.

$$v^* = \frac{neE}{6\pi\mu a} \, C \qquad\qquad\qquad (3\text{-}35)$$

the acceleration time constant becomes (see Equation 3-19)

$$\tau = \frac{m}{6\pi\mu a} \, C \qquad\qquad\qquad (3\text{-}36)$$

and mobilities must be multiplied by $C(Z_{corr} = ZC)$. This has a rather substantial effect upon the magnitude of the mobility and its variation with particle size. The mobilities given in Figure 3.12 are corrected for rarefaction effects in Figure 3.16. At the higher ion densities there is a noticeable minimum in the mobility curve. For those conditions it would be desirable to choose particles whose radius places it near the minimum. This type of behavior was predicted by Ruhnke [3-3] (see Figure 3.17) but does not always occur.

3.2 Previous Nozzles

Several nozzles have been used previously to test out the principles of aerosol precipitation. These nozzles will be briefly described in this section. At the end of the section desirable features of future nozzles, based on the results of Section 3.1, will be discussed. The previous nozzle did not incorporate these design features.

One of the earliest nozzles was designed by Whitby [3-4] to accelerate ions. Ions which were generated in a corona near the needle were accelerated through a sonic orifice (Figure 3.18). Output currents of 16 μA using 2.5 cfm of air at 30 psig through a one-sixteenth inch orifice were achieved.

Ruhnke [3-3] analyzed the charge decay in a jet and constructed a nozzle to check the calculations. A schematic of his apparatus, derived from his written description, is shown in Figure 3.19. The charge in the corona generated at the tip of the hypodermic needle was transferred to the fine mist of water droplets that was created. A space-charge density of about 10^{-2} c/m^3 was built up on the droplets before breakdown occurred. The jet produced a current of about 15 μA, and the current could not be greatly increased without producing a corona
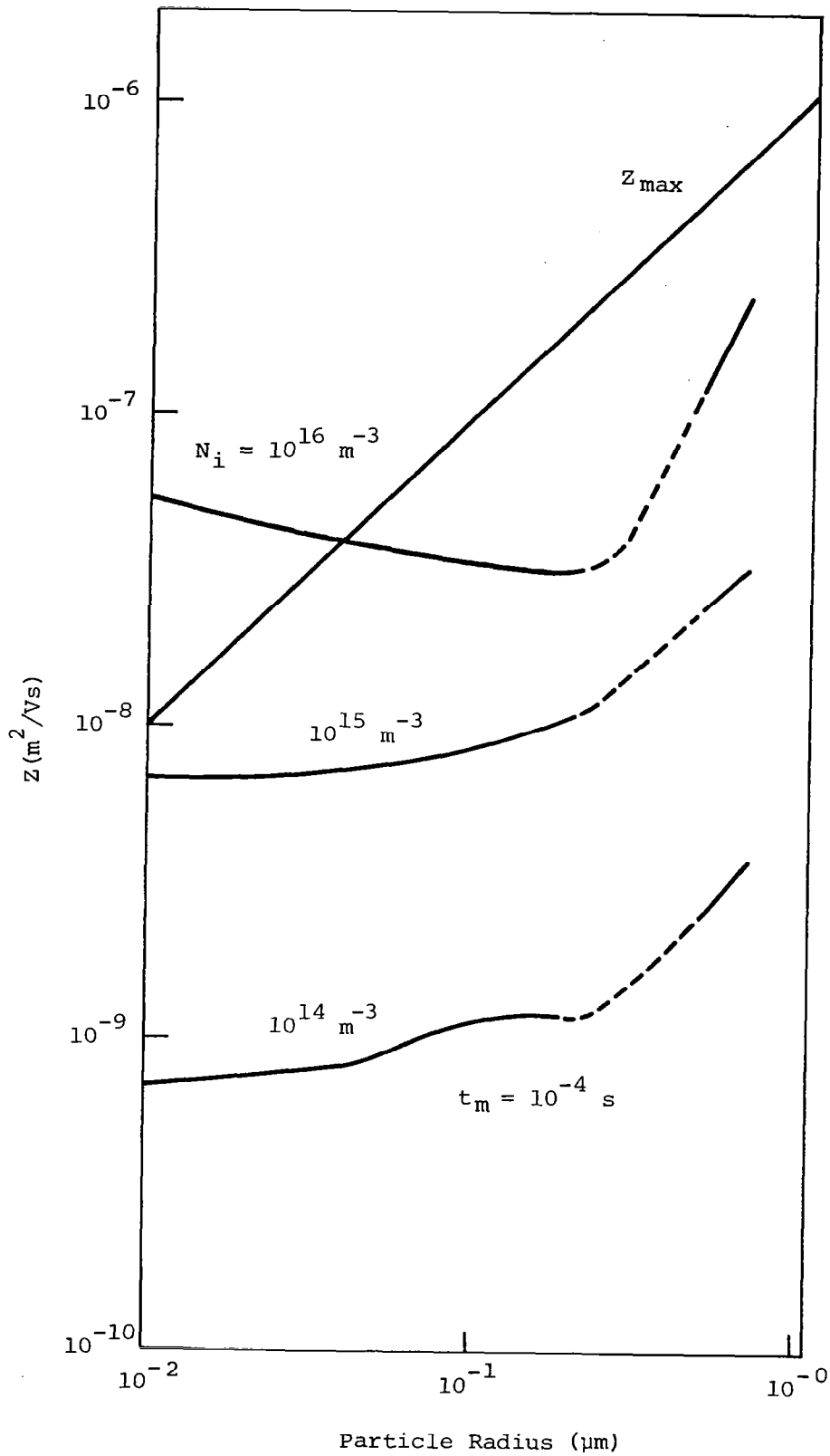
Figure 3.16 Mobility for fixed charging time corrected for rarefraction effects.

55
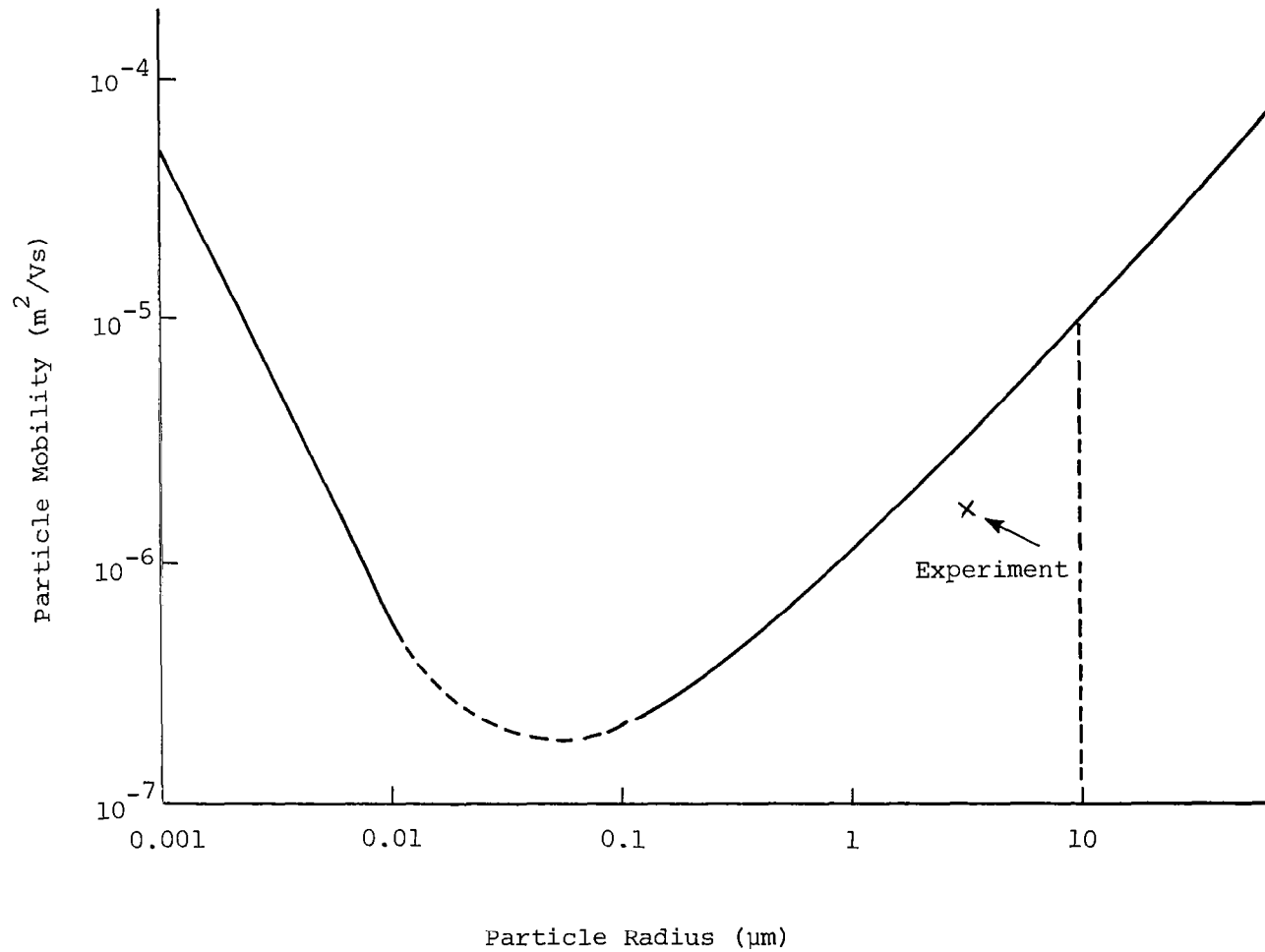
Figure 3.17 Expected variation of mobility with particle size [3-3].
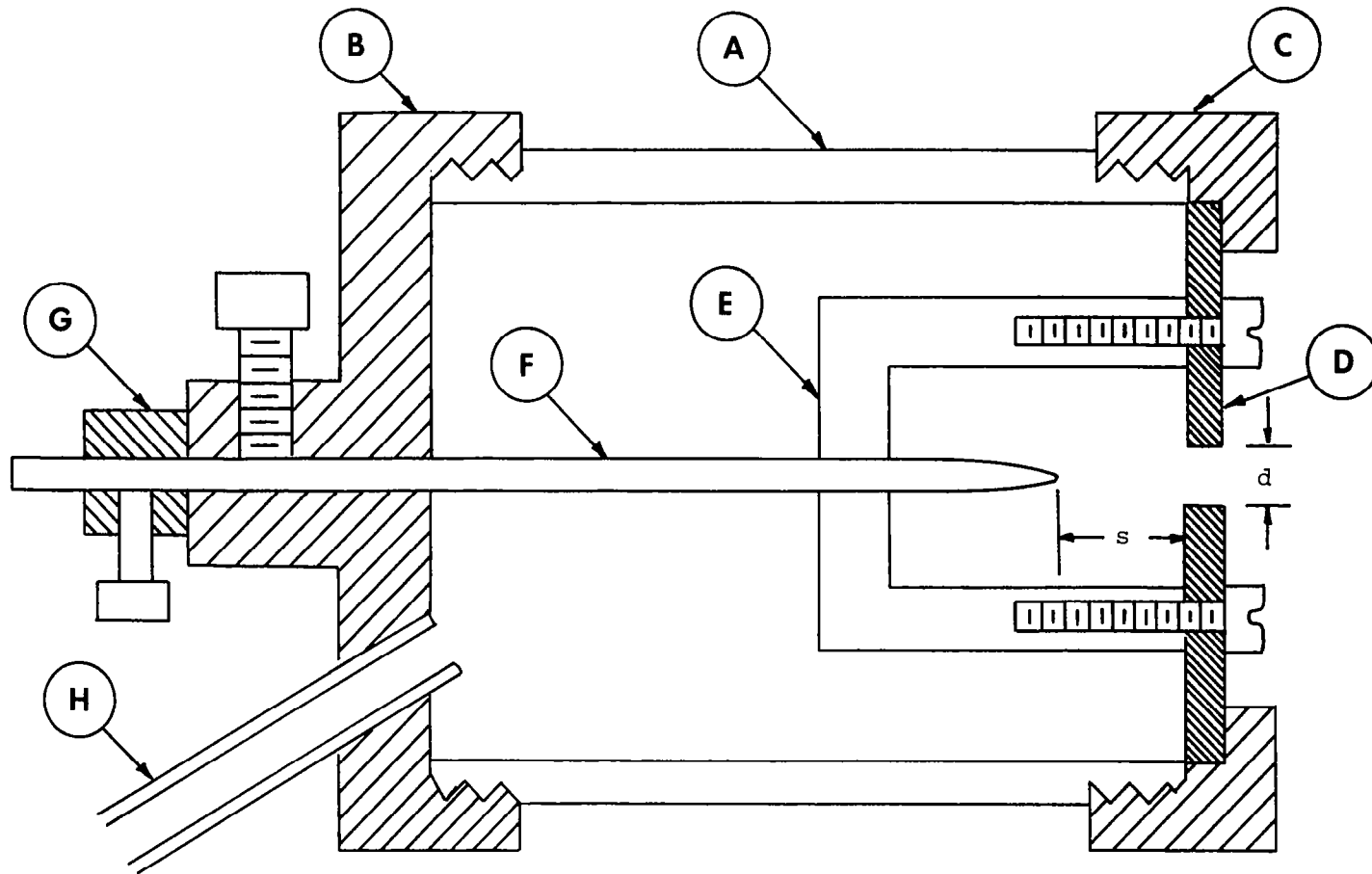
A = lucite tube, B = end caps, C = end cap, D = orifice plate, d = orifice diameter,
E = needle positioning bracket, F = needle, G = needle stop, H = air connection,
s = needle spacing

Figure 3.18   Schematic of sonic jet ionizer [3-4].
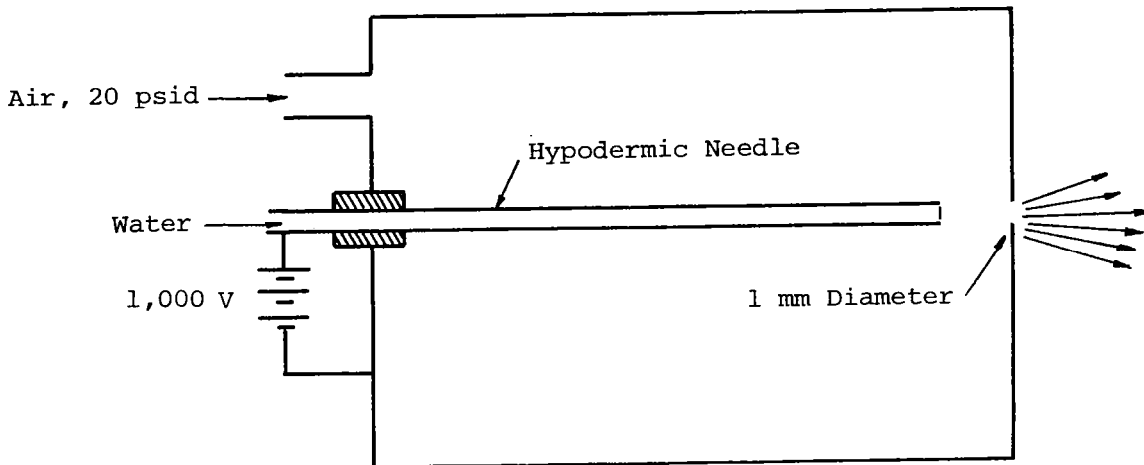
Figure 3.19 Ruhnke charged droplet source [3-3].

discharge at the jet exit. Ruhnke estimated that the average mobility
of his droplets was about 10^{-6} m^2/Vs.

The only field tests of jets of charged particles for warm fog
dispersal used nozzles designed by Gourdine [3-1, 3-2, 3-7]. These
experiments were described in Section 3.1. Details of some of the
nozzles built by Gourdine are shown in Figures 3.20 and 2.5 (page 11).
Saturated air was expanded through a converging-diverging nozzle leaving
the nozzle at a Mach number of about 1.35. During the expansion
process, the saturated air became supersaturated and small water drop-
lets were formed. Near the throat region the droplets passed through a
corona region and acquired a charge.

Properties of the nozzles were given in Table 3.5, page 40.
Nozzle currents were up to 160 μA. The corona region was less than
3×10^{-2} m long, and with a sonic speed of 360 m/s at the throat, the
droplets remained in the corona region of the Gourdine nozzle less than
8×10^{-5} s. Gourdine estimated that the droplets had a radius of about
0.1 μm. From Equation 3-10 the maximum charge to mass ratio for that
size particle is 0.8 c/kg. Measured values of charge to mass ratio were
much less (Table 3.5), and therefore it can be concluded that the

58

Attractor

Stand-Tubing

Ionizer Needle
Assembly

Collar

Cap-Inlet

Ring

O-Ring Seals

EGD Spray Gun

High Voltage
Connector

High Speed
Jet Section
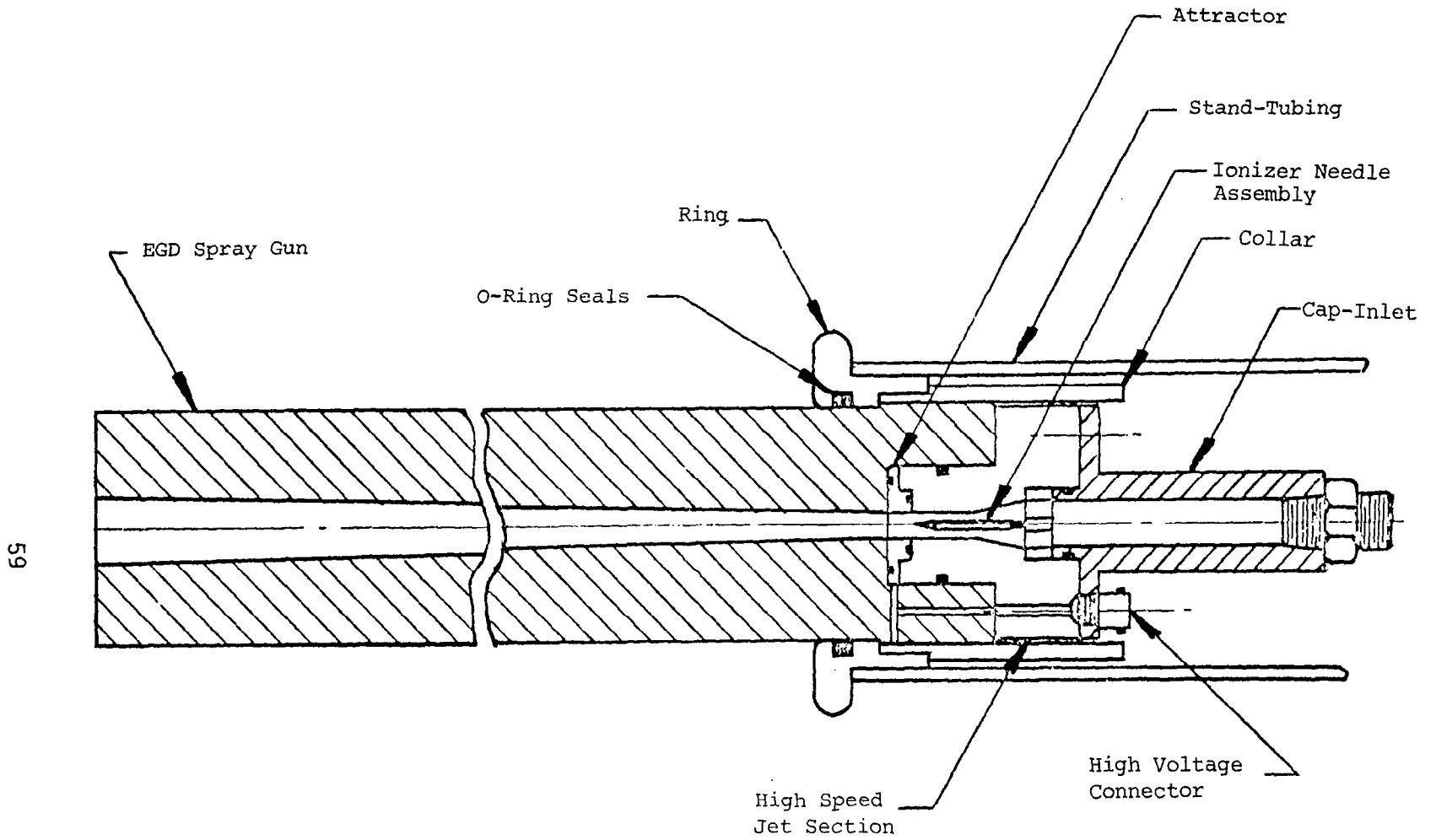
Figure 3.20 Gourdine nozzle [3-7].

particles did not remain in the corona region long enough to acquire the maximum charge.

The following recommendations can be made concerning the design of future nozzles:

1. The water particles should have a radius of about 0.1 μm to minimize the mobility.

2. The ion number density in the corona region should be as large as possible.

3. The water particles should remain in the corona region long enough to acquire the maximum charge to mass ratio. The last feature probably can best be achieved by allowing the droplets to pass through multiple corona discharges.

3.3 Models of Field External to Nozzle Exit

For the CPFDT to be useful the air jet must propel the charged droplets to large heights (at least 50 m) and must create a large charge density to that altitude. It is, therefore, important to develop expressions for predicting both the decay of the charge density in the jet as it proceeds upward and the charge density in the region exterior to the jets. These charge number densities are labeled N_J and N_{BJ}, respectively, in Figure 3.21. Several approximate expressions for these quantities have been derived and they will be given in this section. A program for accurately determining the number density field plus the remaining aspects of the fog dispersal problem will be outlined in the next section.

Because of the relatively low charge densities within the jet, the magnetic field created by the moving charged particles can be ignored. Then only one of Maxwell's equations needs to be kept plus the equation for charge conservation. The relevant equations which describe the charge density in the jet are

$$\nabla \cdot \vec{E} = \rho_e / \epsilon_o \qquad (3\text{-}37)$$

$$\frac{\partial \rho_e}{\partial t} + \nabla \cdot \vec{J} = 0 \qquad (3\text{-}38)$$

$$\vec{J} = \rho_e Z \vec{E} + \rho_e \vec{u} \qquad (3\text{-}39)$$

60

Between Jets

N_J

N_{BJ}

Jet

Jet

Jet

H

← Entrainment →

Ground
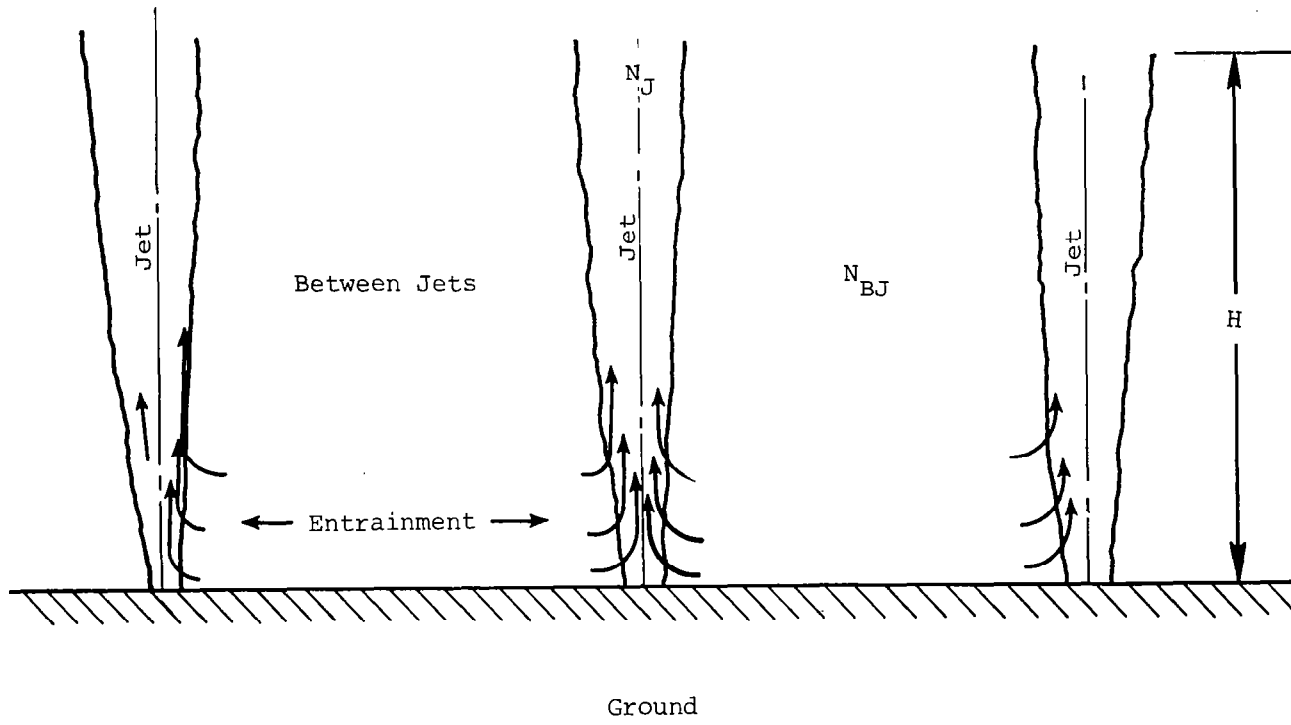
Figure 3.21   Schematic of multiple jet array.

Many analyses can neglect the fluid dynamic velocity term. The results given below all have used these equations as a starting point.

First, consider the analyses for the decay of the charge density in the jet. Whitby [3-4] analyzed the charge number decay in a closed space. He assumed that the particle charge and mobility were constant, the space was not acted upon by fields, and that the particle number density was uniform in space at all times. The number density decay was found by integrating Equation 3-38 yielding the expression

$$\frac{N}{N_0} = \frac{1}{1 + 4\pi N_0 neZt} \tag{3-40}$$

Noting that this expression is independent of geometry, it was then applied to the charge number density decay in a jet by assuming that the charge concentration is only a function of time since a given volume of gas has left the corona region. Using the expression for the gas velocity along the centerline of a circular turbulent jet (subsonic or supersonic--see Harsha [3-12]), $u = b/x$

$$u = \frac{b}{x} \; , \quad t = \int_0^x \frac{dx}{u} = \frac{x^2}{2b} \tag{3-41}$$

then the decay expression becomes

$$\frac{N_J}{N_{Jo}} = \frac{1}{1 + \dfrac{2\pi N_{Jo} neZx^2}{b}} \tag{3-42}$$

where N_{Jo} is the concentration at the jet exit. Measurements by Whitby [3-4] of the decay of a unipolar ion beam confirmed the general correctness of this expression.

Whitby [3-6] assumed that the charge number density outside the region of the jet could be described as that which was generated by a spherical source located some distance downstream from the nozzle exit. Consider a spherical source, shown in the figure, where all properties are functions only of the radial coordinate. Let Q be the total current from the source.

$$\vec{E} = E\hat{r}$$
$$\vec{J} = J\hat{r}$$
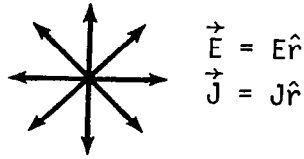
$$\int \vec{J} \cdot \hat{n}dA = 4\pi r^2 N_{BJ} neZE = Q \tag{3-43}$$

The equation to be solved for the electric field is

$$\frac{d}{dr}(r^2E)^2 = \frac{1}{4\pi\epsilon_o}\frac{2r^2Q}{Z} \tag{3-44}$$

Setting the constant of integration equal to zero and assuming that Z is constant, Whitby integrated this equation to give

$$E = \left(\frac{1}{4\pi\epsilon_o}\frac{2}{3}\frac{Q}{Zr}\right)^{1/2}; \quad N_{BJ} = \left(4\pi\epsilon_o\frac{3Q}{2Z}\right)^{1/2}\frac{r^{-3/2}}{4\pi ne} \tag{3-45}$$

Because Equation 3-44 is nonlinear, the usual methods of superposition cannot be used to find the solution for multiple sources, such as would be needed to examine an array of jets (Figure 3.21), nor can the method of images be used to find the solution to the source above the ground plane (Figure 3.22). A general source problem could be determined by numerically solving the following set of equations plus appropriate boundary conditions.

$$\vec{E} = -\nabla V \tag{3-46}$$

$$\nabla^2 V = -\rho_e/\epsilon_o \tag{3-47}$$

$$\nabla V \cdot \nabla \rho_e = \rho_e^2/\epsilon_o \tag{3-48}$$

Whitby measured N_{BJ} on a line perpendicular to the axis of an ion beam and confirmed the correctness of the spatial dependence of N_{BJ} from Equation 3-45 [3-6]. Also, measurements of the electric field between the sources in the Panama Canal Zone field tests [3-7] seemed to indicate that this result was also applicable in that situation [3-13].

Gourdine approached the estimation of N_J and N_{BJ} from a quite different point of view. Gourdine, et al. [3-1] derived an expression
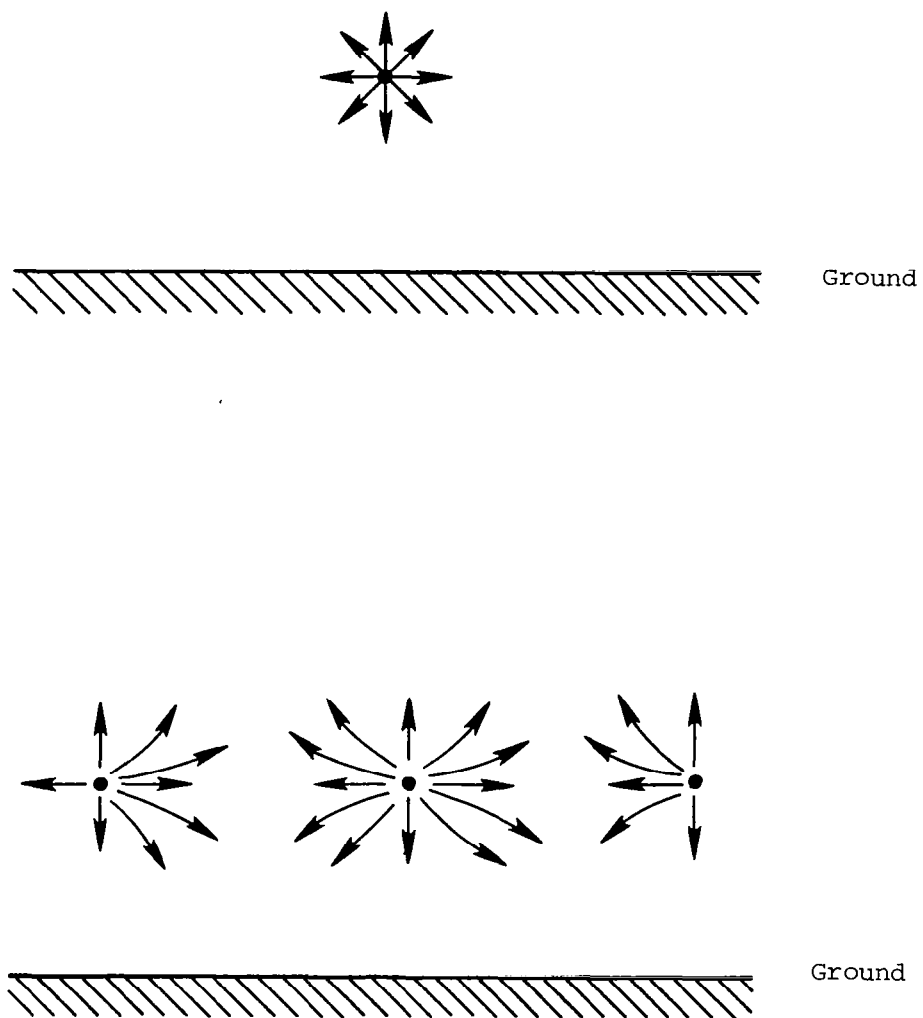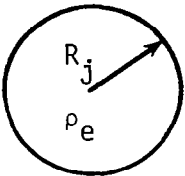
Figure 3.22 Single and multiple sources above ground plane.

for the conservation of charge from a circular turbulent jet by utilizing the spreading rate of a turbulent jet [3-16]

$$r = R_j + \alpha x = R_j + 0.0848x \quad (m) \tag{3-49}$$

and assuming that the electric field at the edge of the jet is equal to that which exists at the edge of an infinitely long cylindrical region of constant radius, R_j, and constant uniform charge density, ρ_e. Applying Gauss's law to such a region the field is given by

$$\vec{E} = \begin{cases} \dfrac{r\rho_e}{2\varepsilon_o} \hat{r} & r \le R_j \\[2mm] \dfrac{R^2 \rho_e}{2r\varepsilon_o} \hat{r} & r > R_j \end{cases} \tag{3-50}$$

Using this result, the charge density equation, as corrected by Christensen and Frost [3-17] is

$$\frac{N_J}{N_{Jo}} = \left\{ 1 + \left[\alpha + \frac{2ZE(o)}{u_j} \right] \frac{x}{R_j} + \frac{2ZE(o)\alpha}{u_j} \left(\frac{x}{R_j} \right)^2 \right\}^{-1} \tag{3-51}$$

where E(o) is the electric field at the edge of the jet ($r = R_j$) at the nozzle exit (x = 0). This expression is plotted, using the parameters for the large nozzle used by Gourdine [3-2], in Figure 3.23. For these parameters this equation predicts a much slower decay of the number density than is predicted by Equation 3-42. There is no experimental confirmation of this prediction.

For the charge number density between the jets Gourdine, et al. [3-1] assumed that the turbulent jet entrainment would create a region of uniform space charge between the jets in a large array, such as would be used near an airport. This model should be contrasted to the spherical source distribution which Whitby used to describe the charge density between the jets (Equation 3-45). Gourdine assumed that the charge density, ρ_a, is constant to a height H where the jet charge density equals the charge density in the surrounding atmosphere (i.e., H is height where $N_{BJ} = N_J$). Then the field and height are given by

65
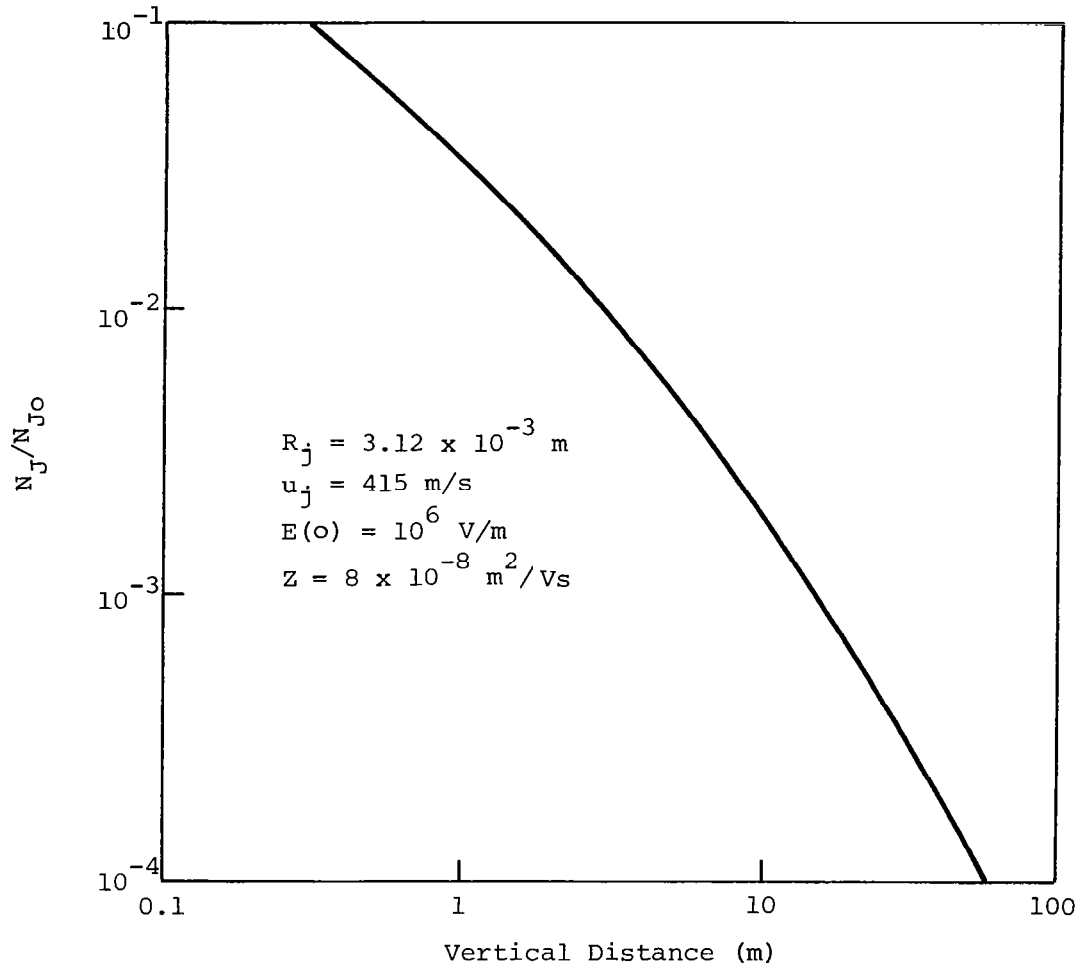
Figure 3.23 Charge number decay according to Gourdine expression [3-2].

$$E(x) = -\rho_a (H - x)/\varepsilon_o \qquad\qquad (3\text{-}52)$$

$$H = 24.5 \frac{R_j u_j}{ZE(o)} \qquad (m) \qquad\qquad (3\text{-}53)$$

$$\rho_a = 0.0408 \left[\frac{\varepsilon_o E(o)/R_j}{u_j/ZE(o)} \right] \qquad (C/m^3) \qquad\qquad (3\text{-}54)$$

The jets were assumed to be noninteracting, at least to an altitude H. It should be noted that these latter equations have not been corrected for the linear term in x/R_j that was added by Christensen and Frost [3-17] to Equation 3-51.

The equations given in this section for the decay of the charge number density in the jets and the region between the jets are recognized to only approximately describe the complicated phenomena which occur. They have not been subjected to close scrutiny because field experiments of enough detail have not been performed. In particular, the particle size and mobility distribution have been very uncertain in the experiments that were performed. A method for obtaining a much more complete description of the space external to the nozzle exits will be described in the next section.

References

3-1. Gourdine, M. C., T. K. Chiang, G. B. Carvin, and A. Brown. "EGD Fog Dispersal System Scaling Laws," Paper presented at the AMS's Fourth National Conference on Weather Modification, Fort Lauderdale, Florida, November 1974.

3-2. Gourdine, M. C., T. K. Chiang, and A. Brown. "A Critical Analysis of the EGD Fog Dispersal Technique," The Cornell Engineer, pp. 14-35, November 1975.

3-3. Ruhnke, L. H. "Warm Fog Modification by Seeding with Unipolar Ions," AMS's Second National Conference on Weather Modification, Santa Barbara, California, pp. 385-388, 1970.

3-4. Whitby, K. T. "Generator for Producing High Concentrations of Small Ions," Rev. Sci. Instrum., Vol. 32, pp. 1351-1355, 1961.

3-5. Whitby, K. T., R. C. Jordan, C. M. Peterson, and L. W. Rees. "Charging and Decay of Monodispersed Aerosols in the Presence of a Unipolar Ion Source," Final report for USPHS, Grant No. AP00136-02, September 1963.

3-6. Whitby, K. T., B. Y. H. Liu, and C. M. Peterson. "Charging and Decay of Monodispersed Aerosols in the Presence of Unipolar Ion Sources," Journal of Colloid Science, Vol. 20, pp. 585-601, 1965.

3-7. Chiang, T. K. "Field Evaluation of an Electrogasdynamic Fog Dispersal Concept," Part I, Report No. FAA-RD-73-33, February 1973.

3-8. White, H. J. "Particle Charging in Electrostatic Precipitation," AIEE Transactions, Vol. 70, pp. 1186-1191, 1951.

3-9. Oglesby, S., Jr., and G. B. Nichols. Electrostatic Precipitation. New York: Marcel Dekker, Inc., 1978.

3-10. Lapple, C. E. "Electrostatic Phenomena with Particulates," Advances in Chemical Engineering. New York: Academic Press, 1970.

3-11. Arendt, P., and H. Kallman. "The Mechanism of the Electrification of Small Particles in Clouds," Z. Physik, Vol. 35, pp. 421-441, 1926.

3-12. Harsha, P. T. "Free Turbulent Mixing: A Critical Evaluation of Theory and Experiment," AEDC TR-71-36, 1971.

3-13. Whitby, K. T. "Analysis of Electrogasdynamic Fog Dispersal," Final report to ERDA Contract E(11-1)-1248, December 1976.

3-14. Crawford, M. *Air Pollution Control Theory*. New York: McGraw-Hill, 1976.

3-15. Cobine, J. D. *Gaseous Conductors*. New York: Dover Publications, 1958.

3-16. Schlichting, H. *Boundary-Layer Theory*, 6th edition. New York: McGraw-Hill, 1968.

3-17. Christensen, L. S., and W. Frost. "Fog Dispersion," NASA CR 3255, March 1980.

4.0 FOG/JET FLUID DYNAMICS

Figure 4.1 illustrates schematically a number of physical effects
which must be considered in attempting to analyze and plan an experi-
mental field program to test warm fog dispersal by charged particle
techniques. The figure illustrates a jet containing charged droplets as
well as some ions which are propelled by the jet momentum into the
atmosphere. Controversy exists as to whether the droplets reach maximum
height simply through momentum imparted by the jet or through turbulent
diffusion. Turbulence will be induced not only by the jet itself, but
also by neighboring jets as well as the natural turbulence in the atmo-
sphere. It is also unknown as to whether the jet contains only charged
droplets or positive and negative ions as well. In general, it is
assumed that the charged droplets are unipolar charged droplets with a
common polarity. In turn, the size distribution of the charged droplets
leaving the nozzle is not well known.

As illustrated schematically in the figure, the charged droplets
can transfer charge to fog droplets by polarization charging and/or
attachment charging, i.e., diffusion charging and electric field
charging. Also, the induced electric fields may enhance coalescence
with subsequent precipitation of the fog droplets.

Additionally, the interaction of the jet with the atmospheric
boundary layer is not fully understood. In Reference [4-1] some simple
jet analysis without concern for the incorporation of charged particles
were investigated to see the effect of crosswind on the jet. These
models, however, do not provide any insight into how far downstream the
charged particles are carried before they effectively cause precipitation
of the fog droplets. This is a very important problem relative to
nozzle spacing and position with respect to the runway.

In this section, a set of equations is developed which can be
utilized to investigate the behavior of the charged jet interaction with
the atmospheric boundary layer. The equations are developed for
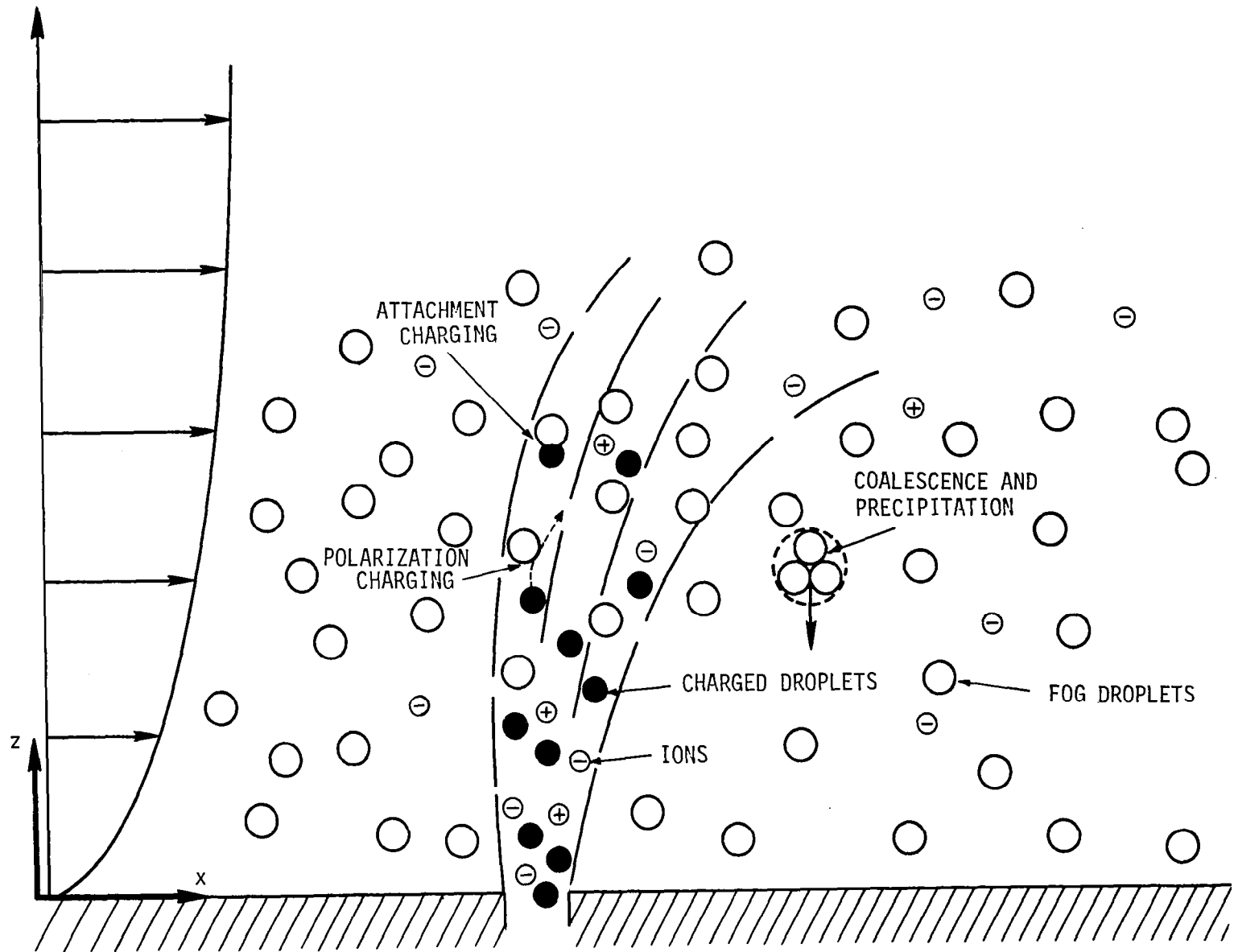
Figure 4.1 Schematic illustration of physical effects involved in warm fog dispersal by a charged droplet jet.

two-dimensional flow. In this case, the jets would be treated as a plane jet perpendicular to a crosswind. Such arrangement would be similar to a line of fog dispersal units perpendicular to the crosswind.

The development of the equations is drawn heavily from [4-2, 4-3]. The former references deal with numerical modeling of the atmospheric boundary layer incorporating turbulence kinetic energy and turbulence length scale transport equations. The latter reference deals with the numerical study of cloud electrification in an axisymmetric, time-dependent cloud model. The equations presented in the aforementioned references are modified to apply to the case of a plane jet discharging from the ground into a logarithmic atmospheric boundary layer wind profile.

In Section 4.1 the standard conservation equations for mass and momentum are described. In Section 4.2 the equations necessary to incorporate the effect of transport of water substances are presented and discussed. The thermodynamic equations are stated in Section 4.3. In Section 4.4 the equations governing the transfer of charge are presented. Models currently used in cloud physics programs for incorporating the effect of polarization charging and/or attachment charging are also described in this section. Solutions to the equations are not given nor are the full complement of boundary conditions developed.

4.1 <u>Momentum Equation</u>

Figure 4.2 lists the momentum equations along with the equation for conservation of mass. Electric force terms are included to model the electrical effects on the air motion. The definition of terms is given in the Nomenclature. Little discussion of these equations is necessary since they are simply the Navier-Stokes equations with the additional electric force terms added. The standard Boussinesq approximation is made and referenced to an environment state having a constant reference pressure, p_o, and a vertical varying density, $\langle \rho \rangle$. Variables in angle

Primitive Variables

$$\frac{Du}{Dt} = -C_p <\theta> (1 + 0.61\ q_v)\frac{\partial \pi'}{\partial x} + \frac{\rho_T}{<\rho>} E_x + F_x \tag{1}$$

$$\frac{Dw}{Dt} = -C_p <\theta> (1 + 0.61\ q_v)\frac{\partial \pi'}{\partial z} + g\left(\frac{\theta'}{<\theta>} + 0.61\ q_v' - \ell_c - \ell_f - \ell_p\right)$$

$$+ \frac{\rho_T}{<\rho>} E_z + F_z \tag{2}$$

$$\pi = (P/P_o)^{R/C_p}; \tag{3}$$

$< >$ designates reference state.

Vorticity and Streamline Variables

$$\omega = \frac{\partial <\rho> u}{\partial z} - \frac{\partial <\rho> w}{\partial x} \tag{4}$$

$$\frac{D\omega}{Dt} = -uw\ \frac{\partial^2 <\rho>}{\partial z^2} + \left(\omega + u\ \frac{\partial <\rho>}{\partial z}\right)\frac{2w}{<\rho>}\ \frac{\partial <\rho>}{\partial z} + <\rho> g\left(\frac{1}{<\theta>}\ \frac{\partial \theta'}{\partial x}\right.$$

$$\left. + 0.61\ \frac{\partial q_v'}{\partial x} - \frac{\partial \ell_c}{\partial x} - \frac{\partial \ell_f}{\partial x} - \frac{\partial \ell_p}{\partial x}\right) + \frac{\partial \rho_T E_z}{\partial x} - \frac{\partial \rho_T E_x}{\partial z} + D_\omega \tag{5}$$

$$\nabla^2 \psi = <\rho> \omega \tag{6}$$

where

$$u = \frac{1}{\rho}\ \frac{\partial \psi}{\partial z} \quad \text{and} \quad w = -\frac{1}{\rho}\ \frac{\partial \psi}{\partial x} \tag{7}$$

where

D_ω is the vorticity source term.

Figure 4.2   Conservation of momentum equations.

brackets represent those of the environmental reference state, and the primed variables represent the deviation.

Equations 5, 6, and 7 of Figure 4.2 express the equations in terms of the vorticity and streamline variables. It is believed this formulation of the governing equations will be more convenient and will have certain advantages relative to numerical solution.

4.2 Conservation Equations for Water Substances

4.2.1 Governing Equations

Figure 4.3 lists the equations governing the transport of water substances. In this set of equations, the relative velocities, V_c, V_f, and V_p, represent the velocity of the average size charged droplet, fog droplet, and precipitating droplets, respectively. The effect of both electrical and gravitational forces on these velocities are taken into account as described later. The term P_{fp} represents the rate of autoconversion of fog droplets to precipitation droplets, the terms P_{fA} and P_{pA} represent the rate of accretion of charged droplets to fog droplets and of charged droplets and fog droplets to precipitation droplets, respectively. Finally, the terms P_{fE} and P_{pE} represent the rate of evaporation of fog drops and the rate of evaporation of precipitation drops, respectively. The water substance variables, q, ℓ_1, ℓ_2, are simply convenient choices of combinations of water content terms. The symbol q represents the sum of the water vapor plus the liquid water content due to charged droplets in the given control volume (pounds per unit mass of air). The quantity ℓ_1 represents q plus the liquid water content of the fog droplets, and the symbol ℓ_2 represents the combined or total water content of the atmosphere.

The terms on the left-hand side of Equations 1, 3 and 5 represent the total rate of change of the respective water content quantities. The first term on the right-hand side of the equality sign, in these same equations, represents the turbulent diffusion of the water substances. The terms appearing in the equations which contain the relative velocities of the various droplets, i.e., V_c, V_f, and V_p, represent the liquid water transport due to the motion of the particles with respect

74

$$\frac{Dq}{Dt} = \frac{1}{<\rho>} \nabla \cdot K\nabla<\rho>q - \frac{1}{<\rho>} \nabla \cdot <\rho>\ell_c V_c - P_{pA} - P_{fA} + P_{fE} + P_{pE} \qquad (1)$$

$$q = q_v + \ell_c \qquad (2)$$

$$\frac{D\ell_1}{Dt} = \frac{1}{<\rho>} \nabla \cdot K\nabla<\rho>\ell_1 - \frac{1}{<\rho>} [\nabla \cdot <\rho>\ell_c V_c + \nabla \cdot <\rho>\ell_f V_f]$$

$$- P_{fp} - P_{pA} + P_{pE} \qquad (3)$$

$$\ell_1 = q_v + \ell_c + \ell_f \qquad (4)$$

$$\frac{D\ell_2}{Dt} = \frac{1}{<\rho>} \nabla \cdot K\nabla<\rho>\ell_2 - \frac{1}{<\rho>} [\nabla \cdot <\rho>\ell_c V_c + \nabla \cdot <\rho>\ell_f V_f$$

$$+ \nabla \cdot <\rho>\ell_p V_p] \qquad (5)$$

$$\ell_2 = q_v + \ell_c + \ell_f + \ell_p \qquad (6)$$

P_{fp} ~ rate of autoconversion of fog droplets to precipitation droplets

P_{fA} ~ rate of accretion of charged droplets to fog droplets

P_{fE} ~ rate of evaporation of fog droplets

P_{pA} ~ rate of accretion of charged and fog droplets to precipitation droplets

P_{pE} ~ rate of evaporation of precipitation droplets

Figure 4.3 Conservation equations for water substances.

to the air flow. That is, these terms express the fact that the droplets
due to gravitational or electric forces will be moving faster or slower
than the surrounding air and will consequently precipitate or move out
of the control volume.

4.2.2 Mathematical Expressions for Sources and Sinks of Water Substances

To solve the governing equation given in Section 4.2.1, mathematical
models of the source and sink terms for the water substances are
required. Expressions for these quantities are given in Figure 4.4.
The expression for the autoconversion of fog droplets to precipitation
droplets is modified from Chiu [4-3]. In this expression, N_f, is the
number of droplets per unit volume, $<\rho>$ is the reference density of the
air, D_0 is the relative dispersion of the droplet distribution, and will
need to be determined from empirical results. The term ℓ_0 is a threshold
value of fog water content for conversion. A value of ℓ_0 equal to
2×10^{-3} grams/gram is recommended for the threshold value of cloud
water content in [4-3]. A similar value is expected to apply for fog.

The accretion term, Equation 2 in Figure 4.4, represents the mass
growth rate of fog droplets due to capture of the charged droplets. A
similar expression exists for the growth of the precipitation droplets.
The mass growth of the droplets occurs due to the charged droplets moving
with velocity V_c through the fog droplets which are either stationary or
moving with a small terminal velocity, V_f. In general, the relative
velocity of the fog droplets will be small, whereas the charged droplets
particularly near the nozzles will be very high and will become smaller
as they reach higher altitudes in the atmosphere. Similarly, the
precipitation droplets falling through the relatively stationary fog
will accrete fog droplets and carry them to the ground. Also, they will
intercept charged droplets and possibly carry them downward.

In the expression given by Equation 2 in Figure 4.4, η represents
the collision efficiency which is defined as the probability that a
charged droplet will collide with a droplet in its path. The growth of
fog droplets by collision and coalescence with charged droplets as well
as precipitation droplets depends not only on η but also on $(1 - <S>)$,

76

$$P_{fp} = \frac{<\rho>(\ell_f - \ell_o)^2}{1.2 \times 10^{-4} + 1.596 \times 10^{-12} \, N_f/D_o\rho(\ell_f - \ell_o)} \; ; \quad \ell_f - \ell_o > 0$$

$$= 0; \quad \ell_f - \ell_o < 0 \tag{1}$$

$$P_{fA} = N_f \, n \, \pi r_f^2 |V_c - V_f| \rho \ell_c (1 - <S>)/<\rho> \tag{2}$$

$$P_{fE} = \frac{N_f 4\pi r_f(1 - s)(1 + 0.22 \, Re^{1/2})}{<\rho>(L^2/k_T R_v T^2 + 1/<\rho>q_{vs}D_v)} \tag{3}$$

Similar expressions for P_{pA} and P_{pE} can be developed.

Figure 4.4   Mathematical expressions for sources and sinks of water substances.

where <S> is defined as the mean separation probability. This expression is described in detail in [4-3]. The expression (1 - <S>) signifies the fraction of colliding droplets that coalesce, i.e., the coalescence efficiency.

Finally, Equation 3 in Figure 4.4 represents the evaporation of the fog and precipitation drops. The charged droplets will also evaporate, but because of their small size this is negligible. In the evaporation expression, L is the latent heat of evaporation, R_v the specific gas constant for water vapor, D_v the diffusivity of water vapor in air, k the thermal conductivity of the air, T the temperature of the air, and s the saturation ratio defined as the ratio of water vapor mixing ratio, q_v, to the saturation vapor mixing ratio, q_{vs}.

4.2.3 Water Substance Parameters

The solution of the expressions for sources and sinks of water describes the governing equations for these parameters. The various parameter equations shown in Figure 4.5 are explained for fog droplets only; however, similar expressions can be developed for the charged droplets and precipitation droplets, respectively. If the fog liquid water content, ℓ_f, is known at a point in spece, one can consider that there exists N_f fog droplets per unit volume of air, with mean radius r_f. The number of fog droplets per unit volume, N_f, and droplet radius, r_f, are related to the liquid water content, ℓ_f, as shown by Equation 1, Figure 4.5. It is necessary to know the distribution function for fog droplet sizes, $n_f(r, \ell_f)$ which appears under the integral in Equation 1, Figure 4.5. This requires further research, but as an example a typical size distribution for raindrops is the Marshall-Palmer distributions;

$$N = N_o e^{-\hat{\lambda} r}$$

with $\hat{\lambda}$ being a function of liquid water content, ℓ_f:

$$\hat{\lambda} = (\pi \rho_w N_o / <\rho> \ell)^{1/4}$$

Number and Radius of Fog Droplets:

$$N_f = \int_0^\infty n_f(r, \ell_f) dr \qquad (1)$$

$$r_f = \frac{3<\rho>\ell_f}{4\pi\rho_w N_f} \qquad (2)$$

Gravitational and Electrical Forces

$$F_G = \frac{4}{3} \pi r_f^3 \rho_w g \qquad (3)$$

$$F_E = q_f E \qquad (4)$$

Terminal Velocity:

$$F_G + F_E = \frac{\pi}{2} r_f^2 C_D \rho |V_f| V_f \qquad (5)$$

Similarly, expressions can be developed for charge carrier droplets and precipitation droplets.

Figure 4.5   Parameter equations for water substances.

79

In the Marshall-Palmer distribution, N_O is given empirically as
0.08 cm^{-4}, r is the radius of the raindrops, ρ_w is the density of water, and $<\rho>$ is the density of air as defined previously. The mean radius of the fog droplets can then be determined from Equation 2, Figure 4.5.

Knowing the average radius of the fog droplets, the gravitational force, F_G, and the electrical force, F_E, exerted on a droplet may be expressed as shown in Equations 3 and 4 of Figure 4.5. q_f is the charge on a droplet of average size. For this study it can be assumed that:

$$q_f = Q_f/N_f$$

where Q_f is the charge density on the total fog liquid water content. The equations governing charge transport and an expression for calculating Q_f is given in a following section.

Finally, the relative velocities of the fog droplets, V_f, can be computed from the drag law where the total force acting on the particle is the sum of the gravitational and electrical forces, Equation 5, Figure 4.5.

The technique described above can also be used to calculate the relative velocities of the average size charged droplets and precipitation droplets, respectively. The number concentration of the charged droplets, however, will depend upon the characteristics of the nozzle. Solution of the proposed system of equations can be used to carry out parametric studies of the best droplet distribution for nozzles. Thus the computational model proposed will allow either (1) determination of the effect of a nozzle of known droplet distribution, or (2) parametric study of droplet distribution to provide design criteria for optimum nozzle performance. The number of droplets is shown in [4-3] to be an important parameter influencing cloud electrification and is expected to be a significant parameter in the fog electrification.

4.3 Thermodynamic Equations

The form of the thermodynamic equations used by Chiu [4.3] follows the work of Orville [4.4] and Wisner, et al. [4.5]. The thermodynamic equation is expressed in terms of the entropy variable, ϕ', as shown in Figure 4.6. The form of the entropy variable for saturated and unsaturated air are given by Equations 2 and 3 of Figure 4.6, respectively. Again, the left-hand term of the equation represents the total rate of change of the entropy, ϕ'. The first term on the right-hand side of the equality sign represents the turbulent diffusion of entropy. The latter terms of the equation represent the thermal energy change due to water mass being advected into a fluid medium and reaching thermal equilibrium with its surroundings.

The saturation mixing ratio, q_{vs}, can be calculated from Equation 4, Figure 4.6, where the equilibrium vapor pressure over water, e_s, is given by Equation 5. The temperature, T, is directly related to the potential temperature, θ', through the definition of potential temperature given by Equation 6, Figure 4.6.

4.4 Equations Governing Electrical Properties

4.4.1 Governing Equations

Figure 4.7 lists the various equations which can be used to simulate the electrical properties of the fog and jet interaction. The total space charge density, ρ_T, is given by Equation 1 of Figure 4.7. It is observed that ρ_T appears in the Navier-Stokes equations relative to the electric force field. This is one of the most important parameters which has not been modeled correctly in previous analyses. If the precipitation process takes place by electrical forces acting on the charged fog droplets, then the development of this space charge and its distribution at steady state is essentially the controlling parameter to assure effective fog dispersal.

In Equation 1, Figure 4.7, the effects of large ions are ignored which assumes that the growth and decay of the fog is not simulated in a contaminated atmosphere where most large ions form. This assumption must be examined for an airport in an urban environment.

81

$$\frac{D\phi'}{Dt} = \frac{1}{\langle\rho\rangle} \nabla \cdot K\langle\rho\rangle\nabla\phi' - \frac{C_w}{C_pT_\infty}[\ell_c(\vec{v} + \vec{V}_c) \cdot \vec{\nabla}T + \ell_f(\vec{v} + \vec{V}_f) \cdot \vec{\nabla}T$$

$$+ \ell_p(\vec{v} + \vec{V}_p) \cdot \vec{\nabla}T] \tag{1}$$

$$\phi' = \theta'/\theta + Lq_v/C_pT_\infty \qquad \text{(unsaturated)} \tag{2}$$

$$\phi' = \theta'/\theta + Lq_{v_s}(\theta')/C_pT_\infty \qquad \text{(saturated)} \tag{3}$$

$$q_{v_s} = 0.622\, e_s/(p - e_s) \tag{4}$$

$$e_s = \exp[19.07\, T - 4782.9/(T - 35.9)] \tag{5}$$

$$T = \langle\theta\rangle\, (P/P_0)^{R/C_p} \tag{6}$$

Figure 4.6   Thermodynamic equations.

$$\rho_T = e(n_1 - n_2) + Q_c + Q_f + Q_p \tag{1}$$

$$E = -\nabla \phi_e \tag{2}$$

$$\nabla^2 \phi_e = -\rho_T / \varepsilon_o \tag{3}$$

$$\frac{Dn_{1,2}}{Dt} = -\nabla(\pm n_{1,2} Z_{1,2} E - K\nabla n_{1,2}) + G - \alpha n_1 n_2$$

$$- \left(\frac{\delta n_{1,2}}{\delta t}\right)_c - \left(\frac{\delta n_{1,2}}{\delta t}\right)_f - \left(\frac{\delta n_{1,2}}{\delta t}\right)_p \tag{4}$$

$$\frac{DQ_c}{Dt} = -\nabla(Q_c V_c - K\nabla Q_c) + e[(\delta n_1/\delta t)_c - (\delta n_2/\delta t)_c] - (\delta Q_c/\delta t)_{coal_f}$$

$$- (\delta Q_c/\delta t)_{coal_p} - (\delta Q_c/\delta t)_{pol_f} - (\delta Q_c/\delta t)_{pol_p} \tag{5}$$

$$\frac{DQ_f}{Dt} = -\nabla(Q_f V_f - K\nabla Q_f) + e[(\delta n_1/\delta t)_f - (\delta n_2/\delta t)_f] + (\delta Q_c/\delta t)_{coal_f}$$

$$- (\delta Q_c/\delta t)_{coal_p} + (\delta Q_c/\delta t)_{pol_f} - (\delta Q_f/\delta t)_{pol_p} \tag{6}$$

$$\frac{DQ_p}{Dt} = -\nabla(Q_p V_p - K\nabla Q_p) + e[(\delta n_1/\delta t)_p - (\delta n_2/\delta t)_p] + (\delta Q_c/\delta t)_{coal_p}$$

$$+ (\delta Q_f/\delta t)_{coal_p} + (\delta Q_c/\delta t)_{pol_p} + (\delta Q_f/\delta t)_{pol_p} \tag{7}$$

Figure 4.7 Equations governing electrical properties.

The electric field strength can be related to an electric potential, ϕ_e (see Equation 2, Figure 4.7). The relationship between the electrical potential and the space charged density is then given by Equation 3, Figure 4.7.

Equations 4, 5, 6, and 7 represent the conservation of ion and charge density. n_1, n_2 represent the positive and negative free small ions, while Q_c, Q_f, and Q_p represent the space charge densities associated with the charged droplets, the fog droplets, and the precipitating droplets, respectively. Again, the left-hand terms of the five equations represent the total rate of change of the quantities indicated. Note that Equation 4 represents two equations--one for negative ions and one for positive ions. The subscript (1,2) is simply a concise notation.

One observes from Equation 4, Figure 4.7, that the current densities for the macroscopic transport of ions is made up of contributions from electrical conduction, $\pm n_{1,2} Z_{1,2} e$, and turbulent diffusion $- K \nabla n_{1,2}$. Besides the transport terms, ions can be formed or generated by cosmic ray ionization at various heights. This is unlikely to be important in the fog problem but is represented by the term G in the equation. The rate of ion loss is mainly controlled by ion attachment to the droplets in the flow field $(\delta n_{1,2}/\delta t)_c$, $(\delta n_{1,2}/\delta t)_f$ and $(\delta n_{1,2}/\delta t)_p$, and by ionic recombination between ions of opposite polarity, $-\alpha n_1 n_2$. The effect of charge on droplets being released as free ions during evaporation of the water droplets is also included in the last three terms of the equation as described later.

In Equations 5, 6, and 7, Figure 4.7, the charge densities associated with all three forms of droplets are transported both by their relative velocities with respect to the air motion and by turbulent diffusion, $\nabla \cdot (Q V_c - K \nabla Q_c)$. The second term in each of these equations represents electric charging of the droplets through ion attachment, $e[(\delta n_1/\delta t)_c - (\delta n_2/\delta t)_c]$. Finally, the droplets can also be electrified and charged due to the polarization charging mechanisms when particles collide with each other and then separate in electric field $(\delta Q/\delta t)_{pol}$ and through charge transfer when charged droplets collide and coalesce with fog droplets and precipitating droplets, $(\delta Q/\delta t)_{coal}$. The charge

84

density related to, say, 'the charged droplets' is considered to be partially transferred to the charge density associated with, say, 'the fog droplets' according to the number of charged droplets coalescing with fog droplets.

4.4.2 Ion Attachment to Droplets

Figure 4.8 lists the equations governing ion attachment to the various droplets. These equations assume that ion attachment occurs by ionic diffusion and electrical attraction only. A physical discussion of droplet charging by these mechanisms is given in Section 3.0. In this section the models are static models where the effect of relative velocity of the droplets with respect to the field and air flow is neglected. The equations given in Figure 4.8, however, take into account the effect of droplet motion at least in an approximate manner. On the other hand, these equations neglect the effects of ambient space charge around the droplets and effects due to physical or chemical properties of the droplet surfaces.

Equation 1 of Figure 4.8 illustrates that the total rate of attachment of ions is expressed in terms of a simple superpositioning of the rate of attachment of ions due to diffusion and the rate of attachment of ions due to electric field effects. The two expressions for the rate of ion attachment are based on the assumption that each works separately. In actual fact, the two attraction processes will operate simultaneously, however, there is no rigorous analytical solution presently available in the literature to compute this effect. Therefore the assumption of superpositioning is made. Evidence given in the literature suggests that the method of superpositioning will not lead to errors greater than 15%. The equations in Figure 4.8 are developed for fog droplets, however, similar expressions pertain to the charged and precipitation droplets.

The expression for the ionic diffusion is given by Equation 2, Figure 4.8. One observes from this equation that when the relative velocity of the fog droplets is zero, the equation reduces to the simple static diffusion attachment described earlier in Section 3.0.

Total Rate of Attachment of Ions (i.e., due to ionic diffusion and electrical (field) attachment)

$$\left(\frac{\delta n_{1,2}}{\delta t}\right)_f = N_f[(\tilde{I}_{1,2})_D + (\tilde{I}_{1,2})_E] \tag{1}$$

Ionic Diffusion

$$(\tilde{I}_{1,2})_D = 4\pi r_f D_{1,2} n_{1,2}[1 + (r_f V_f/2\pi D_{1,2})^{1/2}] \tag{2}$$

Electrical Attraction

1. $q_f > q_s$; $\quad (\tilde{I}_1)_E = 0$, $\quad (\tilde{I}_2)_E = n_2 Z_2(q_f/\varepsilon_0)$ $\tag{3}$

2. $q_f < q_s$; $\quad (\tilde{I}_1)_E = -n_1 Z_1 \, q_f/\varepsilon_0$, $\quad (\tilde{I}_2)_E = 0$ $\tag{4}$

3. $q_s > q_f > -q_s$ $\tag{5}$

Case 1: E same direction as V_f

$$(\tilde{I}_1)_E = 0; \quad q_s > q_f > 0; \quad |V_f| > Z_1|E| \tag{5i}$$

$$(\tilde{I}_1)_E = -n_1 Z_1(q_f/\varepsilon_0); \quad 0 > q_f > -q_s; \quad |V_f| > Z_1|E| \tag{5ii}$$

$$(\tilde{I}_1)_E = n_1 Z_1|E|(3\pi r_f^2)[1 - (q_f/q_s)]^2; \quad |V_f| < Z_1|E| \tag{5iii}$$

$$(\tilde{I}_2)_E = n_2 Z_2|E|(3\pi r_f^2)[1 + (q_f/q_s)]^2 \tag{5iv}$$

Case 2: E opposite direction of V_f

$$(\tilde{I}_2)_E = n_2 Z_2(q_f/\varepsilon_0); \quad q_s > q_f > 0; \quad |V_f| > Z_2|E| \tag{5v}$$

$$(\tilde{I}_2)_E = 0; \quad 0 > q_f > -q_s; \quad |V_f| > Z_2|E| \tag{5vi}$$

$$(\tilde{I}_2)_E = n_2 Z_2|E|(3\pi r_f^2)[1 + (q_f/q_s)]^2; \quad |V_f| < Z_2|E| \tag{5vii}$$

$$(\tilde{I}_1)_E = n_1 Z_1|E|(3\pi r_f^2)[1 - (q_f/q_s)]^2 \tag{5viii}$$

Figure 4.8   Ion attachment.

The mathematical expression for the electrical field attachment of ions is somewhat more cumbersome than that for diffusion attachment. Ion attachment due to electric field attraction to a droplet of radius, r_f, in an electric field, E, can be written in three different forms, depending on the polarity and magnitude of the net charge, q_f, of the droplet. Equation 3 represents the case where the droplet charge is positive and greater than the saturation charge. In this case no positive ions attach. Equation 4 gives a similar result for when the droplet charge is negative and exceeds the magnitude of the saturation charge.

Equation 5, shown in the figure, expresses the fact that for $q_s > q_f > -q_s$, the direction of the electric field relative to the direction of velocity of the droplet is significant. Equation 5, Case 1, illustrates the mathematical form of the expression for the ion attachment rate where the field is in the same direction as the direction of the velocity of the droplet. In this case the rate of attachment of <u>positive</u> ions also depends upon the magnitude of the relative velocity of the droplet to the drift velocity of the droplet, defined as the mobility, $Z_{1,2}$, times the magnitude of the electric field $|E|$. For Case 2 where the electric field is in the opposite direction of the relative velocity of the droplet, the situation is reversed and the rate of attachment of <u>negative</u> ions is dependent upon the magnitude of the relative velocity to the drift velocity.

The expressions for electrical field attachment given in Figure 4.8 are based on the assumption that the electric field is parallel to the direction of droplet motion. No analytical solution is available for the case where the electric field is not parallel to the velocity of the droplet. However, for the simplest method of solution, it is assumed that meaningful results can be obtained by replacing $|E|$ by the components of $|E|$ along the direction of relative velocity.

A physical explanation of the equations in Figure 4.8 may be gained by inspection of Figure 4.9. When a droplet is totally positively or totally negatively charged, the ion fluxes to the droplet have similar mathematical forms. The rate of ion attachment depends only on the net charge of the droplet and has nothing to do with the ambient electric fields nor the terminal velocity of the droplet. If the droplet is
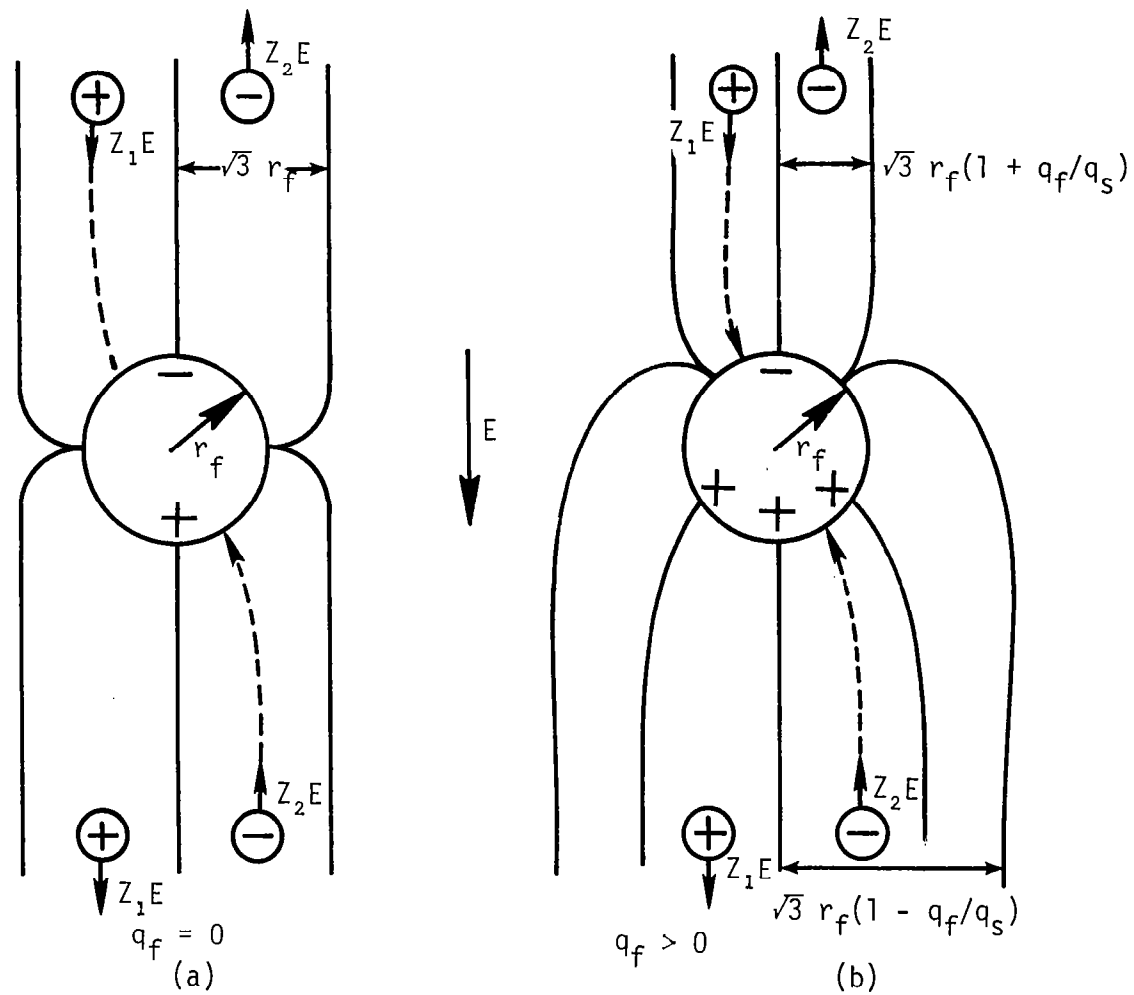
Figure 4.9   Ion capture cross sections of a droplet.

polarized in the electric field and at rest with respect to the ambient air, only positive ions can be attracted directly to the negatively charged region of the droplet, while the negative ions on the same side of the droplet can never become attached to the drop but are driven away by the electric forces. Conversely, on the other side of the droplet, only negative ions can reach the droplet at its positively charged region.

This situation changes when the droplet has a relative velocity with respect to its environment. To illustrate these changes, consider Figure 4.10(a). Here the relative velocity of the droplet is greater than its drift velocity. In this case, focusing attention on the lower left-hand corner of the figure, the velocity imparted to the droplet due to drag of the air is greater than its drift velocity. Therefore, it is carried towards the positive charged region of the droplet, whereas if it were at rest it would be repelled. Since it cannot attach to the positively charged region, it is swept around the particle and can either pass by the droplet if the droplet is completely positively charged or can be attached to the negative region behind the droplet if the droplet has some negative charge.

The negatively charged droplets illustrated in the right lower corner of Figure 4.10(a) will have both the relative velocity and drift velocity directed towards the droplet and therefore will attach on the front portion of the droplet. In turn, the two ions illustrated at the top of Figure 4.10(a) will both move away from the droplet. The positive ion moves away because the droplet's relative velocity is greater than the drift velocity caused by the electric field. Therefore the positive ion can never catch up to the droplet. The negative ion moves away even if the relative velocity of the particle were zero, because the negative region of the droplet repels the ion. This situation is clearly contained in Equations 5i and 5ii, Figure 4.8.

Inspection of Figure 4.10(b) illustrates the case where the relative velocity of the droplet is less than the drift velocity of the ions. This case is exactly identical to the case of zero droplet velocity. However, the negative ions will attach at a faster rate because their velocity relative to the droplet is increased by the

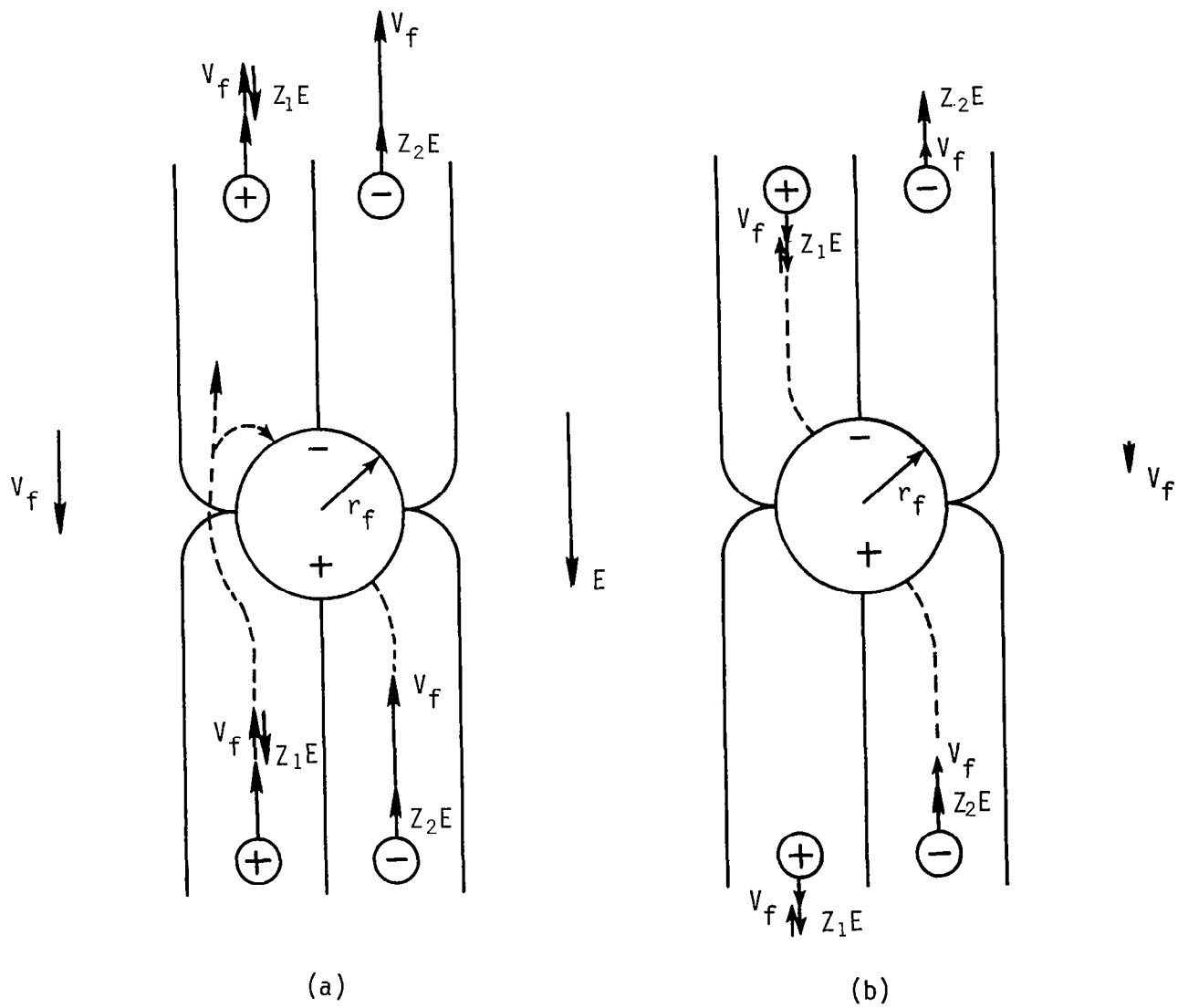(a)   (b)

Figure 4.10   Schematic of ion attachment by electrical field effects with moving droplets.

drift velocity, whereas the positive ions will collect at a slower rate because their velocity relative to the droplet is decreased due to the drift velocity. This effect is contained in Equation 5iii, Figure 4.8. Similar explanation of Equation 5, Case 2, can be given.

4.4.3 Release of Free Ions Due to Evaporation

To account for the increase in free ions in the terms $\delta n_{1,2}/\delta t$ due to evaporation of the droplets, the following rule is proposed by Chiu [4-3]. In his cloud electrification model, he allows part of the net charge associated with cloud water to be released as free ions as the cloud water content decreased because of evaporation. He assumes the amount of net charge released to occur in such a way that the net charge per unit area of droplet surface remains constant during the shrinking of the droplet due to evaporation. Although this is a gross assumption, it at least prevents the charge carried by droplets from becoming too large to be realistic when the droplet shrinks during evaporation.

4.4.4 Polarization Charging Mechanism

An expression for the term $(\delta Q/\delta t)_{pol}$ occurring in the charge transport equations must be developed. The simplest case of charge redistribution due to polarization occurs between two spherical droplets when they contact each other and then separate in an electric field. Consider a large drop of radius, r_f, with net charge, q_f, which collides with a small droplet of radius, r_c, with net charge, q_c, under the influence of an electric field. After the contact, charge will be redistributed between the two droplets so that the net charge of the large droplet becomes q_f, while that of a small droplet becomes q_c. Figure 4.11 shows the mathematical relationships. The term, Δq, is the charge transfer between the droplets. The terms A and B in Equation 2, Figure 4.11, are positive nondimensional coefficients which can be written in terms of the ratio between the radii of droplets as shown in Equation 3. The positive nondimensional constants, γ_1 and γ_2, depend only on the ratio between the radii of the droplets. Latham and Mason [4-6] show for the particular case where $r_c << r_f$, $\gamma_1 = \pi^2/2$ and $\gamma^2 = \pi^2/6$. Inspection of the equation for Δq shows that the amount of

Upon collision but not coalescence of a charge carrier and fog droplet under the influence of an electric field

$$q_f' = q_f - \Delta q; \qquad\qquad q_c' = q_c + \Delta q \qquad\qquad (1)$$

where

$$\Delta q = 4\pi\varepsilon_0\gamma_1|E|\cos(E,r_{fc})r_c^2 + Aq_f - Bq_c \qquad\qquad (2)$$

$$A = \frac{\gamma_2(r_c/r_f)^2}{1 + \gamma_2(r_c/r_f)^2}; \qquad\qquad B = \frac{1}{1 + \gamma_2(r_c/r_f)^2} \qquad\qquad (3)$$

Figure 4.11   Charge redistribution during polarization charging.

charge transferred between a pair of droplets under an electric field E depends on the original net charge on the particles, (q_c, q_f), the sizes of the particles, (r_c, r_f), the strength of the local electric field, $|E|$, and the angle between the electric field vector, E, and the position vector of the small colliding droplet with respect to the center of the large droplet, r_{cf}. The cosine of the angle between E and r_{cf} is denoted with $\cos(E, r_{cf})$. After some algebra, Chiu [4-3] shows that the rate of change of the charge density of the fog liquid water with respect to time is given by the expression shown in Figure 4.12. Where <S>, the mean separation probability and $<\cos \alpha_1>$, the mean value of $\cos \alpha_1$ for all colliding droplets, are given by Equations 2 and 3 of Figure 4.12, respectively. The angle α_1 is a measure of the relative location of the colliding droplet with respect to the impacted droplet.

Equation 1 of Figure 4.12 shows that the charging rate of a droplet depends directly on the size of the droplet, r_f, the collision effi- ciency, η, the separation probability of the colliding drops, <S>, the

$$\frac{\delta q_f}{\delta t} = \eta_f |\dot{V}_{cf}| N_c (\pi r_f^2)\{4\pi\varepsilon_0 \gamma_1 |E| \cos (E,V_{cf}) r_c^2 <\cos \alpha_1> - A q_f + B q_c\} <S> \tag{1}$$

$$<S> = \int_0^{\pi/2} S(\alpha_1) 2\pi r_f^2 \sin \alpha_1 \cos \alpha_1 \, d\alpha_1 / \pi r_f^2 \tag{2}$$

$$<\cos \alpha_1> = \int_0^{\pi/2} 2S(\alpha_1) \sin \alpha_1 \cos^2 \alpha_1 \, d\alpha_1 / <S> \tag{3}$$

Rate of Polarization Charging

$$(\delta Q_c / \delta t)_{pol_f} = N_f (\delta q_f / \delta t) \tag{4}$$

Rate of Coalescence Charging

$$(\delta Q_c / \delta t)_{coal_f} = N_f \{\eta_f |V_{fc}| N_c \pi r_f^2 (1 - <S>) q_c\} \tag{5}$$

Figure 4.12 Polarization and coalescence charging mechanism.

number concentration of the colliding droplets, N_c, and the speed of the small droplets relative to the large droplet, $|V_{cf}|$. The equation indicates that the more droplets which collide with the large droplet and then separate from it per unit time, the faster the large droplet can be charged. For each collision and separation, more charge is separated between droplets. It is apparent that the local electric field increases if (1) the ambient electric field tends to be parallel to V_{cf}, (2) the size of the droplets increases, and (3) the value of $<\cos \alpha_1>$ increases. The charging rate, of course, is also affected by the charge already accumulated on the interacting droplets, i.e., q_f and q_c. The final expression for the term $(\delta Q/\delta t)_{pol}$ is then given by Equation 4, Figure 4.12. This expression assumes that the fog droplets

are separated far enough from one another in the fog that the $\delta q_f/\delta t$ expression in Figure 4.12 can be applied to all of the fog droplets in a unit volume of air.

The above discussion of the polarization charging mechanism is, of necessity, brief and the reader is referred to the more complete derivation given by Chiu [4-3].

4.4.5 Charge Transfer During Coalescence

From Equation 1, Figure 4.12, it is apparent that only <S> fraction of the colliding droplets separate from the larger droplet to make the polarization charging mechanism work. There is, therefore, (1 - <S>) fraction of the colliding droplets which coalesce with the larger droplet. In such conditions, it is assumed that the net charge on the droplet transfer to the larger droplet. If q_c is the average charge on the charged droplets before collision and coalescence, then the form of $(\delta Q_c/\delta t)_{coal}$ in Equations 5, 6, and 7 of Figure 4.7 can be expressed as shown by Equation 5, Figure 4.12.

4.5 Utility of Equations

The preceding equations represent a set of governing equations which, if solved simultaneously by numerical techniques, will provide, at least, qualitative solution to the rate at which fog droplets can be precipitated by electric charged particles sprayed into the atmosphere. Of course, many assumptions in the model are involved and must be examined once solutions are available and experiments are carried out.

A number of the parameters which are needed as input to the various semiempirical expressions appearing in the governing equations are not well known. However, the model can be applied to parametric studies and the sensitivity of the fog dispersal technique to the various parameters can be established.

In addition to the unknown empirical parameters, a complete set of initial conditions and boundary conditions must be established before the solution of the system of equations can be achieved. Work in this area is continuing and will be reported at a later date.

References

4-1. Christensen, Larry S., and Walter Frost. "Fog Dispersion," NASA Contractor Report 3255, prepared by FWG Associates, Inc., Tullahoma, Tennessee, under Contract No. NAS8-33095 for Marshall Space Flight Center, Huntsville, Alabama, March 1980.

4-2. Becker, Bryan R. "Cooling Tower Recirculation as Influenced by the Local Atmospheric Flow Field, a Numberical Study," PhD Dissertation, The University of Tennessee, December 1979.

4-3. Chiu, Chin-Shan. "Numerical Study of Cloud Electrification in an Axisymmetric, Time-Dependent Cloud Model," Journal of Geophysical Research, Vol. 83, No. C10, October 20, 1978.

4-4. Orville, H. D. "A Numerical Study of the Initiation of Cumulus Clouds over Mountainous Terrain," Journal of Atmospheric Science, Vol. 22, p. 684, 1965.

4-5. Wisner, C., H. D. Orville, and C. Myers. "A Numerical Model of a Hail-Bearing Cloud," Journal of Atmospheric Science, Vol. 29, p. 1160, 1972.

4-6. Latham, J., and B. J. Mason. "Electrical Charging of Hail Pellets in a Polarizing Electric Field," Proceedings of the Royal Society of London, Series A, 266, 387, 1962.

5.0 FIELD EXPERIMENT

Simultaneous with the analytical modeling of the fog dispersal technique and the nozzle design study, advanced planning of a field study to verify the charge particle fog dispersal systems is needed. This section discusses meteorological measurements which must be considered (rates and accuracies), site requirements, spatial configurations of units, and necessary instrumentation, i.e., tower, transmissometer, electric field mills, cloud particle and nuclei counters, etc.

5.1 General Requirements

Electrostatic fog dispersal, although shown effective in the laboratory, has not been demonstrated conclusively in the field. It is essential that to accurately assess charged particle fog dispersal techniques, a comprehensive field experiment be designed.

The field experiment must determine if there is any improvement in visibility and the time, duration, location, and degree of improvement. Any natural fog dissipation, warming, advection of dry air, change in spectrum of condensation nuclei, etc. must be accounted for and distinguishable from the conditions produced by the fog dispersal system.

To examine the charging characteristics of particular charge particle spray guns the electric field and changes in the electric field with space and time need to be measured. The charge on the precipitated drops will determine the charge transfer efficiency between the particular fog drops and charge carriers.

There are a number of site requirements for a field experiment of this nature. The aviation industry is the most likely industry to benefit from fog dispersal; therefore, the site should be at an airport or approximate the terrain of an airport. Airports are characterized by flat terrain, low vegetation, and few tall buildings in the runway area. For convenience, an area where fogs occur regularly and predictably has obvious advantages.

96

An area that has different types of fog, i.e., advection, seacoast, and urban fogs under different prevailing weather conditions might eliminate the need for testing at different sites. The size of the field experiment can be reduced if the normal mean wind direction during foggy conditions is known. This allows the field instruments to be arranged along the mean wind thus making an essentially two-dimensional experiment which greatly reduces the number of necessary measurement. Any nearby meteorological recording stations are of obvious value.

One possible geometrical configuration for the proposed field project is shown in Figure 5.1. This shows a minimum configuration. A larger test array is required for runs during higher mean wind conditions. The exact size of the array is under investigation. The number of units required to dissipate fog in crosswind conditions depends on the wind velocity and time required for visibility to improve. The time required for visibility to improve to 457 m (1,500 ft) (required visibility for aircraft landing) is estimated at 14 minutes.

For 2.24 m/s (5 mph) crosswind conditions, the wind drifts 1,878 m (6,160 ft) in 14 minutes. Therefore, to disperse fog with 2.24 m/s (5 mph) crosswind conditions requires a matrix of units at a 58 m spacing. This will be more carefully defined from the results of the on-going studies described in Sections 3.0 and 4.0.

Figure 5.1 illustrates control areas containing an instrumented tower and transmissometer array located at positions of the test site upwind and downwind. A similar arrangement of towers and transmissometers at the test site will allow for realistic three-dimensional analysis of the fog life cycle. The influence of a metal tower on the electrical field is being investigated.

5.2 Required Measurements

The meteorological variables that need to be monitored in order to verify and analyze the effectiveness of charged particle fog dispersal are discussed in this subsection. Criteria for a minimum but effective field project are discussed. A suggested list of rates and accuracies for the proposed field project are given in Table 5.1. It should be
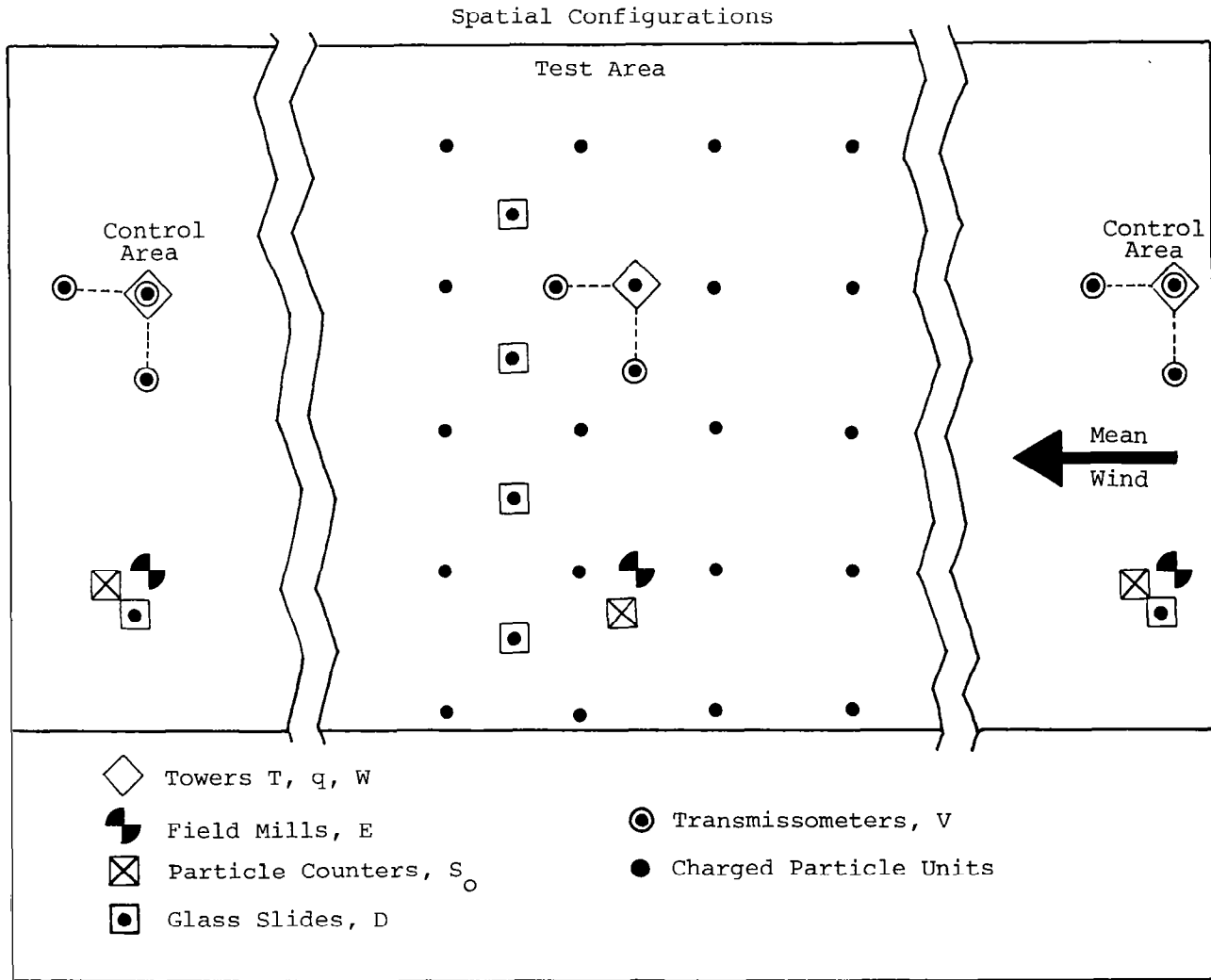
Test Area

Control
Area

Control
Area

Mean

Wind

86

◇ Towers T, q, W

◣ Field Mills, E

⊠ Particle Counters, S$_O$

⊡ Glass Slides, D

◉ Transmissometers, V

● Charged Particle Units

Figure 5.1 Schematic of Site Arrangement for Field Testing.

Table 5.1 Rates and Accuracies of Meteorological Variables.

	Variable	Locations	Accuracy	Frequency
T	Temperature	Three levels, three towers	$0.1°$ C	1/60 Hz
P	Pressure	Local airport	0.1 mb	1/3600 Hz (hourly)
q	Relative humidity	Three towers	1%	1/60 Hz
V	Visibility	Three towers, three axes	1 m	1/60 Hz
W	Turbulent wind	Three levels, three towers	0.1 m/s	1 Hz
E	Electric field	Three locations	10 v/m	1/60 Hz
S_o	Particle spectrum concentration versus size	Three locations	$10^2/m^3$	1/60 Hz
R	Precipitation rate	Three locations	1 drop/ mm^2/min	1/900 Hz (15 min)
C_n	Condensation nuclei	One location upwind	$10^2/m^3$	1/900 Hz
**** Optional Measurements ****				
H_I	Inversion height	One location	10 m	---
W_G	Geostrophic wind	Local airport	10 m/s	1/3600 Hz
γ	Lapse rate above tower height	Local meteorological station	1 $°$ C/m	Twice daily
**** Synoptic Conditions ****				
Hourly synoptic scale weather conditions should be analyzed for fog extent and surrounding conditions. Advection rates of temperature and humidity.				

noted that these accuracies and frequencies can be attained from commercially available instrumentation and that some leniency may be accepted while still producing meaningful data. The rates and accuracies listed for the wind field are for turbulence measurements and need not be that sensitive at all three locations.

5.2.1 Three-Dimensional Wind Field

The three-dimensional wind field needs to be known at a minimum of three locations upwind and downwind from the test site and at the test site. The wind field must be measured to the height of desired fog clearance. If the terrain at and around the test site is flat and homogeneous, turbulence measurements are really needed only at one location, ideally at the test site. The geostrophic wind can be interpolated from maps obtained from surrounding National Weather Service Stations.

5.2.2 Temperature and Humidity Fields

The temperature and humidity fields need to be known at the test site and at both control areas. To determine the stability of the atmosphere the temperature lapse rate must be measured. It is convenient to simply locate a reference thermocouple junction at one level on the meteorological towers and temperature differential instruments at other levels. Humidity need only be measured at one level of each tower if there is sufficient mixing. These measurements are needed to determine if any warm or dry parcels of air advect into the area.

5.2.3 Visibility

The purpose of fog dispersal is to improve visibility. Therefore, one of the more important parameters to measure is visibility. Visibility measurements need to be made on three axes: along wind, crosswind, and in the vertical. It is convenient to mount a transmissometer at the top of each tower for the vertical measurement. The horizontal measurements can be made by either transmissometers or backscatter lidars. It

is important that accurate measurements be made at the site and both control areas.

5.2.4 Cloud Physics

The types and spectrum of condensation nuclei prior to the onset of fog will determine the type of fog which occurs although the gasoline engine exhaust may have some effects which must be considered. Monitoring of the nuclei for changes in number or species should be used as a control to determine what changes are instrumental in the fog dissipation.

The fog droplet spectrum, being the direct cause of reduced visibility, must be monitored as continuously as possible at the site and at both control areas prior to, during, and after the field test. The theory of charged particle fog dispersal is based on changing the number and or sizes of fog droplets. Therefore, any accurate assessment of the dispersal technique must include a complete time history of the droplet spectrums at the control areas as well as at the test site.

Charged particle fog dispersal theory is based on enhanced fog droplet precipitation; therefore, the precipitation rate needs to be monitored as continuously as possible at the test site and at the control areas. The size of the precipitating droplets will aid in determining the mechanism behind charged particle fog dispersal.

5.2.5 Electric Field

Charged particle fog dispersal enhances the precipitation rate by enhancing the local electric field. To determine the efficiency with which the nozzle enhances the electric field, measurements are needed. The electric field need only be monitored at one surface location in the control areas; however, at the test site an array of surface mills and an elevated mill are required for optimum data collection.
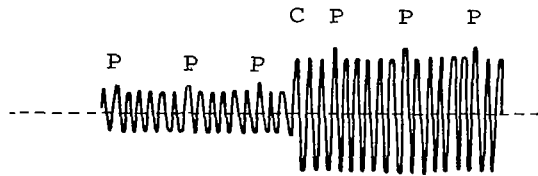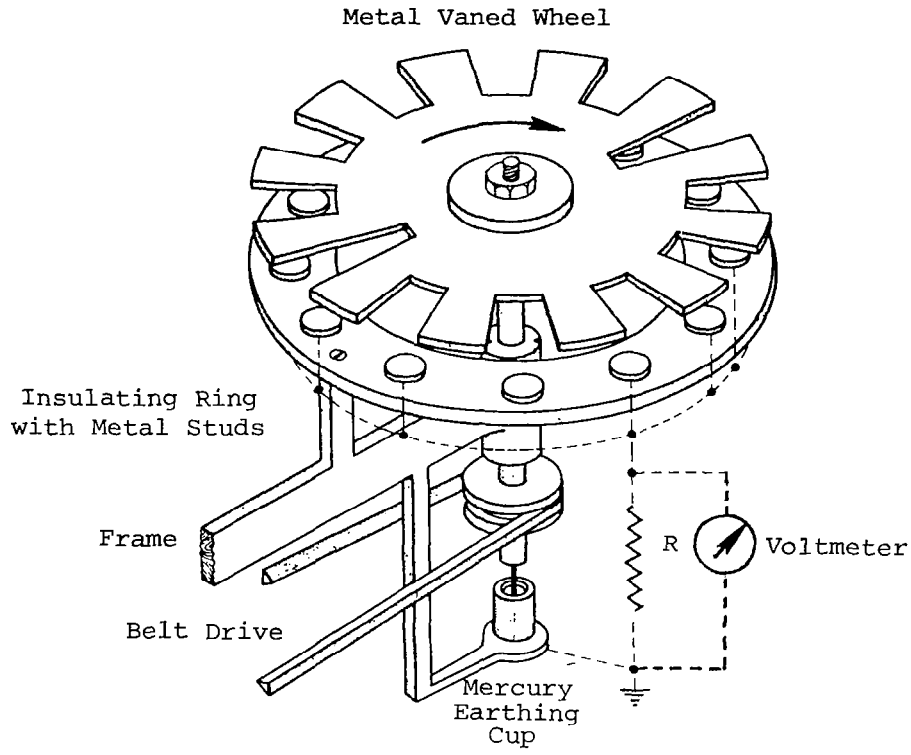
5.3 Instrumentation

Tower instrumentation would consist of standard three-dimensional wind sensors commercially available from a number of manufacturers. Thermocouple junctions at a number of heights on each tower with an

internal electric reference in the recorder will provide the absolute temperatures and the temperature lapse rates up to the height of the towers. An aspirated humidity sensor on each tower will provide continuous monitoring of the relative humidity and aid in interpretation of the natural onset and breakup of fog.

Visibility measurements can be made by either of two methods: transmission or backscatter. Transmissometers measure the percent of light received to that transmitted a chosen distance away. Backscatter instrumentation measures the percent of light scattered back to the transmitter. Transmissometers use either a chopped incandescent transmit signal or a continuous laser transmitter. The incandescent instrumentation utilizes a full-band photo-electric cell receiver while the laser utilizes a selective small-band photo cell. The laser circuit allows the beam to be split into the three orthogonal directions by use of partial reflectors thus requiring only one transmit circuit at each site. However, the incandescent instrumentation has the advantage of low cost.

The electric field is measured with electric field mills. Electric field mills are of many different designs but most field mills are based on alternately exposing and shielding an electrical plate to the atmosphere. One particular design is illustrated in Figure 5.2 [5-1]. A rotating disk with slots, exposes and shields a number of metal studs. The larger slots allow for the direction of the electric field to be determined. A sample output is shown illustrating the peaks formed by the larger slots indicated with a "P." A change in intensity is shown and indicated with a "C." Since large structures significantly alter the electric field, the meters must be located in a region at least ten times the height of such structures or trees away. The measurement of electric fields is not at all a routine measurement. Considerable research is currently going on to improve field mill technology. The most current instrumentation should be used.

To measure the electric field at tower height, a field mill could be mounted at the top of the tower. A graph of the ratio of the resultant field at the top of a structure, E_T, to the inducing field, E, as a

Metal Vaned Wheel

Insulating Ring
with Metal Studs

Frame

Belt Drive

Mercury
Earthing
Cup

R ⊘ Voltmeter

C P   P   P

P   P   P

Oscilloscope Output

Figure 5.2 Electric field mill [5-1].

103

function of structure dimension, H/R, (height divided by the radius) is shown in Figure 5.3 [5-2].

The cloud droplet spectrum can be measured with gelatin slides or a backscatter lidar. The gelatin slides are inexpensive, but require labor-intensive viewing with a microscope; moreover, they did not prove very successful during the Panama experiments and would require careful preparation and application to provide meaningful results. The backscatter lidar gives a continuous measure of the droplet spectrum but is expensive. The condensation nuclei can be measured with standard aiken counters.

The preceding brief discussion of instrumentation illustrates that most instrumentation required to verify the charged particle fog dispersal technique is commercially available. Some of the instrumentation needed to make measurements of the accuracy desired, however, are relatively expensive, for example, backscattering lidar. Obviously, cost of the experiment is an important consideration, and work in developing a meaningful experimental plan is on going.

The one area where measurement techniques may require development is electric field measurements. Presently, a program is being carried out at the Naval Research Laboratories, Washington, D.C., to develop a new electric field mill. Work carried out at Socorro, New Mexico, has produced a successful electric mill, but these are not commercially available and require appreciable amounts of machining when built on an individual basis [5-3]. Evaluation of electric field measurement techniques is continuing.

References

5-1. Mason, G. J. The Physics of Clouds, 2nd edition. Oxford: Claredon Press, 1971.

5-2. Anderson, R. B. Lightning, Vol. 1. Academic Press, 1977.

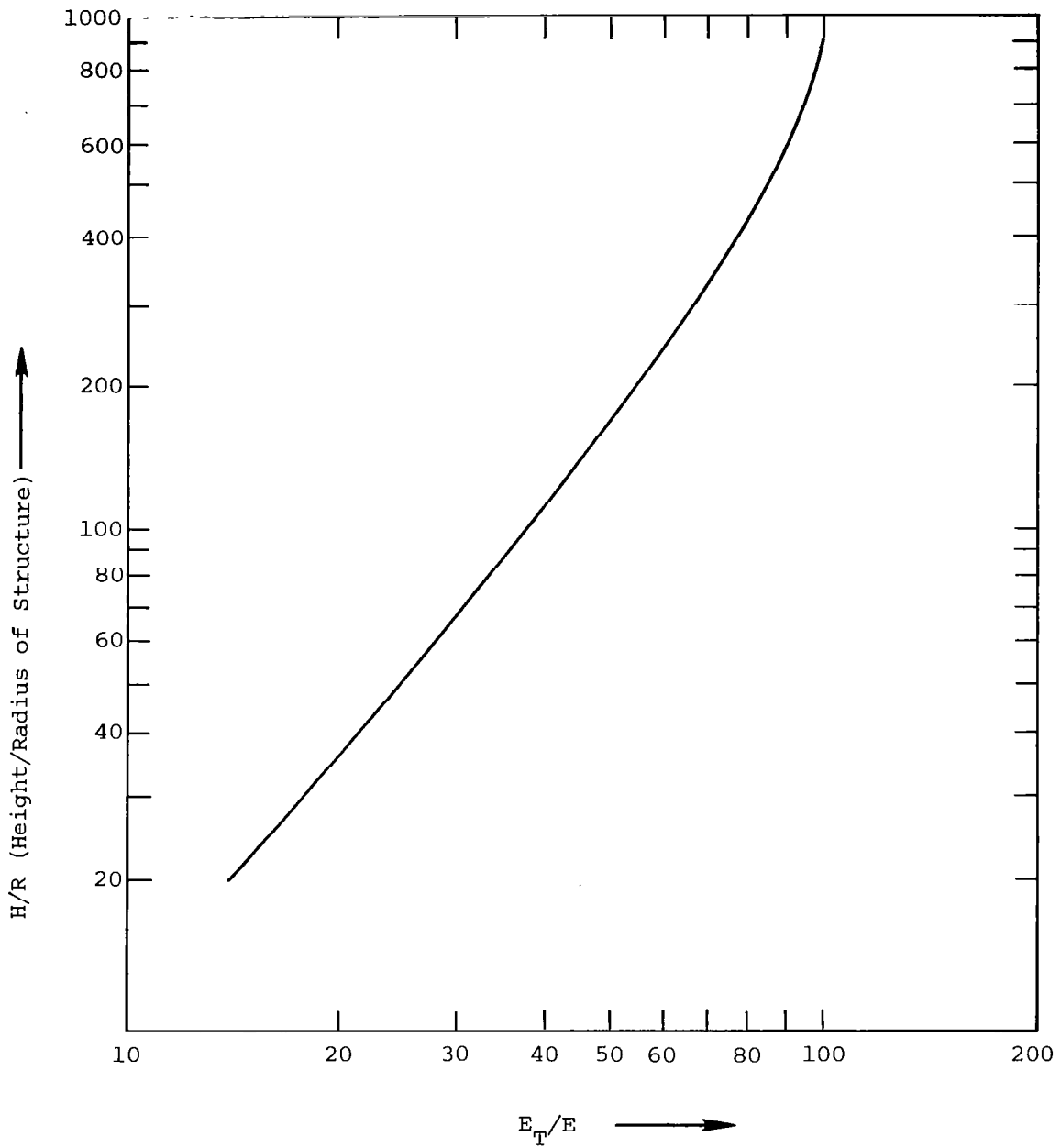5-3. Christian, Hugh, Personal communication, July 1980.

Figure 5.3   Influence of tower structure on local electrical field [5-2].

6.0 CONCLUSIONS

This study has reviewed the Panama Canal charged particle, fog dispersal field test program, looked in-depth at the nozzle characteristics of a charged particle spray nozzle, formulated the basic governing equations to analyze a charge jet interaction with the fog environment and outlined some basic requirements of a field program which would verify the charged particle fog dispersal technique.

The review of the Panama Canal experiment indicates that the results are inconclusive as to whether a cleared region can be maintained for a sufficient period of time and as to the values of certain physical parameters required to modify and improve the design of the fog dispersal system hardware.

The in-depth study of charged particle nozzle characteristics suggests that certain modifications to the design of the previous nozzle used in the Panama Canal experiment may significantly enhance the amount of charge which can be induced on the charge carriers. Since the time for maximum charging of particles in a corona region are on the order of milliseconds, and the droplets pass through the supersonic nozzle used in previous experiments on the order of microseconds, techniques for exposing the particle charge carriers to the corona discharge for a longer period should be developed. Work in this area is proceeding.

The basic equations which govern the jet interaction within a fog environment once the charged particles have left the nozzle have been formulated. The system of equations is essentially the same as used in cloud electrification studies; however, modification of the boundary conditions is required for solution of the problem.

A study of the instrumentation needed and its availability to carry out a full, in-depth field study of the fog dispersal technique utilizing charged particles indicates that much of the instrumentation is commercially available. For several of the measurements such as droplet size distributions, a tradeoff between cost and accuracy is an important

consideration, e.g., the use of backscattering lidar versus gelatin slide techniques. Measurements of electric field strengths is one area where commercial instruments are apparently not available. Electric field mills have been developed by a number of separate research groups. These mills can be built on an individual unit basis to carry out the necessary measurements for verification of the charged particle warm fog dispersal system. Thus extensive development costs of instrumentation are not anticipated.

1. REPORT NO. NASA CR-3440	2. GOVERNMENT ACCESSION NO.	3. RECIPIENT'S CATALOG NO.
4. TITLE AND SUBTITLE Charged Particle Concepts for Fog Dispersion		5. REPORT DATE June 1981
		6. PERFORMING ORGANIZATION CODE
7. AUTHOR(S) Walter Frost, Frank G. Collins, and David Koepf		8. PERFORMING ORGANIZATION REPORT #
9. PERFORMING ORGANIZATION NAME AND ADDRESS FWG Associates, Inc. R.R. 2, Box 271-A Tullahoma, TN 37388		10. WORK UNIT NO. M-352
		11. CONTRACT OR GRANT NO. NAS8-33541
		13. TYPE OF REPORT & PERIOD COVERED
12. SPONSORING AGENCY NAME AND ADDRESS National Aeronautics and Space Administration Washington, D.C. 20546		Contractor Report
		14. SPONSORING AGENCY CODE 505 44 19

15. SUPPLEMENTARY NOTES

Marshall Technical Monitor: Dennis W. Camp
Final Report

16. ABSTRACT

     Charged particle techniques hold promise for dispersing warm fog in the terminal area of commercial airports. This report focuses on features of the charged particle technique which require further study. The basic physical principles of the technique and the major verification experiments carried out in the past are described. The fundamentals of the nozzle operation are given. The nozzle characteristics and the theory of particle charging in the nozzle are discussed, including information from extensive literature on electrostatic precipitation relative to environmental pollution control and a description of some preliminary reported analyses on the jet characteristics and interaction with neighboring jets. The equation governing the transfer of water substances and of electrical charge is given together with a brief description of several semi-empirical, mathematical expressions necessary for the governing equations. The necessary ingredients of a field experiment to verify the system once a prototype is built are described.

17. KEY WORDS Warm fog Fog dispersal Aviation safety Aviation meteorology	18. DISTRIBUTION STATEMENT Unclassified – Unlimited Subject Category 47
19. SECURITY CLASSIF. (of this report) Unclassified	20. SECURITY CLASSIF. (of this page) Unclassified	21. NO. OF PAGES 120	22. PRICE A06